

**ACTIVITY ENHANCEMENT OF COPPER DOPED TiO<sub>2</sub>/ZnO PHOTO  
CATALYST FOR DEGRADATION OF RECALCITRANT  
POLLUTANTS**

**MOHAMMAD REZA DELSOUZ KHAKI**

**FACULTY OF ENGINEERING  
UNIVERSITY OF MALAYA  
KUALA LUMPUR**

**2017**

ACTIVITY ENHANCEMENT OF COPPER DOPED  $\text{TiO}_2/\text{ZnO}$  PHOTO  
CATALYST FOR DEGRADATION OF RECALCITRANT  
POLLUTANTS

MOHAMMAD REZA DELSOUZ KHAKI

THESIS SUBMITTED IN FULFILLMENT OF THE  
REQUIREMENTS FOR THE DEGREE OF DOCTOR  
OF PHILOSOPHY

FACULTY OF ENGINEERING  
UNIVERSITY OF MALAYA  
KUALA LUMPUR

2017

**UNIVERSITI MALAYA**  
**ORIGINAL LITERARY WORK DECLARATION**

**Name of Candidate:** Mohammad Reza Delsouz Khaki

**Registration/Matric No:** KHA110060

**Name of Degree:** DOCTOR OF PHILOSOPHY

**Title of Project Paper/Research Report/Dissertation/Thesis (“this Work”):**

ACTIVITY ENHANCEMENT OF COPPER DOPED TiO<sub>2</sub>/ZnO PHOTO  
CATALYST FOR DEGRADATION OF RECALCITRANT POLLUTANTS

**Field of Study:** Environmental Engineering

**I do solemnly and sincerely declare that:**

- (1) I am the sole author/writer of this Work;
- (2) This Work is original;
- (3) Any use of any work in which copyright exists was done by way of fair dealing and for permitted purposes and any excerpt or extract from, or reference to or reproduction of any copyright work has been disclosed expressly and sufficiently and the title of the Work and its authorship have been acknowledged in this Work;
- (4) I do not have any actual knowledge nor ought I reasonably to know that the making of this work constitutes an infringement of any copyright work;
- (5) I hereby assign all and every rights in the copyright to this Work to the University of Malaya (“UM”), who henceforth shall be owner of the copyright in this Work and that any reproduction or use in any form or by any means whatsoever is prohibited without the written consent of UM having been first had and obtained;
- (6) I am fully aware that if in the course of making this Work I have infringed any copyright whether intentionally or otherwise, I may be subject to legal action or any other action as may be determined by UM.

**Candidate’s Signature**

**Date:**

**Subscribed and solemnly declared before,**

**Witness’s Signature**

**Date:**

## ABSTRACT

Industrial wastewaters contain a variety of chemical pollutants such as phenolic compounds, dyes, organophosphate insecticide. Treatment of these chemical compounds is of importance due to the toxic nature of these chemical compounds. Advance Oxidation Processes (AOPs) have been introduced as a potential method to produce highly oxidative ion species including  $\text{OH}^\bullet$  and  $\text{O}^{2-}$  for water treatment. Photocatalysts such as  $\text{TiO}_2$  and  $\text{ZnO}$  have been extensively and successfully used in AOPs to remove chemical pollutants. However, these photocatalysts suffer from limited activities and applications under UV light due to large band gap. Doping is the process of adding transition metals to a photocatalyst or combining two different photocatalysts to alter their properties, especially their band gap energy level. In this study, a new photocatalyst, Cu-doped  $\text{TiO}_2/\text{ZnO}$  nanocrystals were fabricated by entrapping copper ions in the crystalline matrix of  $\text{TiO}_2/\text{ZnO}$  through sol-gel method in order to improve the photocatalytic activity of  $\text{TiO}_2$ . Different copper concentrations were loaded into the photocatalyst matrix and the photocatalysts were calcinated at two different temperatures of 500 and 700°C. Thermal property, crystalline structure, surface morphology, band gap and absorption spectra of Cu-  $\text{TiO}_2/\text{ZnO}$  were characterized by thermogravimetric analysis, X-ray diffraction, scanning electron microscopy, transmission electron microscope and UV-Vis spectroscopy. The minimum crystal size and maximum surface area were observed in the samples with Cu amount of 5wt%. It was also observed that the Cu- $\text{TiO}_2/\text{ZnO}$  complex was in cylindrical shape, depending on the concentration of the compounds. Furthermore, the band gap of Cu- $\text{TiO}_2/\text{ZnO}$  was reduced to about 2.20eV as the Cu loading increased to almost 3%. The photocatalytic activity and stability of the photocatalyst with the best characterization result were then evaluated based on its capability of degrading *methyl orange* and *methylene blue* dyes based on colour, COD and TOC removal under visible light irradiation. The

characterization results implied that the synergistic effect of Cu ions considerably narrowed the band gap of TiO<sub>2</sub> and ZnO compared to TiO<sub>2</sub>, ZnO, TiO<sub>2</sub>/ZnO, Cu-TiO<sub>2</sub> and Cu-ZnO. The synthesized photocatalysts also showed enhanced absorption in the visible light region, exhibiting the ability of Cu-TiO<sub>2</sub>/ZnO for photocatalytic degradation of these model dyes. Cu- TiO<sub>2</sub>/ZnO with a Cu content of 3wt% was found to have the maximum activity, giving C/C<sub>0</sub> value of 0.03 after 150 min. The maximum colour removal of 85.45%, COD removal of 70.56% and TOC removal of 48.70% were achieved for MO while the maximum colour removal of 73.20 %, COD removal of 59.92% and TOC removal of 38.77% were achieved for MB under optimal conditions. ANFIS (*Adaptive Neuro Fuzzy Inference System*) was used to analyse the sensitivity of photoactivity of Cu-TiO<sub>2</sub>/ZnO towards operating conditions in advanced oxidation reaction for photodegradation of dyes. According to variables selection using ANFIS analysis, catalyst concentration 0.6 g/l and reaction time 120 min were the most effective parameters for MO degradation whereas dye concentration 35 ppm and pH > 7.5 were the most influential on MB removal using Cu-TiO<sub>2</sub>/ZnO.

## ABSTRAK

Air sisa industri mengandung pelbagai bahan pencemar kimia seperti sebatian fenol, pewarna, racun serangga organofosfat dan lain-lain. Rawatan sebatian-sebatian kimia ini adalah penting disebabkan oleh sifat toksik sebatian-sebatian ini. Rawatan Pengoksidaan Lanjutan (RPL) telah diperkenalkan sebagai satu cara yang berpotensi untuk menghasilkan spesies ion yang mempunyai upaya pengoksidaan yang tinggi termasuk  $\text{OH}^\bullet$  dan  $\text{O}^{2-}$  untuk rawatan air. Pemangkin foto seperti  $\text{TiO}_2$  dan  $\text{ZnO}$  telah digunakan secara ekstensif dan berjaya dalam RPL untuk menyingkirkan bahan pencemar kimia dari air sisa. Walau bagaimanapun, pemangkin foto mempunyai aktiviti dan penggunaan yang terhad di bawah pancaran UV disebabkan oleh jurang jalur yang luas. Pembauran merupakan satu proses penambahan logam peralihan ke dalam pemangkin foto atau penggabungan dua pemangkin foto yang berlainan untuk mengubah ciri-ciri pemangkin tersebut, terutamanya tahap tenaga jurang jalur. Dalam kajian ini, satu pemangkin foto yang baru, kristal nano  $\text{TiO}_2/\text{ZnO}$  yang terbaur dengan kuprum telah dihasilkan dengan memasukkan ion kuprum ke dalam matriks kristal  $\text{TiO}_2/\text{ZnO}$  melalui cara sol-gel untuk menambahbaiki aktiviti pemangkinan foto  $\text{TiO}_2$ . Kuprum dengan kepekatan yang berlainan telah dimasukkan ke dalam matriks pemangkin foto dan dibakar pada dua suhu, iaitu 500 dan 700°C. Ciri-ciri haba, struktur kristal, morfologi permukaan, jurang jalur dan spektra penyerapan  $\text{Cu-TiO}_2/\text{ZnO}$  telah ditentukan oleh analisa termogravimetrik, pembelauan sinaran X, Mikroskopi Imbasan Electron, Mikroskop Transmisi Electron dan Spektroskopi UV-Vis. Saiz kristal minimum dan luas permukaan maximum telah diperhatikan di dalam sampel yang mengandungi 5wt% kuprum. Kompleks  $\text{Cu-TiO}_2/\text{ZnO}$  adalah dalam bentuk silinder, yang bergantung pada kepekatan sebatian. Selain daripada itu, jurang jalur  $\text{Cu-TiO}_2/\text{ZnO}$  telah dikurangkan ke 2.20eV apabila kuprum bertambah sebanyak kira-kira 3%. Aktiviti pemangkinan foto dan kestabilan untuk pemangkin foto dengan

ciri-ciri yang terbaik kemudian diuji berdasarkan keupayaan pemangkin tersebut untuk merawat pewarna *methyl orange* (MO) and *methylene blue* (MB) mengikuti tahap penyingkiran warna, COD dan TOC bawah pancaran cahaya boleh dilihat. Keputusan pencirian menunjukkan bahawa kesan sinergistik ion kuprum dapat mengurangkan jurang jalur TiO<sub>2</sub> dan ZnO dengan ketara berbanding dengan TiO<sub>2</sub>, ZnO, TiO<sub>2</sub>/ZnO, Cu-TiO<sub>2</sub> dan Cu-ZnO. Pemangkin foto yang dihasilkan juga mempunyai daya penyerapan yang lebih baik dalam kawasan pancaran cahaya boleh dilihat. Ini telah menunjukkan keupayaan Cu-TiO<sub>2</sub>/ZnO untuk merawat pewarna model melalui aktiviti pemangkinan foto. Cu-TiO<sub>2</sub>/ZnO dengan kepekatan kuprum sebanyak 3wt% mempunyai aktiviti pemangkinan yang maximum dengan nilai C/C<sub>0</sub> sebanyak 0.03 selepas 150 min. Penyingkiran warna sebanyak 85.45%, COD sebanyak 70.56% dan TOC sebanyak 48.70% telah dicapai untuk MO manakala penyingkiran warna maximum sebanyak 73.20 %, COD sebanyak 59.92% dan TOC sebanyak 38.77% telah dicapai untuk MB di bawah keadaan optimum. ANFIS (*Adaptive Neuro Fuzzy Inference System*) telah digunakan untuk menganalisa sensitiviti aktiviti foto Cu-TiO<sub>2</sub>/ZnO terhadap keadaan operasi dalam RPL. Berdasarkan analisa ANFIS atas pembolehubah, kepekatan pemangkin 0.6 g/l dan masa tindak 120 min balas merupakan parameter yang paling berpengaruh ke atas penyingkiran MO manakala kepekatan pewarna 35 ppm dan pH > 7.5 adalah paling berpengaruh ke atas penyingkiran MB apabila Cu-TiO<sub>2</sub>/ZnO digunakan.

*Dedicated to my father, my mother and my sister who have been a source of inspiration  
and contributed immensely to the success of this thesis*

University of Malaya



## ACKNOWLEDGEMENTS

I would like to express my sincere appreciation and gratitude to my supervisor Prof. Ir. Dr. Abdul Aziz Abdul Raman who has provided me the opportunity and conducive environment to undertake this study. Under his supervision, I have built the confidence to pursue laboratory investigations with patience and optimism.

There is no way I would have been able to make this journey without the care, unconditional support and encouragement of my co-supervisor Prof. Dr. Wan Mohd Ashri Bin Wan Daud. His busy schedule has never been an obstacle; his almost daily presence, mentorship and encouragement helped me to overcome difficult times during the course of this study.

Throughout this study, my friends have also extended exceptional and invaluable cooperation. I would like to especially acknowledge the contribution of Dr. Baharak Sajjadi. Special thanks go to each and every staff member of the Department of Chemical Engineering. Without their assistance, the journey would have been more difficult and the laboratory work more laborious.

Most of all, I will always be grateful to my parents, whose love and prayers made everything possible. They gave me all the encouragement to be resilient and endure when situations at times became depressive. By remaining close through constant contact and being there when I needed them, they made me feel as if I am with them even though they are thousands of miles away. My deep appreciation goes to my loving sister Negin for sharing many happy memories together. Foremost, it is the continuous support and prayers of my dearest father that have kept me moving at times when the task ahead appeared overwhelming.

## TABLE OF CONTENTS

TITLE PAGE .....	i
ORIGINAL LITERARY WORK DECLARATION FORM.....	ii
ABSTRACT .....	iii
ABSTRAK .....	v
ACKNOWLEDGEMENTS .....	viii
TABLE OF CONTENTS .....	ix
LIST OF FIGURES .....	xiii
LIST OF TABLES .....	xvi
LIST OF SYMBOLS AND ABBREVIATIONS .....	xviii
<b>1 CHAPTER 1: INTRODUCTION.....</b>	<b>1</b>
1.1 Background .....	1
1.2 Problem statement .....	2
1.3 Research objectives .....	3
1.4 Thesis organization.....	3
<b>2 CHAPTER 2: LITERATURE REVIEW .....</b>	<b>5</b>
2.1 Introduction .....	6
2.2 Water treatment methods.....	7
2.3 Advance oxidation process.....	8
2.4 Photocatalyst .....	9
2.5 TiO <sub>2</sub> and ZnO photocatalyst.....	15
2.6 TiO <sub>2</sub> Photocatalyst.....	24

2.7	Dopants effects on TiO <sub>2</sub> photocatalyst .....	30
2.8	Doping processes.....	31
2.8.1	Effect of metal doping.....	33
2.8.2	Effect of non-metal doping .....	36
2.8.3	Effect of metalloid and halogen doping.....	38
2.8.4	Effect of Co-doping.....	40
2.8.5	Coupling of TiO <sub>2</sub> with other semi-conductors.....	40
2.9	Operational factors effecting the photocatalytic degradation.....	42
2.9.1	Effect of calcination temperature of nano-doped-TiO <sub>2</sub> .....	42
2.9.2	Effect of dopant concentration.....	43
2.9.3	Effect of initial concentration.....	43
2.9.4	Effect of photocatalyst concentration.....	43
2.9.5	Preparation methods of doped-photocatalysts .....	46
2.9.6	Sol-gel method .....	47
2.10	Summary of literature review.....	52
<b>3</b>	<b>CHAPTER 3: METHODOLOGY .....</b>	<b>53</b>
3.1	Material .....	53
3.2	Photocatalyst preparation .....	53
3.3	Characterization.....	56
3.4	Experimental design and statistical analysis .....	57
3.5	Adaptive neuro-fuzzy inference (ANFIS).....	59
3.5.1	Variable selection methodology.....	60

3.5.1.1	Input and output variable .....	60
3.5.1.2	Variable selection using ANFIS .....	60
3.6	Photocatalytic activity .....	68
3.7	Safety Aspects .....	70
<b>4</b>	<b>CHAPTER 4: RESULTS AND DISCUSSION .....</b>	<b>71</b>
4.1	Introduction .....	71
4.2	Physico–chemical properties of new doped photocatalyst .....	72
4.2.1	Effect of calcinate temperature .....	72
4.2.2	Structure characterize of Cu-TiO <sub>2</sub> /ZnO .....	74
4.2.3	Crystal size, specific surface area and particle size of Cu- TiO <sub>2</sub> /ZnO .....	79
4.2.4	Morphology of Cu- doped TiO <sub>2</sub> /ZnO .....	82
4.2.5	Analysis of optical absorption of Cu-doped TiO <sub>2</sub> /ZnO .....	85
4.2.6	Band gap energy level of Cu-doped TiO <sub>2</sub> /ZnO .....	88
4.2.7	The photocatalytic mechanism of Cu-doped TiO <sub>2</sub> /ZnO under visible light irradiation .....	92
4.3	Photocatalytic activity of Cu-doped TiO <sub>2</sub> /ZnO .....	94
4.3.1	Effect of light irradiation intensity .....	98
4.3.2	Effect of solution acidity .....	98
4.3.3	Effect of dye and catalyst concentration .....	100
4.3.4	Effect of irradiation time on photocatalysis reaction .....	102
4.3.5	ANOVA analysis .....	104
4.4	Kinetic analysis of MO degradation .....	107

4.5	Sensitivity using (ANFIS) methodology .....	109
4.6	Removal process optimization .....	119
<b>5</b>	<b>CHAPTER 5: CONCLUSION AND RECOMMENDATION FOR FUTURE WORK.....</b>	<b>123</b>
5.1	Conclusion.....	123
5.2	Recommendation for future work .....	125
	REFERENCES.....	126
	LIST OF PUBLICATIONS .....	146

University of Malaya

## LIST OF FIGURES

Figure 2.1:	The diagram of topic presented in Chapter II.....	5
Figure 2.2:	Advanced oxidation technologies for hydroxyl radical Generations.....	8
Figure 2.3:	Energy band gap diagram of a TiO <sub>2</sub> spherical particle.....	27
Figure 2.4:	TiO <sub>2</sub> Crystal structure .....	28
Figure 2.5:	Process of Sol-gel method.....	47
Figure 3.1:	Diagram of catalyst synthesis process.....	54
Figure 3.2:	ANFIS structure.....	66
Figure 3.3:	The photoreactor Set-up	69
Figure 4.1:	TGA curves of the Cu- TiO <sub>2</sub> /ZnO composite powder. with Heating speed of 10°C/min.....	73
Figure 4.2:	XRD patterns of synthesized Cu- TiO <sub>2</sub> /ZnO calcined at a) 500°C b) 700°C.....	76
Figure 4.3:	SEM images of Cu-ZnO/TiO <sub>2</sub> Calcined at 500°C, a) Cu=1wt%, b) Cu=2wt%, b) Cu=5wt%.....	83
Figure 4.4:	SEM images of Cu-ZnO/TiO <sub>2</sub> , a) Cu=5wt%, Calcined at 500°C, b) Calcined at 700°C.....	84
Figure 4.5:	TEM images of Cu-TiO <sub>2</sub> /ZnO with Cu=3wt% calcined at 500 °C (a, b) and 700 °C (c,d).....	85
Figure 4.6:	The optical absorption curves of Cu- TiO <sub>2</sub> /ZnO, calcined at a) 500°C b) 700°C.....	86
Figure 4.7:	The rate of light absorption spectra of Cu (3wt%) doped TiO <sub>2</sub> /ZnO calcined at 500°C.....	87

Figure 4.8:	$(\alpha h\nu)^2$ versus energy curve (Kubelka–Munk plots) to estimate the band gap energies of Cu- TiO <sub>2</sub> /ZnO with different copper content .....	89
Figure 4.9:	Estimation of the band gap energy of Cu (3wt%) doped TiO <sub>2</sub> /ZnO calcined at 500°C by Perkin Elmer.....	90
Figure 4.10:	Schematic diagram illustrating the charge-transfer process in Cu-TiO <sub>2</sub> /ZnO under simulated solar light irradiation.....	92
Figure 4.11:	Photocatalytic degradation of methylene orange using different Cu- TiO <sub>2</sub> /ZnO with copper concentrations of □:Cu(1wt%) , ◇ Cu(2wt%), Δ:Cu(3wt%), *:Cu (4wt%) , ) :Cu (5wt%).....	95
Figure 4.12:	The response surface plot of Color, COD and TOC removal efficiency (%) as a function of BA, BC, BD and BE effects. ....	97
Figure 4.13:	The response surface plot of Color removal (%) as a function of visible light irradiation intensity.....	99
Figure 4.14:	The response surface plot of COD removal (%) as a function of visible light irradiation intensity and dye concentration, (a):MO and (b):MB.....	100
Figure 4.15:	The response surface plot of COD removal (%) as a function of visible light irradiation intensity and catalyst concentration, (a):MO and (b): MB.....	101
Figure 4.16:	The response surface plot of TOC removal (%) as a function of visible light irradiation intensity and	

	reaction time, (a):MO and (b):MB.....	103
Figure 4.17:	Effect of irradiation time on $\diamond$ :Colour, $\square$ : COD  $\Delta$ : TOC removals (%), Orange colour: MO, Blue Colour: MB.....	104
Figure 4.18:	Cycling photocatalytic degradation of MO (Orange Colour) and MB (Blue Colour) using Cu(3wt%) doped ZnO/TiO <sub>2</sub> calcined at 500°C.....	106
Figure 4.19	Pseudo-first-order kinetics for heterogeneous photocatalytic degradation of Methylene orange.....	109
Figure 4.20:	ANFIS predicted relationship for Color, COD and TOC removal efficiency (%) as a function of BA, BC, BD and BE effects .....	111
Figure 4.21:	The every input parameter's influence .....	117
Figure 4.22:	ANFIS predicted relationship between the most influential parameters .....	118



## LIST OF TABLES

Table 2.1:	Application of ZnO-TiO <sub>2</sub> hetro-junction in degradation of water pollutants.....	12
Table 2.2:	A review on doped ZnO-TiO <sub>2</sub> based photocatalys in degradation of water pollutants.....	19
Table 2.3:	Properties of various metal dopants of TiO <sub>2</sub> .....	34
Table 2.4:	Properties of various non-metal dopants of TiO <sub>2</sub> .....	37
Table 2.5:	Properties of various metalloid-and halogen dopants of TiO <sub>2</sub> .....	39
Table 2.6:	Effect of photocatalyst concentration and operational condition on degradation of industrial pollutant.....	44
Table 2.7:	Sol gel method for preparation doped catalyst.....	50
Table 3.1:	Amount of Titanium Oxide, Copper Nitrate and Zinc Sulphate in two groups of synthesised catalyst.....	56
Table 3.2:	Independent numerical variables and their levels (Input parameters for ANFIS).....	60
Table 3.3:	Experimental design matrix and the final results of Methyl Orange & Methylene Blue removals Using Response Surface Methodology (RSM) based on a 3 level and 5 factor.....	61
Table 3.4:	Output parameters (MO).....	64
Table 3.5:	Output parameters (MB).....	64
Table 3.6:	The main properties of the investigated dyes.....	69
Table 4.1:	Crystallite size and surface area of the Cu- TiO <sub>2</sub> /ZnO	

	photocatalyst prepared at various calcination temperatures and compound concentrations.....	80
Table 4.2:	Band gap energies of Cu- TiO <sub>2</sub> /ZnO with different copper content .....	89
Table 4.3:	Analysis of individual and interaction effects of operational parameters.....	105
Table 4.4:	Fitness versus coefficients of determination .....	105
Table 4.5	The calculated parameters of the zero- and pseudo-first- order kinetic models for photocatalytic degradation of Methylene orange.....	108
Table 4.6:	ANFIS regression errors for (a) COD (MO) and (b) COD (MB) prediction.....	114
Table 4.7:	ANFIS regression errors for (a) TOC (MO) and (b) TOC (MB) prediction.....	115
Table 4.8:	ANFIS regression errors for (a) UV (MO) and (b) UV (MB) prediction.....	116
Table 4.9:	Predicted and experimental values of the studied responses at optimum conditions.....	120
Table 4.10:	Available and similar literatures in terms of TiO <sub>2</sub> doped Photocatalysts.....	122

## LIST OF SYMBOLS AND ABBREVIATIONS

<b>Symbols</b>	<b>Description &amp; Unit</b>
$b_0$	Constant coefficient, [-]
$C$	Total concentration in the bulk phase, [mg L <sup>-1</sup> ]
$C_0$	Initial concentration, [mg L <sup>-1</sup> ]
$e^- - h^+$	Electron-hole pairs, [-]
$Err$	Normalized standard deviation, [%]
$k$	kinetic rate constant, [-]
$m$	Mass, [g]
$M$	Molecular weight, [-]
$R^2$	Regression coefficient, [-]
$t$	Time, [-]
$V$	Volume, [L]
$\lambda$	Wavelength, [-]
$\eta$	Effectiveness, [%]
$\sigma^2$	Residual mean square, [-]
$\mu_{AB}$	Membership Functions, [-]
$\mu_{CD}$	Membership Functions, [-]
$C_S$	Scherrer Constant, [-]
$\beta$	Full-Width of The Half Maximum, [-]
$\theta$	Contact Angle, [degree]

### Abbreviations

ANOVA	Analysis of variance
AOPs	Advanced Oxidation Processes
BET	Brunauer-Emmett-Teller
COD	Chemical oxygen demand
DO	Dissolved Oxygen
MB	Methylene blue
MO	Methyl orange
•OH	Hydroxyl radical

PZC	Point of zero charge
TOC	Total organic carbon
UV-Vis	Ultra violet-visible light
WWTP	Wastewater treatment plant
XRD	X-ray diffraction
MO	Methyl Orange
MB	Methylene Blue
COD	Chemical Oxygen Demand, mg L
ANOVA	Analysis Of Variance
BET	Brunauer, Emmette and Teller
TOC	Total Organic Carbon, mg L
AOPs	Advance Oxidation Processes
eV	Electron Volt, J
CCD	Central Composite Design
TGA	Thermo-Gravimetric Analysis
XRD	X-Ray Diffractometer
FESEM	Field Emission Scanning Electron Microscope
FWHM	Full Width Half Maximum
<i>t</i>	Time, min
<i>hν</i>	Photon Energy, eV
<i>vis</i>	Visible Light
TEM	Transmission Electron Microscope
<i>E<sub>g</sub></i>	Band gap Energy, eV
<i>A</i>	Anatase
<i>R</i>	Rutile
<i>B</i>	Brookite
<i>Y</i>	Predicted Response
<i>pH<sub>PZC</sub></i>	Zero Charge Point
<i>MF<sub>s</sub></i>	Variable Membership Functions
JCPDS	Standard Patterns
<i>R</i>	Reflectance
RSM	Response Surface Method

## CHAPTER 1: INTRODUCTION

### 1.1 Background

To date, more than 8000 different types of dyes and 6900 additives are known to be the cause of different organic and inorganic water pollution (Simphiwe & Buthelezi, 2012). These effluents enter waterways and adversely affect the quality of water, since they encompass a wide range of potential contaminants and concentrations. Most organic contaminants in water are not easily biodegradable and are often not fully removed in conventional biological plants. The reason is the presence of surfactants in the effluents that promote emulsion formation and impose additional load on wastewater biotreatment facilities. Most of the processes currently in use, such as adsorption, ozone or electrochemical oxidation, membrane separation, coagulation and filtration for water treatment suffer from different limitations. For instance, contaminants are only transferred from one medium to another in activated carbon adsorption, therefore another step is required to eliminate the organic compounds. Moreover, the process is slow and poses some difficulties with operation at high concentrations of organic contaminants. Chemical oxidation cannot completely mineralize organic compounds and it is only economically favourable for specific pollutant concentrations. In terms of biological treatment, drawbacks include low reaction rate, difficulty with activated sludge disposal and a very narrow pH range (Nadia et al., 2013).

Among various advanced chemical and physical treatment techniques, photocatalytic degradation is the only process that results in the complete mineralization of organic substances (Nadia et al., 2013). This process is also fast, economically feasible and chemically stable. Among different semiconductor photocatalysts, there is growing interest in Titanium Oxide ( $\text{TiO}_2$ ) due to its low price, environmentally friendly characteristic, chemical stability and absence of toxicity.

One of the most pivotal limitations of  $\text{TiO}_2$  or  $\text{ZnO}$  based lattices is their photocatalysis activity under visible light irradiation. In this study, a hybrid photocatalyst was generated by doping  $\text{TiO}_2/\text{ZnO}$  lattice with copper in order to improve their photo-activity. Cu-doped  $\text{TiO}_2/\text{ZnO}$  nanocrystals were fabricated by entrapping copper ions in crystalline matrix of  $\text{TiO}_2/\text{ZnO}$  through sol-gel synthesis method. Different copper concentrations were loaded into the photocatalyst matrix. The main aim was to analyse the sensitivity of photoactivity of  $\text{Cu-TiO}_2/\text{ZnO}$  toward operating conditions in advanced oxidation reaction for photodegradation of two different dyes.

## 1.2 Problem statement

A multitude of wastewater pollutants are found in effluents from dyestuff. Photocatalytic oxidation technology is commonly used for the treatment of these types of pollutants and environmental protection. However, there are some drawbacks related to this treatment:

1.  $\text{TiO}_2$  can be potentially used under visible light. However, the efficiency of photodegradation is trivial under visible-light irradiation. The reason is that this catalyst has a wide band gap of around 3.2eV at room temperature, therefore it should be mainly used under Ultraviolet (UV) irradiation.
2.  $\text{TiO}_2$  also suffers from low surface area, which reduces its efficiency.
3. The unsuitable band gap energy level of this photocatalyst is another limitation.
4. Moreover, the photocatalytic activity of  $\text{TiO}_2$  depends on the relative degree of branching of the reactive electron-hole pairs into interfacial charge-transfer reactions.

In order to overcome these limitations, the crystalline  $\text{TiO}_2$  catalyst matrix can be modified. To achieve this aim, the heterojunction of  $\text{TiO}_2/\text{ZnO}$  with Cu integrated into the structure is investigated, with the goal to narrow the band gap energy of  $\text{TiO}_2$  and

enhance the hybrid photocatalyst's photoactivity under visible light irradiation. In this study, Cu was selected for doping the TiO<sub>2</sub> photocatalyst, since its structure is similar to Fe. The low energy level of Cu enables it to improve the TiO<sub>2</sub> band gap. Besides, Cu has proven to enhance the photocatalytic band gap of Cu-TiO<sub>2</sub> and Cu-ZnO separately. This is attributed to the presence of two electrons in the valence layer of Cu, which enables electron transfer.

### **1.3 Research objectives**

The aim of this research is to study the performance of Cu-doped TiO<sub>2</sub>/ZnO photocatalyst for wastewater treatment and the degradation of two dyes, i.e. methyl blue (MB) and methylene orange (MO) dyes under visible light irradiation. Hence, the objectives of this study are to:

1. To synthesize and characterize a new nanocrystal photocatalyst by doping copper ions in the crystalline matrix of TiO<sub>2</sub>/ZnO.
2. To analyse the effects of the synthesis parameters on the physicochemical properties of the synthesized Cu-doped TiO<sub>2</sub>/ZnO.
3. To evaluate the physicochemical properties of the new synthesized Cu-doped TiO<sub>2</sub>/ZnO and the photoactivity of the new photocatalyst in the degradation of methyl orange as an anionic-dye and methylene blue as a cationic-dye under visible light irradiation.
4. To statistically analyse the sensitivity of Cu-doped TiO<sub>2</sub>/ZnO to operational parameters under visible light irradiation.

### **1.4 Thesis organization**

This thesis consists of five chapters dealing with different aspects related to the research topic.

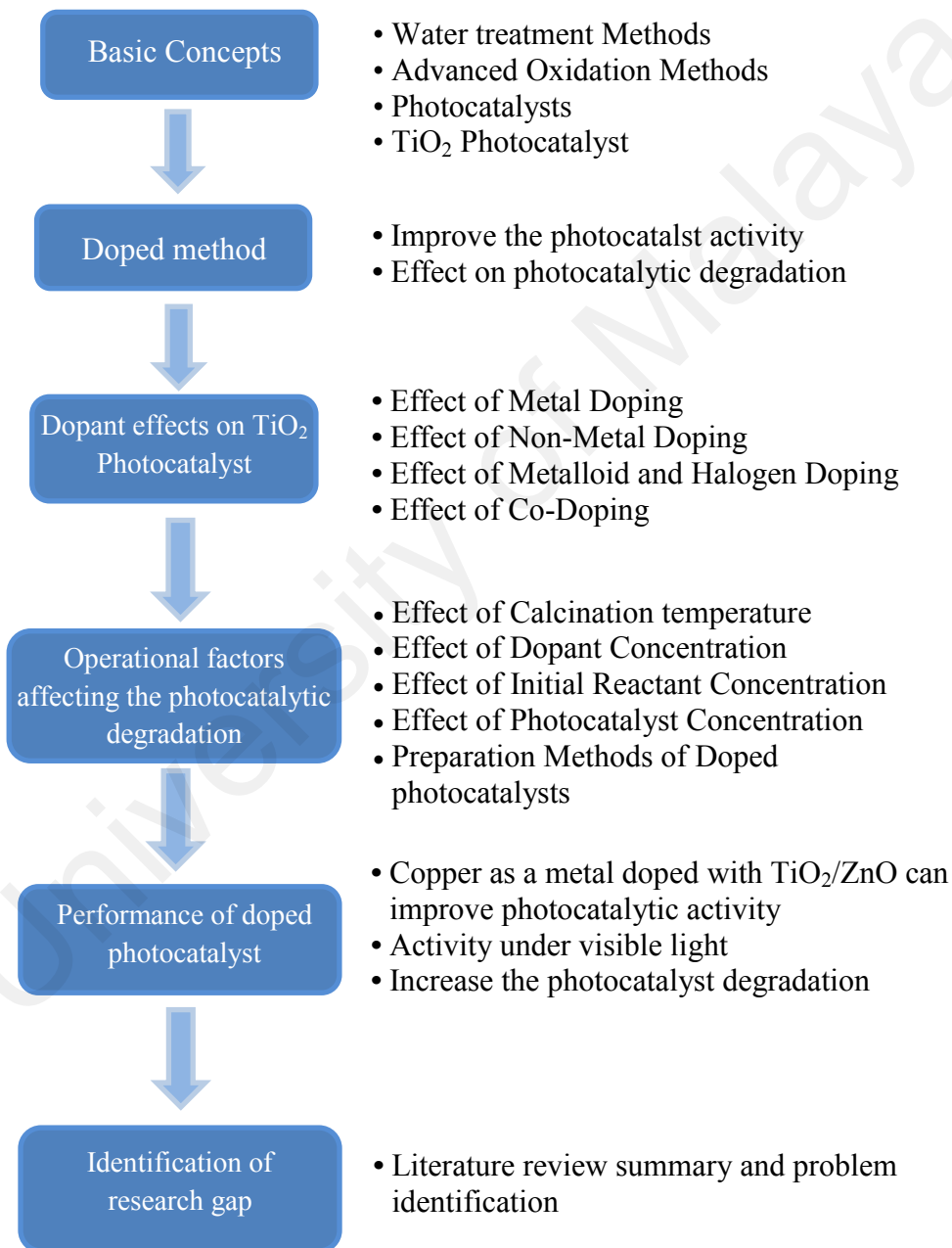
- CHAPTER 1 includes a brief introduction to the research project.

- CHAPTER 2 contains a comprehensive literature survey of Advanced Oxidation Processes (AOPs), followed by an overview of the  $\text{TiO}_2$  photocatalyst for photocatalytic degradation under UV light irradiation.
- CHAPTER 3 describes the materials and process setup for the synthesis and characterization of the new photocatalyst Cu doped  $\text{TiO}_2/\text{ZnO}$ . Furthermore, all experimental design techniques and analysis equipment and processes are explained in detail.
- CHAPTER 4 presents the results and data obtained from laboratory experiments. Efficiency evaluation of the new hybrid photocatalyst is carried out in terms of absorption, crystal size, morphology, and band gap energy level. The degradation of two types of dyes (MO and MB) under visible light irradiation is investigated and ANFIS analysis is done to examine how the mentioned operating parameters influence the photoactivity of Cu-doped  $\text{TiO}_2/\text{ZnO}$ . In addition, a comprehensive discussion and explanation of the experimental results are presented.
- CHAPTER 5 summarizes the conclusions according to the study results and findings, followed by a list of recommendations for further studies.



## CHAPTER 2: LITERATURE REVIEW

Figure 2.1 illustrates a simplified flow diagram of the main review topics presented in this chapter. The advanced oxidation process with a base for the generation of hydroxyl radicals has high potential to completely destroy hazardous organic components in wastewater processing without generating secondary pollutants.



**Figure 2.1:** Overview of the literature review.

## 2.1 Introduction

Various dyes and organic compounds that are commonly used in industry cause environmental contamination and must be removed from wastewater (Alem & Sarpoolaky, 2010). Dye colours are a copious source of coloured organics emanating as waste from textile dyeing processes. Due to the high concentrations of organic compounds in wastewater and the higher stability of modern synthetic dyes, conventional treatment methods are ineffective in the degradation of dyes and organic compounds or complete colour removal (Zhang, 2011). According to the last report of the United Nations World Water Development, untreated industrial wastewater, which contains several kinds of organic pollutants, flows into productive land, and surface and underground water sources (Gleick, 2004). Therefore, there is growing concern regarding the effectiveness and environmental compatibility of pollutant removal methods to prevent hazardous pollutants from entering the environment. A wide range of chemical, physical and biological processes have been applied to remove pollutants through chemical coagulation, oxidation, flocculation, precipitation, froth floatation, reverse osmosis and biological techniques (Akpan & Hameed, 2011). However, chemical methods are unable to mineralize all organic pollutants and they generate new environmental pollutants (Takeda, 1988). Physical methods like adsorption are not able to remove all hazardous waste from effluents. Biological methods are also slow, selective and sensitive to ambient conditions such as pH and temperature (Krumme, 1988 ; Aviam, 2004). Advanced Oxidation Processes (AOPs), such as photocatalytic processes including Fenton, photo-Fenton and electro-oxidation are powerful and non-selective (Fujishima, 2000 ; Carp, 2004). These methods have been used to mineralize persistent organic pollutants in the environment.

## 2.2 Water treatment methods

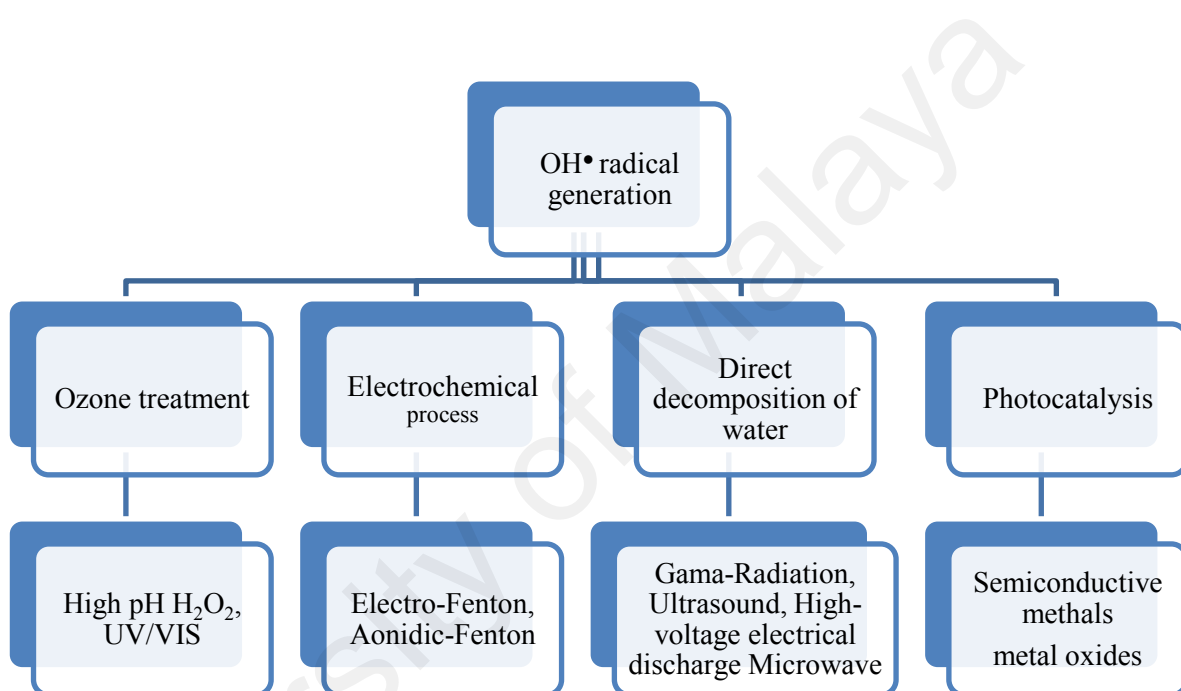
Non-biodegradable organic waste materials are compounds that cannot be recycled into the life cycle naturally since they cannot break down into natural components. Therefore, such pollutants should be removed from wastewater using different technologies, including biological treatment, coagulation/precipitation techniques, Fenton oxidation treatment and photocatalytic advanced oxidation technology. Biological treatment processes that employ microbial metabolism are safe, economical and reliable; however, these technologies require high levels of sludge and their efficacy is not stable.

Fenton oxidation is a treatment method of breaking down organic matter by exploiting the oxidation power of iron salts (Fenton's reagent) and the generation of OH radicals. This treatment method includes an oxidative reaction caused by the Fenton's reagent, neutralization and a coagulation process to remove the iron salts. Therefore, this process is simpler, easier to manage and does not require added devices like other photo-oxidation or oxidation methods. However, this method produces excessive amounts of sludge and operation is costly due to secondary processing.

Coagulation/precipitation treatment methods precipitate suspended solids by adding inorganic coagulants or polymer coagulators and forming flocs. In fact, polymer coagulants create sludge flocs to separate or precipitate dissolved or suspended solids from wastewater. Meanwhile, inorganic coagulants coagulate with pollutants and are moved by using a water-soluble metal salt. Advanced Oxidation Technology (AOT) is a strong wastewater treatment process for non-biodegradable compounds. This process can treat large water quantities with low operational and installation costs. AOT generates  $\cdot OH$ , which has stronger oxidation power (oxidation potential: 2.80 eV), and the organic compounds are decomposed into HCl, H<sub>2</sub>O or CO<sub>2</sub>, which are relatively harmless compounds.

### 2.3 Advance oxidation process

Four different methods are employed in AOP to generate hydroxyl radicals and treat wastewater, namely (i) ozone treatment, (ii) electrochemical processes, (iii) direct decomposition of water, and (iv) photocatalysis. Figure 2.2 displays the advanced oxidation technologies for hydroxyl radical generation.



**Figure 2.2:** Advanced oxidation technologies for hydroxyl radical generations

Ozone treatment is commonly used for water treatment by directly inserting ozone gas into wastewater. The ozone directly reacts with organic compounds or indirectly reacts with  $\text{OH}^\bullet$ , resulting in indirect oxidative decomposition. The organic pollutants' properties are a determinant factor of the ozone decomposition mechanism by either promoting or inhibiting ozone decomposition. Therefore, the un-decomposable organic compounds or those that cannot be easily decomposed undergo ozone treatment.

Fenton oxidation technology also generates OH<sup>•</sup> through decomposing H<sub>2</sub>O<sub>2</sub> by Fe<sup>2+</sup> in liquid medium with or without light irradiation, or with UV radiation.



However, the Fenton oxidation reaction is not applicable for conditions with pH > 4. Therefore, the pH should be controlled and adjusted for this method, which may increase operational costs (barbuslinski, 2009).

Direct decomposition of water molecules through external energy sources like microwaves, ultrasound, and electromagnetic beams, is also a method of OH<sup>•</sup> generation. Water molecules are decomposed into H<sup>+</sup>, OH<sup>•</sup> and aqueous electrons by irradiation. As high voltage pulses of about 10 kV are discharged in water through two electrodes installed within a short distance, localized heat is generated, decomposing the water molecules. The same conditions occur under ultrasound or microwave irradiation, where over-heated regions named hot spots are generated.

Photocatalysis is another OH<sup>•</sup> generation technology that entails the activity of semiconducting metal oxides, e.g. SrTiO<sub>3</sub>, BiTiO<sub>3</sub>, WO<sub>3</sub>, ZnWO<sub>4</sub>, ZnO, CuS/ZnS, Bi<sub>20</sub>Ti<sub>20</sub>, ZnS, Ag<sub>2</sub>CO<sub>3</sub>, Bi<sub>2</sub>WO<sub>6</sub>, Nb<sub>2</sub>O<sub>5</sub>, Fe<sub>2</sub>O<sub>3</sub>, TiO<sub>2</sub>, etc. The process involves a semiconductor as a photocatalyst, which is activated under light irradiation (Gaya, 2008). The Semiconductor Photocatalyst (SP) structure contains Valence bands (VB) and Conduction bands (CB) that are separated by Band gap (E<sub>g</sub>).

## 2.4 Photocatalyst

Among various AOPs, the heterogeneous photocatalytic processes can successfully reduce a broad range of pollutants at ambient temperature and pressure without generating harmful intermediates (Daneshvar, 2007 ; Abdollahi, 2011). The processes

are initiated with the excitation and transfer of an electron from the VB, which is full of electrons to the empty CB. In photocatalysis, the photocatalyst absorbs enough energy, which is nearly equal to its band gap energy level, to become excited. This process generates an electron-hole pair that reacts with water and oxygen molecules or hydroxyl groups to generate highly reactive oxygen species, i.e. superoxide anions ( $O_2^{\bullet-}$ ) and hydroxyl radicals ( $\bullet OH$ ). Then the oxy-radical species attack vital organic components and decompose them through oxidation reactions. Photo-excitation occurs through the absorption of photon energy ( $h\nu$ ), which is equal to or higher than the photocatalyst's band gap energy ( $E_g$ ). Therefore, an electron-hole pair ( $e^-h^+$ ) is generated at the surface of the photo-excited catalyst. Among different semiconductors, titanium dioxide ( $TiO_2$ ) and zinc oxide ( $ZnO$ ) are the most successful and popular photocatalysts with good photosensitivity and chemical stability. They are non-toxic and low-cost. However, they suffer from some limitations pertaining to optical and electronic properties (Li & Li, 2002).  $TiO_2$  and  $ZnO$  are highly active photocatalysts under UV light irradiation since their photogenerated electrons and holes are efficient oxidizing and reducing agents. However, the large band gaps of  $TiO_2$  and  $ZnO$ , which are roughly 3.2eV (Khan et al., 2014) and 3.37eV (Ahmad et al., 2013)) respectively, restrict their photoelectrochemical application under visible light irradiation. The easy recombination of photo-induced holes and electrons also reduces their efficiency. Adding an oxide to these photocatalysts and supporting them on an oxide are ways to improve their photoactivity and thermal stability during catalyst preparation.

Among various oxides like  $TiO_2$ ,  $SnO_2$ ,  $SiO_2$ ,  $CeO_2$ ,  $ZnO$ ,  $WO_3$  and  $ZrO_2$ , previous works have demonstrated that the heterojunction of  $TiO_2$  and  $ZnO$  can have synergic effects due to the injection of conduction band electrons from  $ZnO$  to  $TiO_2$ , which

decreases the recombination rate and increases the electron-hole pair lifetime (Zheng et al. 2015) .

TiO<sub>2</sub> and ZnO, with wide band gaps of 3.2 eV and 3.3 eV, and two photocatalysts, require excitation light with wavelengths below 400 nm to begin photoreaction. The doping method has been considered for improving the photoactivity of TiO<sub>2</sub> and ZnO. Doping of two photocatalysts is a method employed for retarding the rapid charge recombination and enabling visible light absorption by creating defect states in the band gap. In the former case, the valance band holes or conduction band electrons are trapped in the defect sites, inhibiting the recombination of photo-induced holes and electrons and improving the interfacial charge transfer. In the latter case, electronic transitions from the defect states to the conduction band or from the valance band to the defect states can occur under sub-band gap irradiation. Table 2.1 presents the application of ZnO-TiO<sub>2</sub> heterojunction in water pollutant degradation.

**Table 2.1:** Application of ZnO-TiO<sub>2</sub> hetero-junction in degradation of water pollutants

Catalyst	ZnO:TiO <sub>2</sub> Ratio	Morphology	Synthesis Method	Synthesis Conditions	Pollutant	Light, λ(nm)	Time min	Dye ppm	Cat g/L	Efficiency (Y) ZnO/TiO <sub>2</sub>	Y ZnO	Y TiO <sub>2</sub>	Ref.
ZnO/TiO <sub>2</sub>	1.23:1 (w/w)	NP, Ring SH	Pyrolysis	400°C	MO	SL, 320-800	120	5	-	94.8	28.9	19.1	(Zheng, Li et al. 2015)
ZnO/TiO <sub>2</sub>	50:50%	NP, non-uniform	Sol-Gel	380°C 500°C	B, T, X	VIS	120	100	1	44.8, 45.7, 49.1 36.9, 39.5, 45.1	-	-	(Ferrari-Lima, de Souza et al. 2015)
ZnO/TiO <sub>2</sub> Thin film	3:1 (w/w)	Z:nanowires T:nanoparticle	Spin Coating	320°C, 3h	Orange II	UV, 315-400 VIS,	210 210	20	0.5	27.5 36.9	52.9 74.1	-	(Siuleiman, Kaneva et al. 2014)
ZnO/TiO <sub>2</sub>	20,50,80wt%	NP, non-uniform	SS	450°C, 6h	4CHI	UV, 303-578	75	25	2	100, 87, 78	75	84	(Pozan and Kambur 2014)
ZnO/TiO <sub>2</sub>	1:1 MR	NP, hollow spheres	Hydrothermal	180°C, 2,6,12,24h	MO	UV, >400 VIS,	25 25	20	1	80.5, 88.4, 91.92 57.4, 66.6, 69, 74.4	92.4 -	29.3 -	(Wang, Zhu et al. 2014)
ZnO/TiO <sub>2</sub>	1:0.2 MR	NP	MW Sol-Gel	500°C, 7 h	RhB	SS, VIS, MV	30	50	1.7	82.4, 68.8, 25.7	89.7, 78.8, 36.7	-	(Li, Zhang et al. 2014)
ZnO/TiO <sub>2</sub>	10,20,30,40%M	Porous Thin film	Sol-Gel	500°C, 0.5h	MO	SS	280	10	4	79.6, 60.3, 7.3, 9.3	-	48.1	(Chen, Zhang et al. 2014)
ZnO/TiO <sub>2</sub>	1:1 (w/w)	NF, Flower SH	Electrospinning	500°C, 4 h	ARS	UV	70	100	2.5	99.4	51.3, 67.9	-	(Murugan, Babu et al. 2013)
TiO <sub>2</sub> /ZnO	1:10,2:10,3:10MR	NP, Irregular	Sol-Gel	500°C, 5 h	MB	UV	90	5	1	91.3, 94.9, 73.6	-	87.5	(Moradi, Aberoomand-Azar et al.)
TiO <sub>2</sub> /ZnO	1:1 MR	NF, Non-woven	Electrospinning	500°C, 2 h	MO 4NPh	UV	40	10	0.01	84.99 70.6	49.9, 52.9 30.3, 29.5	-	(Zhang, Shao et al. 2012)
TiO <sub>2</sub> /ZnO	1:7,1:5,1:3.5wt%	NF	Electrospinning	500°C, 5h	RhB	UV, 365nm	24h	8	0.5	84, 98.1, 90.1	-	NF:80 NP:65	(Liu, Ye et al. 2010)
ZnO/TiO <sub>2</sub>	-	NP<10-20nm	Hydrolysis	180-200°C,-	MO	UV, 365nm	20	20	2.5	81.7	76.3	51.8	(Zhang, An et al. 2010)
ZnO coated- TiO <sub>2</sub>	-	NP-amorphous	MW Sol-Gel	120°C, 3h	OG	UV, 340nm	90	-	-	98.9	58.2	-	(Bahadur, Furusawa et al. 2010)

(continued on next page)



Table 2.1, continued<sup>a</sup>

Catalyst	ZnO:TiO <sub>2</sub> Ratio	Morphology	Synthesis Method	Synthesis Conditions	Pollutant	Light, λ(nm)	Time min	Dye ppm	Cat g/L	Efficiency (Y) ZnO/TiO <sub>2</sub>	Y ZnO	Y TiO <sub>2</sub>	Ref.
TiO <sub>2</sub> /ZnO nanofiber	-	poly-nanocrystal	Electrospinning	550,650,750, 850°C, 2 h	RhB	UV-vis,420	60	1e <sup>-6</sup> M	1	53.9, 86.8, 55.4, 36.2, 33.7	-	35.2	(Pei and Leung 2013)
ZnO/TiO <sub>2</sub>	Z:0.5,2,4,10%M	NP	Wetness impregnation	400°C, 2 h	Cr(VI)	UV-vis,365	-	20	1	Max forZnO:2%	-	-	(Ku, Huang et al. 2011)
ZnO/TiO <sub>2</sub>	1:1 MR	Mesoporous Plate	Tape Casting & lamination	600,650,700/2h	RBR	UV	90	50	1	76.9, 68.5, 31.5	C700= 55	-	(Konyar, Yatmaz et al. 2012)
ZnO/TiO <sub>2</sub>	ZnO=6wt%	composite	Sol-Gel & SS	500, 3h	MO	VIS, >400 UV	300 40	50	1	11.7 45.38	- -	- 76.4	(Yang, Yan et al. 2012)
ZnO/TiO <sub>2</sub>	2:0.1 M	NP	MW-Assisted	500, 0.5h	Cr(VI)	UV	240	10	1	29.5	42	-	(Liu, Pan et al. 2012)
ZnO/TiO <sub>2</sub>	1:1 (w/w)	NP	Chemical	100°C, 3 h	Diazinon	UV<390	120	20	0.5	12.7	-	-	(Jonidi-Jafari, Shirzad-Siboni et al.)
ZnO/TiO <sub>2</sub>	1.97:1.11 (w/w)	NP Round-SH	Hydrothermal	180°C, 20 h	Cr(VI)	UV,365	120	10	0.5	16.3	10.9	-	(Johra and Jung 2015)
TiO <sub>2</sub> coated ZnO	-	NP, nanorod	Sol-Gel	T: 70°C, 2-3h Z: 150°C	MB	UV, 365	20	5	0.5	98.9	Z: 67.3	-	(He, Li et al. 2010)
ZnO/TiO <sub>2</sub>	0.36:0.66 (w/w)	NP/NF	Electrospinning	500°C, 4h	MB	UV,365	60	12.8	2.5	NP:25,NF: 31.6	NF:10	NF:7	(Wang, Yang et al. 2010)
ZnO/TiO <sub>2</sub>	Z:15,30,45,60wt%	NF	Electrospinning	500°C, 4h	RhB	Visible,420 UV,365	40 40	1e <sup>-6</sup> M	0.5 1	78, 93, 83.2, 81 79	-	94.2	(Pei and Leung 2013)
TiO <sub>2</sub> /ZnO	Zn:Ti=1:3	NP Irregular	Sol-gel	350°C, 1h 150°C, 24h	MO	UV,254nm	3h	25e <sup>-6</sup> M	0.5	27.9 47.5	- -	-	(Xu, Wang et al. 2011)

(continued on next page)

Table 2.1, continued

Catalyst	ZnO:TiO <sub>2</sub> Ratio	Morphology	Synthesis Method	Synthesis Conditions	Pollutant	Light, λ(nm)	Time min	Dye ppm	Cat g/L	Efficiency (Y) ZnO/TiO <sub>2</sub>	Y ZnO	Y TiO <sub>2</sub>	Ref.
ZnO/TiO <sub>2</sub>	Z:T=-	NP:Nano flower	Electrospinning	250°C, 3h	MB	UV,365nm	120	25	0.8	68	46.1	58	(Pant, Pant et al. 2013)
ZnO/TiO <sub>2</sub>	1:1	NP	Sol-Gel	100°C, 3h	Cr(VI)	UV, 247.3nm	120	20	1	99.9	82.3	86.1	(Naimi-Joubani, Shirzad-Siboni et al.)
ZnO/TiO <sub>2</sub>	11.7:1 (Atomic R)	NP Nano flower	hydrothermal	140°C, 2h	RB5	UV,-	120	10	0.3	47.2	52.6	-	(Pant, Pant et al. 2013)
core-shell TiO <sub>2</sub> /ZnO	-	Nano wires	pulsed laser deposition	450°C, 1h	RhB	UV, 320-400	15,30 45,60	5e <sup>-6</sup> M		59.7,76.5 54.8,59	60 min, 32.2	31.9	(Tao, Wu et al. 2013)
TiO <sub>2</sub> -ZnO	1:1,1:2,1:3,1:4	NP on Glass film	roll-coating	120°C, 12h	MO	UV,300-600	120	10	0.01	57.6,65,73.5,80	46.5	87.8	(Jlassi, Chorfi et al. 2013)
ZnO/TiO <sub>2</sub>	96:4 atomic R	NP, Nano flower	Hydrothermal	140°C, 2h	MB	UV,365nm	180	10	0.8	69.7	47.7	66.6	(Pant, Park et al. 2012)
ZnO/TiO <sub>2</sub>	1:1,2:1	Tiny Particle	Microwave		MB	671nm	150	5e <sup>-6</sup> M	14	96.7, 94.3	Zn <sub>2</sub> TiO <sub>4</sub> :91.6	-	(Arin, Thongtem et al. 2013)
NP		<10nm			Cr <sub>2</sub> O <sub>7</sub> <sup>2-</sup>	UV				33.8, 31	Zn <sub>2</sub> TiO <sub>4</sub> :4.7		
TiO <sub>2</sub> /ZnO thin film	-	TiO <sub>2</sub> :Nanorod on ZnO buffer layer	laser deposition	Z: 200°C, 0.5h T: 600°C, 1h	MO	VIS	10h	20	-	32.9	25.5	19	(Zhao, Xia et al. 2012)
TiO <sub>2</sub> /ZnO	Zn:Ti=1:1	NP Irregular	Sol-Gel	500,600,700°C,2h	MO	UV,254nm	3h	25e <sup>-6</sup> M	0.5	30.8, 34.2, 54.8	-	-	(Wang, Mi et al. 2013)
ZnO-TiO <sub>2</sub>	7.5%:92.5%	NP	ammonia-induced synthesis	450°C, 4h	MO	UV-A,365nm	30	50	0.8	41.2	-	81.8	(Karunakaran,
					SSY					68.9		93.0	Abiramasundari et al. 2011)
					RHB					44		99.4	

Note: MO: Methylene Orange, MB: Methyl Blue, 4CH: 4chloropheno, RhB: Rhodamine B. RBD: Remazol Brilliant Red, RB5: reactive black 5, OG: Orange G, 4NPh:4-nitrophenol, SSY: SunSet Yellow, T:TiO<sub>2</sub>, Z:ZnO. SS: Solid-State, MW:MicroWave, SH: Shaped, R:Raio. NF: Nano Fiber, NW: Nano Wire, NP: Nano Particle.

The most important works on TiO<sub>2</sub>/ZnO photocatalyst from the past five years are listed in Table 2.1. This table summarises the most important results obtained from various research works aimed at investigating the effects of a number of variables on the TiO<sub>2</sub>/ZnO lattice, e.g. the synthesis method, calcination temperature, TiO<sub>2</sub>:ZnO ratios, photocatalysis reaction time, light irradiation, etc. As per Table 2.1, TiO<sub>2</sub>/ZnO has mostly been synthesized at temperatures ranging from 100 to 500°C. Depending on the ratio of TiO<sub>2</sub> to ZnO, incrementing the temperature beyond 500°C reduces the photoactivity of the TiO<sub>2</sub>/ZnO lattice in most cases. In terms of calcination time, it is suggested that calcination at lower temperatures but for longer durations yields more favourable results. The TiO<sub>2</sub>-to-ZnO ratio is another effective factor. According to Table 2.1, the optimum TiO<sub>2</sub>:ZnO ratio yields the highest TiO<sub>2</sub>/ZnO photoactivity depending on the synthesis method and conditions employed. In short, TiO<sub>2</sub>/ZnO has demonstrated superior photocatalytic degradation of most organic contaminants compared to pure TiO<sub>2</sub> or ZnO. However, it should be noted that the majority of works have been conducted using UV irradiation, indicating there remains room for improvement so the TiO<sub>2</sub>/ZnO lattice can be efficiently used for visible light photocatalysis. Additional details are given in Table 2.1.

## **2.5 TiO<sub>2</sub> and ZnO photocatalyst**

TiO<sub>2</sub> and ZnO are two of the most promising photocatalysts. However, their wide band gap limits their photocatalytic activity in the UV wavelength region that contributes to 3-5% of the total solar spectrum (Zheng et al. 2015). The fast recombination of photogenerated electron-hole pairs is another limitation of these two semiconductors. This is significant in the absence of electron donors or acceptors, as it results in major energy loss and very low photocatalytic reaction yield. Accordingly, enhancing the photocatalytic activity of TiO<sub>2</sub> and ZnO has been studied by many researchers (Wang et

al. 2013a).

Results have indicated that coupling two semiconductors produces a composite with higher photocatalytic efficiency in most cases. The synergistic effect between the two semiconductors modifies the electronic states of the composite, allowing the transfer of photogenerated charge carriers between the two semiconductors, thus promoting electron-hole pair separation and modifying the carrier's lifetime. Compared to  $\text{TiO}_2$ , ZnO has higher electron mobility that causes a negative shift in its valence and conduction band potentials. Accordingly, ZnO is considered suitable for coupling with  $\text{TiO}_2$  (Shaheen et al. 2013). Besides, since ZnO and  $\text{TiO}_2$  have similar band gap energy, they can effectively improve each other's photocatalytic performance. In the  $\text{TiO}_2$ -ZnO heterojunction, the conduction band (CB) of ZnO is positioned above the CB of  $\text{TiO}_2$  and the valence band (VB) of ZnO is positioned between the VB and CB of  $\text{TiO}_2$ , which suppresses the electron-hole pair recombination and promotes its separation, consequently improving the photocatalytic activity. As an example, ZnO- $\text{TiO}_2$  binary oxide catalysts were successfully prepared by solid-state dispersion in a study by Pozan et al. (Pozan & Kambur, 2014). It was then used in the degradation of 4-chlorophenol and the authors indicated that 20wt% ZnO- $\text{TiO}_2$  photocatalyst exhibited much higher photocatalytic activity than pure  $\text{TiO}_2$ , ZnO and P-25. In another work, Zheng et al (Zheng-Li et al., 2015) prepared a ZnO/ $\text{TiO}_2$  photonic crystal (ZnO/ $\text{TiO}_2$ -PC) heterostructure by pyrolysis. The authors evaluated the performance of ZnO/ $\text{TiO}_2$ -PC on the degradation of methyl orange. They found that the synthesised heterostructure had superior photocatalytic activity compared to ZnO,  $\text{TiO}_2$ -PC and P25. Amorphous  $\text{TiO}_2$ -modified ZnO nanorod film was also synthesized to enhance the photocatalytic activity of ZnO film by Xiao et al. (Xiao- Zhao et al., 2014). The photocatalytic analysis revealed that the  $\text{TiO}_2$ -modified film exhibited superior photocatalytic efficiency in the decomposition of methyl orange under ultraviolet-visible excitation compared to ZnO

nanorod arrays. Wang et al. (Wang et al., 2014) prepared mesoporous ZnO/TiO<sub>2</sub> hollow microspheres by a facile one-step hydrothermal route without a template. The authors concluded that the ZnO/TiO<sub>2</sub> hollow microspheres had a significant positive effect on photocatalytic degradation performance compared to the pristine TiO<sub>2</sub> hollow microspheres or ZnO nanosheets.

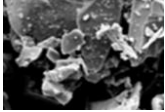
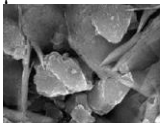

Other strategies have also been developed for utilizing a wide spectrum of incident photon energies by tailoring the band gap absorption of different photocatalysts like TiO<sub>2</sub> and ZnO through metal/non-metal ion doping, co-doping with foreign ions, noble metal deposition, self-doping, sensitization by inorganic complexes or organic dyes, and surface complexation. Among the aforementioned methods, incorporating main group elements (especially metal and non-metal ions) into TiO<sub>2</sub> or ZnO lattices has gained much attention due to these elements' ability to modify the surface electronic properties. The redox energy states of transition metal ions (e.g. Cu, Co, Ni, Cr, Mn, Mo, Nb, V, Fe, Ru, Au, Ag, Pt) mostly lie within the band gap states of TiO<sub>2</sub> or ZnO. This introduces an intra-band state close to the CB or VB edge, which induces visible light absorption at sub-band gap energies. Moreover, metal ions affect the charge carrier equilibrium concentration by serving as electron-hole traps and increasing the degradation rate. As reported by Yi et al (Cui et al., 2014), metal species increase the electron capturing capacity of semiconductors. In Yi et al.'s work (Cui et al., 2014), iron-doped zinc oxide nanoflowers were synthesized via a simple hydrothermal process. These showed enhanced photocatalytic activity under visible light irradiation.

The photocatalytic visible light activity of titanium dioxide can be improved by nonmetal- doping. In terms of non-metal doping (e.g. N, S, C, B, P, I, F) (Szkoda et al. 2016), three methods have been suggested for TiO<sub>2</sub> modification: band gap narrowing, (Sun et al. 2012), impurity energy levels (Di Valentin and Pacchioni 2013) and oxygen vacancies (Bharti et al. 2016). Yalçın et al. (2010) prepared a series of N, C and Sdoped

photocatalysts with different dopant contents using a simple wet impregnation method. They explained that band-gap energy level reduction arises from the contribution of N 2p, C 2p and S 3p orbitals to the O 2p and Ti 3d states in the valence band of titanium dioxide. Di Valentin and Pacchioni (2013) doped TiO<sub>2</sub> with non-metal boron, carbon, nitrogen, and fluorine. Results showed that localized states are formed in the band gap of the material which allow for electronic transitions in the visible range. Among all, non-metal nitrogen is the most beneficial due to the low ionization energy, metastable centre formation, stability and atomic size comparable to oxygen. Oxygen vacancies existence in TiO<sub>2</sub> doped N can improve the photocatalysis in visible light (Wu et al. 2013). Substituting nitrogen affects both the surface structure and electronic properties of TiO<sub>2</sub>, with the former controlling the surface transfer of charge carriers and the latter determining the light response range and redox power of carriers (Asahi et al. 2001).

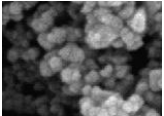
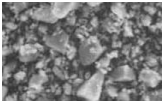
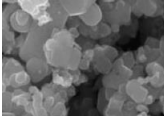
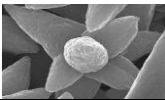
Recently, two methods have been considered in parallel to further improve the photoactivity of TiO<sub>2</sub> and ZnO. Amongst the aforementioned methods, the heterojunction of two photocatalysts along with metal or non-metal doping has gained considerable interest for increasing the photoactivity of different photocatalysts. The related work is summarised in Table 2.2. The tabulated information only highlights the photocatalytic activity of TiO<sub>2</sub>/ZnO-based photocatalysts on dye degradation (Ahmed et al., 2006). For more details, refer to the most recent reviews on ZnO- and TiO<sub>2</sub>-based photocatalysts (Zhang-Tang et al., 2010 ; Chen-Zhang et al., 2013; Han, Yang et al., 2014 ; Yang, Zhang et al., 2014).

**Table 2.2:** A review on doped ZnO-TiO<sub>2</sub> based photocatalys in degradation of water pollutants

Photocatalyst Synthesis method Compounds/Ratio	Drying & Calcination Temp& Time	Morphology	Activity analysed by decomposition	Compound	Photocatalytic Efficiency	Objective/Result	Ref
N-TiO <sub>2</sub> /ZnO Sol-Gel Method C <sub>12</sub> H <sub>28</sub> O <sub>4</sub> Ti (TTIP) Zn(O <sub>2</sub> CCH <sub>3</sub> ) <sub>2</sub> NH <sub>4</sub> OH TiO <sub>2</sub> : ZnO =50:50wt%	D: 80 °C/- C: 380°C/ 5 h C: 500°C/ 5 h C: 380°C/ 5 h C: 500°C/ 5h	non-uniform nano crystals 	Benzene (B), Toluene (T), Xylenes(X) D: 100 mg/L C: 1.0 g/L Visible light Time: 2h	TiO <sub>2</sub> /ZnO TiO <sub>2</sub> /ZnO N-TiO <sub>2</sub> /ZnO N-TiO <sub>2</sub> /ZnO	B T X 55.2 54.3 50.9 63.1 60.5 54.9 73.9 71.4 69.0 85.9 87.1 86.3	<ul style="list-style-type: none"> <li>The nitrogen doping caused a red shift in the absorption band affecting the photocatalysis directly</li> <li>Annealing at 500°C was necessary to induce formation of crystallinity</li> <li>Degradation and reaction rate was enhanced by nitrogen incorporation into the TiO<sub>2</sub> matrix.</li> <li>Degradation was enhanced by calcination temperature.</li> </ul>	(Ferrari-Lima, de Souza et al. 2015)
Er <sup>3+</sup> :YAlO <sub>3</sub> /Fe-TiO <sub>2</sub> /ZnO Sol-Gel Method under ultrasound (C4H9O)4Ti Zn(O <sub>2</sub> CCH <sub>3</sub> ) <sub>2</sub> Fe(NO <sub>3</sub> ) <sub>3</sub> ·9H <sub>2</sub> O, Al(NO <sub>3</sub> ) <sub>3</sub> ·9H <sub>2</sub> O TiO <sub>2</sub> :ZnO=10:3 Fe:Ti molar ratio=1.00%	D: 130 °C / 24 h C: 550 °C/50min	Nubby particles Size: 0.5–1.0 µm 	Acid Red B D: 100 mg/L C: 1.0 g/L Solar Light Time: 30 min	Er <sup>3+</sup> :YAlO <sub>3</sub> 0% 1% 2% 3% 4% 5%	74% 78% 80% 82% 84% 79.5%	<ul style="list-style-type: none"> <li>Degradation on the basis of calcination temperature: 400&gt;550&gt;700.</li> <li>Degradation on the basis of calcination time: 50&gt;30&gt;70min.</li> <li>Degradation on the basis of dye concentration: 15 &gt;10 &gt;20&gt;5&gt;25mg/L</li> <li>Degradation on the basis of catalyst amount: 1&gt;1.25&gt;0.75&gt;0.5&gt;0.25&gt;0g/L.</li> <li>Degradation for different dyes: CG-R&gt;AF&gt;MV&gt;MO&gt;RM-B</li> </ul>	(Gao, Luan et al. 2011)
Mn-TiO <sub>2</sub> /ZnO Mn-TiO <sub>2</sub> (Core), ZnO (Shell) Sol-Gel Method using polyethylene glycol (PEG) 4,000 or 20,000 Zn(O <sub>2</sub> CCH <sub>3</sub> ) <sub>2</sub> MnTiO <sub>3</sub> nano-powder MnTiO <sub>3</sub> :ZnO=1:22	D: 80 °C f: 6 h C: 500 °C: 2 h	Nano-spherical core-shell Particles Size: 20-40 nm 	Methylene Blue D: 0.025 g C: 9.3 mg/L O <sub>2</sub> (airflow):7.8 mL/S UV A light Time: 60 min	Mn-TiO <sub>2</sub> Mn-TiO <sub>2</sub> /ZnO (PEG 4k) Mn-TiO <sub>2</sub> /ZnO (PEG 20k)	6% 46% 80%	<ul style="list-style-type: none"> <li>The charge-transfer resistance of the core-shell nanoparticles is less than that of pristine ZnO nanoparticles.</li> <li>The direct band gap was in order of Mn-TiO<sub>2</sub> &gt;Mn-TiO<sub>2</sub>/ZnO.</li> <li>The indirect band gap was in order of Mn-TiO<sub>2</sub> ~Mn-TiO<sub>2</sub>/ZnO.</li> <li>The specific conductance was in order of Mn-TiO<sub>2</sub>&gt; Mn-TiO<sub>2</sub>/ZnO&gt;ZnO.</li> </ul>	(Karunakaran, Vinayagam oorthy et al. 2013)
SO <sub>4</sub> <sup>2-</sup> -TiO <sub>2</sub> /ZnO (S-T/Z) Sol-Gel Method modified by sulfating treatment <i>n</i> -butyl titanate C <sub>10</sub> H <sub>14</sub> O <sub>4</sub> Zn · xH <sub>2</sub> O C <sub>6</sub> H <sub>8</sub> O <sub>7</sub> ZnO=10%	D:80°C/48h Treat: 200°C /1h Sulfating the dry gel at 200°C C: 400°C/4 hC: 550°C/4 h	---	Methyl Orange D: 0.1–1 g/L C: 10 g/L Visible light Time:5h	Calcining Temp 300 400 500 550 600 700	T/Z S-T/Z 51.4 - 55.6 59.7 50.7 61.4 48.5 63.3 46.8 56.8 45.2 46.6	<ul style="list-style-type: none"> <li>After sulfating, the catalytic activity of ZnO/TiO<sub>2</sub> (400°C,4h) improved nearly 30% and self-made pure TiO<sub>2</sub> (400°C,4h) improved about 24%</li> <li>The stronger the acidity, the higher was the catalytic activity.</li> </ul>	11a

(continued on next page)

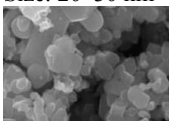

Table 2.2, continued

Photocatalyst Synthesis method Compounds/Ratio	Drying & Calcination Temp& Time	Morphology	Activity analysed by decomposition	Compound	Photocatalytic Efficiency	Objective/Result	Ref
N-ZnO/TiO <sub>2</sub> decomposition of zinc nitrate and ball milling of TiO <sub>2</sub> in N-ZnO TiO <sub>2</sub> (100% anatase) Zn(NO <sub>3</sub> ) <sub>2</sub> -6H <sub>2</sub> O ZnO=0-20wt%	Zn(NO <sub>3</sub> ) <sub>2</sub> -6H <sub>2</sub> O Decomposed @ 300 350°C/1h/air N-ZnO/TiO <sub>2</sub> D:110°C/air	ball shaped particles Size: 20-40 nm 	Reduction of Cr <sub>2</sub> O <sub>7</sub> <sup>2-</sup> : D: 2.9×10 <sup>-4</sup> (mol/L) Oxidation of MO D: 1.0×10 <sup>4</sup> (mol/L) C: 2g/L UV light Time: 20min	p-ZnO :wt% 0.0 0.5 1.0 2.0 5.0 10 20	Cr <sub>2</sub> O <sub>7</sub> <sup>2-</sup> MO 16.3 68.5 23.9 45.9 37.7 33.9 42.9 26.4 35.7 21.6 26.2 19.9 22.1 13.3	<ul style="list-style-type: none"> <li>Compared to TiO<sub>2</sub>, the p-n junction photocatalyst N(p)-ZnO/TiO<sub>2</sub> has higher photocatalytic reduction, but lower oxidation activity.</li> <li>The photoreduction activity is reduced after the optimum concentration of doped N(p)-ZnO.</li> <li>The photooxidation efficiency decreased rapidly with the increase in the ball milling time.</li> <li>The photoreduction efficiency increased gradually with the increase in ball milling time up to 12 h.</li> </ul>	(Chen, Zhao et al. 2008)
N- TiO <sub>2</sub> /ZnO Sol-Gel Method and ammonia treatment (C <sub>4</sub> H <sub>9</sub> O) <sub>4</sub> Ti Zn(O <sub>2</sub> CCH <sub>3</sub> ) <sub>2</sub> Ti:Zn=3:1 (atomic molar ratio)	D: 80 °C: 2 h C: 500 °C: 2 h C: 600 °C: 2 h C: 700 °C: 2 h	non-uniform Diameter 15 nm 	Methyl Orange D: 0.025 mmol/L, C: 0.5g/L UV A light Time: 3 h	NH <sub>3</sub> mass fraction 0% 7% 28%	NH <sub>3</sub> 0% 7% 28% 41 56 60 35 68 78 42 66 71	<ul style="list-style-type: none"> <li>The increase of the calcining temperature from 500 to 700, the particle crystallization of the composite power was actually promoted.</li> <li>With the ammonia treating process, the phase transformation of anatase to rutile was retarded.</li> </ul>	(Tian, Wang et al. 2009)
Er <sup>3+</sup> :YAlO <sub>3</sub> /TiO <sub>2</sub> -ZnO sol-gel under ultrasound & auto-combustion method TiO <sub>2</sub> (anatase phase) ZnO (zincite phase) Er <sub>2</sub> O <sub>3</sub> Y <sub>2</sub> O <sub>3</sub> Al(NO <sub>3</sub> ) <sub>3</sub> -9H <sub>2</sub> O	Er <sup>3+</sup> :YAlO <sub>3</sub> D:85°C C: 1200°C/2 h Er <sup>3+</sup> :YAlO <sub>3</sub> /TiO <sub>2</sub> -ZnO C:350,550,750 °C /30,60,90 min	Grainy balls Size: 20-30 nm 	Acid Red B dye D:10 mg/L C:1.0g/L Under ultrasound in dark Time: 150 min	Er <sup>3+</sup> :YAlO <sub>3</sub> =5% Ti: Zn = 9:1 7:3 1:1 3:7 1:9	Calcined at 550C During 60 min 54.0 64.7 76.2 61.7 43.6	<ul style="list-style-type: none"> <li>The Er<sup>3+</sup>:YAlO<sub>3</sub>/TiO<sub>2</sub> and Er<sup>3+</sup>:YAlO<sub>3</sub>/ZnO sonocatalysts had a higher sonocatalytic activity compared with the catalysts synthesized without ultrasound.</li> <li>Degradation on the basis of calcination temperature: 350~550&gt;750°C.</li> <li>Degradation on the basis of reaction time: 90&gt;&gt;60&gt;30.</li> <li>Degradation on the basis of Ti:Zn: 1:1&gt;&gt;7:3~3:7&gt;9:1&gt;1:9.</li> <li>Degradation on the basis of Er<sup>3+</sup>:YAlO<sub>3</sub> content: 20&gt;15&gt;25&gt;10&gt;5&gt;0wt.</li> <li>Degradation on the basis of solution acidity: 3&gt;5&gt;7&gt;9&gt;11.</li> </ul>	(Wang, Li et al. 2010, Gao, Jiang et al. 2011)
Ag-TiO <sub>2</sub> /ZnO Hydrothermal Process TiO <sub>2</sub> (80% anatase, 20% rutile) Zn(NO <sub>3</sub> ) <sub>2</sub> -6H <sub>2</sub> O AgNO <sub>3</sub> ZnO: TiO <sub>2</sub> : Ag= 88.6:8.6:2.7 wt%	Hydrothermal in an autoclave @ 140°C/2h D: 130°C/12h/air	Ag & TiO <sub>2</sub> on sunflower, shaped, micro sized ZnO 	Reactive black 5 D: 10 ppm, C: 0.4 g/l UV light Time: 210 min	Pristine ZnO TiO <sub>2</sub> /ZnO Ag- TiO <sub>2</sub> /ZnO	65.4% 69.6% 80.4%	<ul style="list-style-type: none"> <li>The efficacy of initially used and reused composite photocatalyst up to three cycles slightly reduced (2%) in each recycling usage.</li> <li>The as-prepared photocatalyst on gram negative <i>E. coli</i> bacteria under mild (20% intensity) UV radiation was also significantly effective with the order of Ag- TiO<sub>2</sub>/ZnO&gt;&gt;TiO<sub>2</sub>/ZnO&gt; ZnO.</li> </ul>	(Pant, Pant et al. 2013)

(continued on next page)

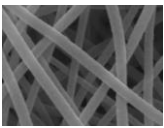

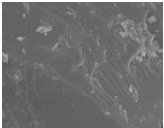
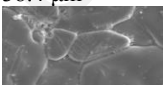


Table 2.2, continued

Photocatalyst Synthesis method Compounds/Ratio	Drying & Calcination Temp & Time	Morphology	Activity analysed by decomposition of:	Compound	Photocatalytic Efficiency	Objective/Result	Ref
Er <sup>3+</sup> :YAlO <sub>3</sub> /TiO <sub>2</sub> -ZnO sol-gel under ultrasound & auto-combustion method TiO <sub>2</sub> (anatase phase) ZnO (zincite phase) Er <sub>2</sub> O <sub>3</sub> Y <sub>2</sub> O <sub>3</sub> Al(NO <sub>3</sub> ) <sub>3</sub> -9H <sub>2</sub> O	Er <sup>3+</sup> :YAlO <sub>3</sub> D:85°C C: 1200°C/2 h Er <sup>3+</sup> :YAlO <sub>3</sub> /TiO <sub>2</sub> -ZnO C:350,550,7 50°C /30,60,90 min	Grainy balls Size: 20–30 nm 	Acid Red B dye D:10 mg/L C:1.0g/L Under ultrasound in dark Time: 150 min	Er <sup>3+</sup> :YAlO <sub>3</sub> =5% Ti: Zn = 9:1 7:3 1:1 3:7 1:9	Calcined at 550C During 60 min 54.0 64.7 76.2 61.7 43.6	<ul style="list-style-type: none"> <li>The Er<sup>3+</sup>:YAlO<sub>3</sub>/TiO<sub>2</sub> and Er<sup>3+</sup>:YAlO<sub>3</sub>/ZnO sonocatalysts had a higher sonocatalytic activity compared with the catalysts synthesized without ultrasound.</li> <li>Degradation on the basis of calcination temperature: 350~550&gt;750°C.</li> <li>Degradation on the basis of reaction time: 90&gt;&gt;60&gt;30.</li> <li>Degradation on the basis of Ti:Zn: 1:1&gt;&gt;&gt;7:3~3:7&gt;9:1&gt;1:9.</li> <li>Degradation on the basis of Er<sup>3+</sup>:YAlO<sub>3</sub> content: 20&gt;15&gt;25&gt;10&gt;5&gt;0wt.</li> <li>Degradation on the basis of solution acidity: 3&gt;5&gt;7&gt;9&gt;11.</li> </ul>	(Wang, Li et al. 2010, Gao, Jiang et al. 2011)
CeO <sub>2</sub> / La <sub>2</sub> O <sub>3</sub> -TiO <sub>2</sub> /ZnO Sol-Gel Method tetrabutyl titanate Zn(NO <sub>3</sub> ) <sub>2</sub> -6H <sub>2</sub> O La(NO <sub>3</sub> ) <sub>3</sub> -6H <sub>2</sub> O Ce(NO <sub>3</sub> ) <sub>3</sub> -6H <sub>2</sub> O TiO <sub>2</sub> :ZnO=85:15wt%	500°C/2 h 600°C/2 h 700°C/2 h	---	---	CeO <sub>2</sub> : - La <sub>2</sub> O <sub>3</sub> : 0.0wt%,0.0wt% 0.5wt%,0.5wt% 1.0wt%,1.0wt% 1.5wt%,1.5wt% 2.0wt%,2.0wt%	---	<ul style="list-style-type: none"> <li>La<sup>3+</sup>/Ce<sup>3+</sup> doping decreased the transformation temperature of gel to anatase, whereas it enhanced the transformation temperature of anatase to rutile</li> <li>With the increase of Ce<sup>3+</sup> content, the transformation temperatures of gels to anatase and anatase to rutile, respectively, present the slight increase and then decrease trends.</li> <li>With the increase of La<sup>3+</sup> content, both of the transformation temperatures roughly sustain invariable.</li> </ul>	(Liao, Donggen et al. 2004)
Ag/ZnO-TiO <sub>2</sub> Sol-Gel Method under micro wave (m) and hydrothermal treatment(c) Zn(Ac) <sub>2</sub> -2H <sub>2</sub> O,Ac AgNO <sub>3</sub> C <sub>12</sub> H <sub>28</sub> O <sub>4</sub> Ti	c-Ag/ZnO-TiO <sub>2</sub> Hydrothermal in an autoclave @ 200°C/6h m-Ag/ZnO-TiO <sub>2</sub> D: 80°C C:500°C/7 h	nano-composite materials 	Rhodamine B D:50mg/L,C: 1.7g/L Simulated Sunlight (SS), Visible Light (VL),Microwave- Irradiation (MI) Time: 30 min	Phoyolysis P25 m-ZnO m-ZnO-TiO <sub>2</sub> c-Ag/ZnO-TiO <sub>2</sub> m-Ag/ZnO-TiO <sub>2</sub>	SS VL MI 5.0 5.3 52.2 6.2 7.6 55.5 10.3 21.2 63.3 17.6 31.2 74.3 21.7 45.9 76.0 26.6 61.0 81.9	<ul style="list-style-type: none"> <li>m-Ag/ZnO-TiO<sub>2</sub> presented regular shape with smooth surface whereas, the surfac of c-Ag/ZnO-TiO<sub>2</sub> was rough with irregular shape.</li> <li>m-Ag/ZnO-TiO<sub>2</sub> presented stable photoactivity under ultraviolet light after three cycles experiment.</li> <li>Microwave-assisted synthesis increased the crys-tallite sizes and the BET specific surface area, reduced the energy band gaps of the samples.</li> <li>Photocatalytic activity for different dyes: MB&gt;CV&gt;RB&gt;MO.</li> </ul>	(Li, Zhang et al. 2014)

(continued on next page)

Table 2.2, continued

Photocatalyst Synthesis method Compounds/Ratio	Drying & Calcination Temp& Time	Morphology	Activity analysed by decomposition	Compound	Photocatalytic Efficiency	Objective/Result	Ref
Au nanoparticles on TiO <sub>2</sub> /ZnO Electrospinning (for TiO <sub>2</sub> /ZnO nanofibers) and in situ reduction (for embedding Nanoparticles) Ti(OC <sub>4</sub> H <sub>9</sub> ) <sub>4</sub> , Zn(Ac) <sub>2</sub> HAuCl <sub>4</sub> Ti:Zn=1:1 molar ratio, Au:10.5wt%	ZnO/TiO <sub>2</sub> C:500°C/2h/air  Au- ZnO/TiO <sub>2</sub> D:40°C/24h/ Vacuum	Nano fibers Size: 80-120 nm 	MO, 30 min 4 nitrophenol, 40 min, D: 10 mg/L C: 0.1g/L UV light irradiation	ZnO TiO <sub>2</sub> ZnO/TiO <sub>2</sub> Au-ZnO/TiO <sub>2</sub>	MO 4-NP 97.0% 96.9% 85.2% 70.0% 52.7% 29.6% 50.0% 30.6%	<ul style="list-style-type: none"> <li>The band gap of TiO<sub>2</sub>/ZnO NFs and TiO<sub>2</sub>/ZnO/Au NFs has been narrowed to 3.16 and 3.17eV from 3.26eV of the pristine ZnO NFs.</li> <li>An stable photoactivity was presented by Au-TiO<sub>2</sub>/ZnO after three cycles experiment.</li> </ul>	(Zhang, Shao et al. 2012)
RGO-TiO <sub>2</sub> /ZnO solution-based reduction of graphite oxide (GO) Zn(CH <sub>3</sub> COO) <sub>2</sub> ·2H <sub>2</sub> O TiF <sub>4</sub> Graphite Oxide (GO)	180°C for 20 h.	TiO <sub>2</sub> &ZnO particles embedded in RGO 	Photoreduction of Cr(VI) D: 10 mg/L C: 1g/L UV irradiation 120 min	ZnO ZnO/TiO <sub>2</sub> RGO-ZnO/TiO <sub>2</sub> RGO-ZnO/TiO <sub>2</sub> RGO=42wt%	11% 17% 41% 63%	<ul style="list-style-type: none"> <li>ZnO and TiO<sub>2</sub> particles were dispersed on RGO with a chemical bonding that contributed to exfoliation of the GO.</li> <li>The photocurrent response also increased with increasing RGO ratio.</li> <li>With increasing RGO mass ratio in the composite, the photocatalysis rate reached to almost 8.97 times higher than the rate for pure ZnO.</li> </ul>	(Johra and Jung 2015)
SnO <sub>2</sub> -ZnO/TiO <sub>2</sub> Sol-Gel (SG) and Solid-State (SS) methods C <sub>16</sub> H <sub>36</sub> O <sub>4</sub> Ti SnCl <sub>4</sub> ·5H <sub>2</sub> O (CH <sub>3</sub> COO) <sub>2</sub> Zn·2H <sub>2</sub> O Sn:Zn=1:1	D:80°C/1h C: 500°C /3h  Sn: Zn=1:1 (MR) Sn(Zn)/Ti molar ratio of 0.05	Non-Uniform 	Methyl Orange D: 10 ppm C: 1g/L SG synthesized Visible light Time:3h UV light Time:40 min SS synthesized Visible light Time:4h	Molar ratio Sn(Zn):Ti-0.05 Sn(Zn):Ti-0.10 Sn(Zn):Ti-0.15 Sn(Zn):Ti-0.20 Sn/Ti-0.15 Zn/Ti-0.15 Wt%Sn(Zn):Ti-3wt% Sn(Zn):Ti-6 wt% Sn(Zn):Ti-9wt%	SG/Vis SG/ UV 48.0% 84.9% 25.8% 71.8% 12.9% 53.2% 25.8% 61.9% 43.5% 44.9% 48.0% 74.3% SS synthesized 24.6% 26.8% 22.9%	<ul style="list-style-type: none"> <li>Degradation rate for the SS synthesized photocatalyst on the basis of the weight ratio of SnO<sub>2</sub> and ZnO to TiO<sub>2</sub>: 6 wt%&gt;3 wt% &gt;9 wt%.</li> <li>The composite catalysts synthesized by sol-gel method represented a much stronger photocatalytic activity than that of the catalysts synthesized by solid-state method.</li> <li>The Sn and Zn ions doped in TiO<sub>2</sub> promoted the phase change from anatase to rutile TiO<sub>2</sub> in the range of annealing temperature from 400 °C to 600 °C</li> <li>Sample heated at 500 °C showed a main rutile structure, with some anatase peaks.</li> </ul>	(Yang, Yan et al. 2012)
ZnO-Bi <sub>2</sub> O <sub>3</sub> -TiO <sub>2</sub> Solid-State Route Method ZnO Bi <sub>2</sub> O <sub>3</sub> TiO <sub>2</sub> powder ZnO: Bi <sub>2</sub> O <sub>3</sub> : TiO <sub>2</sub> powder= 99: 0.5: 0.5 mol%	D: 70°C/air C: 800°C/2h/air	Irregular grains Size: 26 to 38.4 μm 	-	sintered at 1140°C 1170°C 1200°C 1230°C 1260°C	Band gap energy 2.95eV 2.98eV 2.96eV 2.92eV 2.94eV	<ul style="list-style-type: none"> <li>Abnormality and the average grain size increased from with the increase of sintering temperature.</li> <li>Doping TiO<sub>2</sub> in ZnO-Bi<sub>2</sub>O<sub>3</sub> system slightly reduces the <i>E<sub>g</sub></i>.</li> <li>Optical band gap energy decreases with the increase of sintering temperature.</li> </ul>	(Sabri, Azmi et al. 2011)

(continued on next page)

Table 2.2, continued

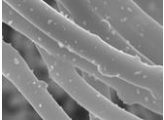
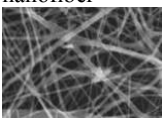
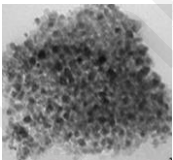
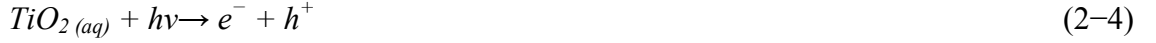
Photocatalyst Synthesis method Compounds/Ratio	Drying & Calcination Temp& Time	Morphology	Activity analysed by decomposition	Compound	Photocatalytic Efficiency	Objective/Result	Ref
Carbon(C)nano fibers decorated with binary TiO <sub>2</sub> /ZnO (T/Z) combined electrospinning and hydrothermal processing TiO <sub>2</sub> (80% anatase, 20% rutile) Zinc Powder & Zn(NO <sub>3</sub> ) <sub>2</sub> ·6H <sub>2</sub> O Bis-Hexa Methylene Triamine Carbon (C)	Vacuum dried at 70°C/12h stabilized in air at 250°C/3h carbonized under argon at 900°C/5h	(T/Z) nano flowers on (C) nano fibers, Size: 470nm 	Methylene blue (MB) D: 10 ppm C: 0.8g/L under UV irradiation Time:150 min	ZnO TiO <sub>2</sub> ZnO/TiO <sub>2</sub> C-ZnO/TiO <sub>2</sub>	46.9% 62.6% 69.4% 99.8%	<ul style="list-style-type: none"> <li>The combination of the high surface area of carbon nano fibers and the photocatalytic property of the TiO<sub>2</sub>/ZnO system presents a fast degradation catalyst along with and antibacterial performance.</li> <li>The C- TiO<sub>2</sub>/ZnO presented stable photocatalytic activity up to almost two cycles, after that, the activation decreased by about 10% for the third cycle.</li> </ul>	(Pant, Pant et al. 2013)
Zn-TiO <sub>2</sub> /ZnO electrospinning of TiO <sub>2</sub> (anatase) nanofibers and metal-organic chemical vapor deposition C <sub>12</sub> H <sub>28</sub> O <sub>4</sub> Ti Zn(tta) <sub>2</sub> tmeda zinc(II) ions	ZnO shell nano structure 600°C/1h/air  Zn-doped TiO <sub>2</sub> 500°C/3h/air	ZnO nano grains/rods on Zn-TiO <sub>2</sub> nanofiber 	-	Zn/Ti% 3% 5% 15%	-	<ul style="list-style-type: none"> <li>Upon increasing the Zn content in the nanofibers, this feature slightly moved towards lower binding energy.</li> <li>Upon increasing the ZnO loading and/or calcination time, ZnO shape was changed from nano grains to nano rods.</li> <li>The Zn-doped TiO<sub>2</sub>-ZnO nanofibers had an hydroxyl rich surface and showed intense emissions in the UV-Vis regions, representing a potentially appealing system for photocatalysts.</li> </ul>	(Fragala, Cacciotti et al. 2010)
Ni-ZnO/TiO <sub>2</sub> Sol-Gel approach tetraethyl titanate Zn(NO <sub>3</sub> ) <sub>2</sub> ·6H <sub>2</sub> O Ni(NO <sub>3</sub> ) <sub>2</sub> ·6H <sub>2</sub> O ZnO loading=8wt%	D: 100°C/12h C: 450°C/2h/ in microwave furnace	Nano grains Size:10-20 nm 	reactive brilliant blue C:1g/L D: 50 mg/L simulated solar light Time:120 min	TiO <sub>2</sub> Ni(0.1)-ZnO/TiO <sub>2</sub> , Ni(0.3)-ZnO/TiO <sub>2</sub> Ni(0.4), ZnO/TiO <sub>2</sub> Ni(0.5) ZnO/TiO <sub>2</sub> Ni(0.7)-ZnO/TiO <sub>2</sub>	32.86% 52.36% 56.24% 60.91% 51.96% 46.22%	<ul style="list-style-type: none"> <li>Ni expanded light absorption of TiO<sub>2</sub> to visible region, increased amount of surface hydroxyl groups and physically adsorbed oxygen and then enhanced separation rate of photo-generated carriers.</li> <li>The photo-degradation rate of methyl orange (MO) over the as-synthesized Ni doped ZnO-TiO<sub>2</sub> is lower than that of KN-R.</li> <li>Photo degradation on the basis of solution acidity: 4&gt;8&gt;10. <ul style="list-style-type: none"> <li>Photo degradation based on catalyst loading 1.25~1.1&gt;&gt;0.75&gt;0.5 g/L.</li> </ul> </li> </ul>	(Zou, Dong et al. 2014)

Table 2.2 shows the heterojunction of two photocatalysts, titanium dioxide and zinc oxide, along with metal or non-metal doping to improve photocatalytic activity. In terms of non-metal doping, nitrogen (N) has been suggested. Calcination temperatures also affect the crystal structure, with calcination at 500°C being necessary to induce the formation of doped crystallinity. Photocatalyst activity and degradation rate can be enhanced by incorporating N into the ZnO/TiO<sub>2</sub> matrix. Moreover, doping of metal ions such as Fe, Mo and Ag shift the absorption edge of both photocatalysts towards the visible region and increase the photocatalytic activity.

## 2.6 TiO<sub>2</sub> Photocatalyst

Titanium dioxide (TiO<sub>2</sub>), an n-type semiconductor, is one of the most applicable photocatalysts that can be used in a wide range of applications, such as H<sub>2</sub> generation, self-cleaning, defogging, water purification, air purification, sterilization, etc. (Robinson & McMullan, 2001). TiO<sub>2</sub> is non-toxic, abundant, economical, versatile and stable (Krumme & Boyd 1988; Aviam, Bar-Nes et al., 2004). Generally, TiO<sub>2</sub> is a semiconductor with a wide band gap ( $E_g = 3.0 \sim 3.2 eV$ ) that requires excitation light with a wavelength lower than 400 nm ( $E_g = hc/\lambda \cong 1240/\lambda$ ) to begin photoreaction (Fujishima et al., 2000; Carp, Huisman et al., 2004). When the surface of TiO<sub>2</sub> (or any other photocatalyst) is irradiated with UV light, electrons ( $e_{CB}^-$ ) and holes ( $h_{VB}^+$ ) are created in the conduction (CB) and valence bands (VB), respectively (Gaya & Abdullah 2008). The generated electrons and holes are subsequently trapped and recombine with each other. In short, the photo-induced formation procedure follows four steps, which are photoexcitation (Eq. 2-4) charge-carrier trapping of  $e^-$  (Eq. 2-5), charge-carrier trapping of  $h^+$  (Eq. 2-6) and electron-hole recombination (Eq. 2-7):

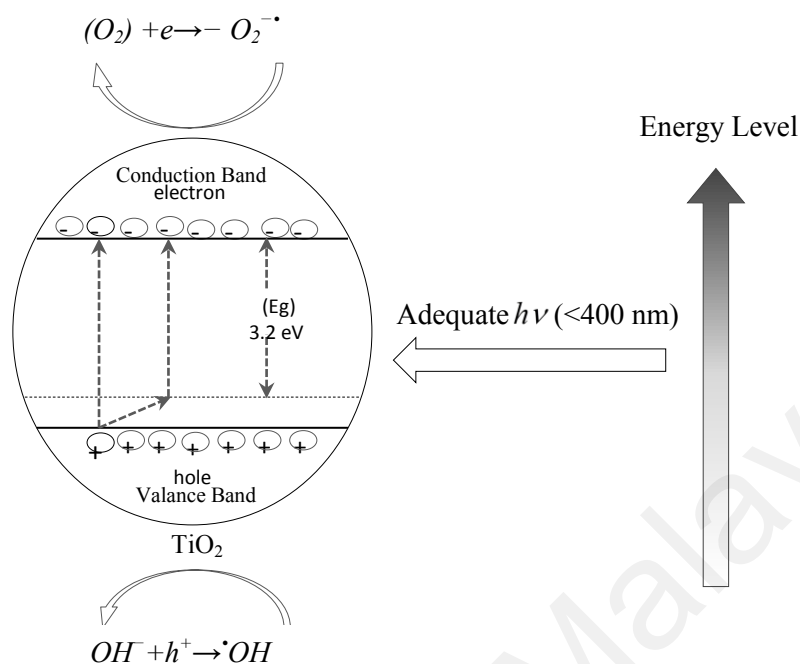


In the next step, the photo-induced electrons in the CB are trapped by aqueous-adsorbed oxygen and participate in the reduction process, producing superoxide radical anions ( $O_2^{\cdot-}$ ) (Eq. 2-8). The superoxide is protonated (Eq. 2-9) by  $H^+$ , which is produced by water ionization in the generated holes ( $h^+$ ) (Eq. 2-10).  $HOO^{\cdot}$  then traps another excited electron to produce  $HO_2^-$  (Eq. 2-11), followed by the protonation of  $HO_2^-$  to generate hydrogen peroxide, as shown in Eq. (2-12). Finally, hydrogen peroxide is decomposed to produce hydroxyl radicals ( $OH^{\cdot}$ ) (Eq. 2-13). Meanwhile, the photo-induced holes in the VB diffuse to the surface of the photocatalyst and then react with the adsorbed water molecules, generating another hydroxyl radical (Eq. 2-14) (Daneshvar, Aber et al., 2007; Kansal, Singh et al. 2008, Abdollahi1, Abdullah et al. 2011, Abdollahi, Abdullah et al. 2011).



A variety of organisms as well as organic and inorganic pollutants can be deactivated, decomposed or transformed by the synergistic interaction of hydroxyl radicals, electrons, holes and other oxidizing radicals (Takeda & Teranishi, 1988).

TiO<sub>2</sub> also has a favourable combination of electronic structure, light absorption properties, charge transport characteristics, and excited-state lifetime (Hadj Benhebal, 2013). Furthermore, TiO<sub>2</sub> is a stable compound either photo-chemically or chemically in contrast with other semiconductors such as GaP or CdS, which can easily solve and produce toxic by-products. Furthermore, TiO<sub>2</sub> presents excellent advantages during environmental purification processes, including an oxidative reaction that is normally employed to decompose the polluting materials. Such reaction is improved by increasing the oxidative power of VB holes. TiO<sub>2</sub> with a band gap of about 3.0–3.2eV and wavelength of about 400 nm presents more powerful oxidative of the VB holes compared to the reducibility of photo-induced electrons. Generally, different TiO<sub>2</sub> structures have very strong oxidation power (3.0eV for rutile and 3.2eV for anatase TiO<sub>2</sub>) considering approximately 1.2 eV for the oxidation potential of water and approximately 3.0 eV for the hydrogen reference potential. Furthermore, organic compounds are decomposed completely into carbon dioxide and water by irradiating TiO<sub>2</sub> with UV light below 400 nm. The reason is the surface temperature of TiO<sub>2</sub>, which increases tremendously to almost 30°C. In such conditions, all materials can be easily oxidized. Figure 2.3 shows the band gap energy level of TiO<sub>2</sub> photocatalyst.

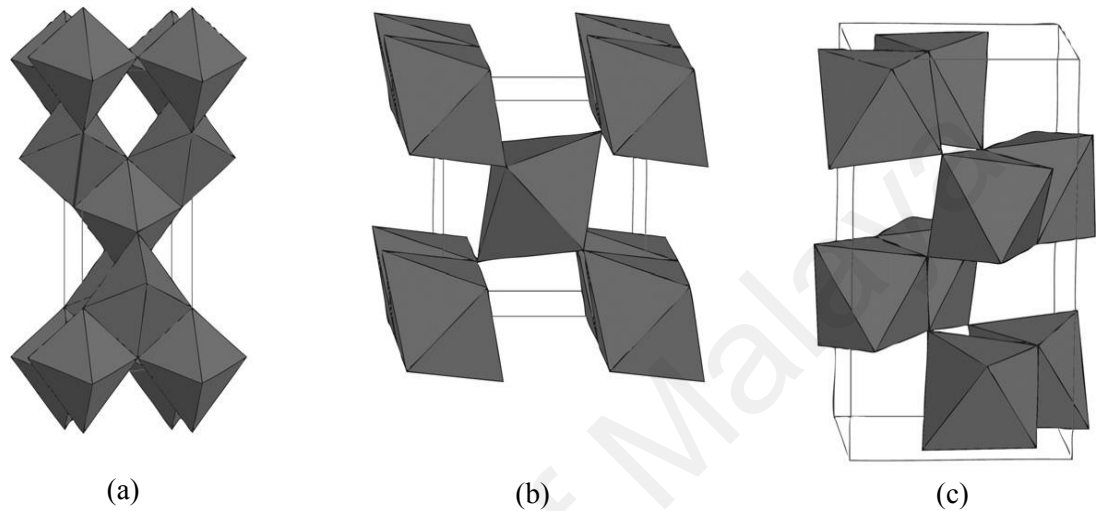


**Figure 2.3:** Energy band gap diagram of a TiO<sub>2</sub> spherical particle

For TiO<sub>2</sub> photocatalyst, the CB energy level is slightly higher than the reduction potential of oxygen ( $E_{CB}=-0.51V$ ,  $E_O=-0.33V$ ), which is a predominant electron acceptor (or oxidant) and it can ease the transfer of  $e^-_{CB}$  to O<sub>2</sub>. On the other hand, its VB energy level ( $E_{VB}=+2.69V$ ) is much lower than the oxidation potentials of most electron donors (either organic or inorganic compounds). Accordingly, the highly oxidative holes can be transferred to the surface-adsorbed hydroxide groups or water by devising a surface-bound hydroxyl radical. Generally, it can be concluded that TiO<sub>2</sub> encourages the redox transformation of pollutants owing to the positions of its bands.

Figure 2.4 displays the TiO<sub>2</sub> crystal structure. TiO<sub>2</sub> has three main crystalline structures: anatase (tetragonal), rutile (tetragonal) and brookite (orthorhombic). Anatase is the phase normally fabricated in the sol-gel process but brookite is mostly found as a by-product when precipitation is performed in an acidic medium at low temperature. Rutile

is a stable structure while both brookite and anatase are metastable and usually transfigure to rutile when heated.



**Figure 2.4:** TiO<sub>2</sub> crystal structure Anatase (a), Rutile (b), Brookite (c)

Brookite is generally more reactive than anatase. However, preparing pure brookite without rutile or anatase is rather difficult, and therefore it has not been widely investigated (Paola, Bellardita et al. 2013). Besides, anatase presents higher photocatalytic activity compared to rutile because the higher  $E_{CB}$  ( $\sim 0.2$  eV) results in higher driving force for transferring electrons to O<sub>2</sub>. This is because the  $E_{CB}$  position affects electron transfer rate and consequently the charge recombination rate. Therefore, it is a determining factor in the efficiency of photocatalysis. It has always been reported that the photocatalytic activity of both anatase and rutile structures is highly influenced by the type of substrate applied (Serpone, Sauvé et al. 1996, Du and Rabani 2003, Ryu and Choi 2007, Tryba, Toyoda et al. 2007).

The surface properties of TiO<sub>2</sub>, particularly the pH dependence of the surface charge, are additional determinants of photocatalytic reaction. TiO<sub>2</sub> is known as a diprotic acid



due to the amphoteric nature of the surface hydroxyl groups. Accordingly, the surface titanol group of this photocatalyst follows the following acid–base equilibrium reaction:



The averaged  $\text{pK}_a$  is defined as the pH zero point of charge ( $\text{pH}_{\text{zpc}}$ ), at which the surface charge of the photocatalyst is null. For the  $\text{TiO}_2$  photocatalyst,  $\text{pK}_{a1}=4.5$ ,  $\text{pK}_{a2}=8$  and the  $\text{pH}_{\text{zpc}}$  value is estimated to be 6.2 (Carraway, Hoffman et al. 1994, Yogi, Kojima et al. 2009). Therefore, the protonation reaction takes place and the catalyst surface is positively charged at  $\text{pH}<6.2$ , while the catalyst surface is negatively charged at  $\text{pH}>6.2$  due to the deprotonation reaction.

Apart from the mentioned properties of  $\text{TiO}_2$ , this photocatalyst is highly reactive during photocatalysis for water treatment and it has great response even under weak light irradiation. However,  $\text{TiO}_2$  is inappropriate for a mass processing system and is inactive and inapplicable with visible light. Numerous efforts have been proposed to overcome such limitations and enhance the photocatalytic activity of  $\text{TiO}_2$  through surface modification/complexation, sensitization, impurity doping, and heterojunction with semiconductors of similar band gaps, etc.

As the suspension of  $\text{TiO}_2$  catalyst and water is irradiated with UV light, the photo-induced electrons in the CB generally react with dissolved oxygen and produce superoxide radical anions ( $\text{O}_2^{\bullet-}$ ). Besides, the photo-induced holes in the VB diffuse to the  $\text{TiO}_2$  surface and react with the adsorbed water molecules, forming  $\text{OH}^{\bullet}$ .

In addition, this photocatalyst can easily be synthesised since it is an industrially mass-produced material. The ease of applying  $\text{TiO}_2$  is another advantage of this photocatalyst that encourages its industrial application.

Although  $\text{TiO}_2$  decomposes pollutant compounds even under weak light easily and fast, it is inactive and unsuitable for a mass processing system under visible light. Therefore,

TiO<sub>2</sub> applications are extremely limited especially with solar energy, since only 3% of solar light is absorbed from solar energy. Moreover, the photocatalytic activity of TiO<sub>2</sub> depends on the relative degree of branching of the reactive electron–hole pairs into interfacial charge-transfer reactions. Low surface area is one more limitation of this photocatalyst.

## **2.7 Dopants effects on TiO<sub>2</sub> photocatalyst**

The most important effect of dopants is improved TiO<sub>2</sub> electronic structure to eliminate its light sensitivity and broaden its effective range from the ultra-violet range to visible light (Jaiswala et al. 2012). Although doping techniques are susceptible to thermal instability, they indicate excellent physicochemical properties, such as small crystallite size, high specific surface area and high crystallinity (Pongwan et al. 2016).

The rutile, anatase and brookite phases are the three main crystalline phases of TiO<sub>2</sub> (Reyes-Coronado et al. 2008). The rutile and anatase phases are common crystallographic phases of TiO<sub>2</sub>, with the latter particularly favoured for its exceptional thermodynamic stability and high photocatalytic activity. The formation of these phases or transformation from rutile to anatase or vice versa is extremely dependent on the thermal dehydration mechanism during which time Ti–O–Ti bonds are formed by the interaction between the protonated surfaces and –OH groups. Specific surface area is another important characteristic that determines the morphology of TiO<sub>2</sub> in photocatalysis. The photocatalytic degradation rate of organic pollutants is enhanced by the production of doped TiO<sub>2</sub> with large specific surface area, warranting the availability of active sites in TiO<sub>2</sub>. The crystallite size of TiO<sub>2</sub> is one of the aspects affecting the quality of TiO<sub>2</sub>, with large crystallite sizes up to a certain limit enhancing the photocatalytic activity of TiO<sub>2</sub> (Diebold 2003).

With the presence of dopants in the formation of TiO<sub>2</sub>-doped photocatalyst, the phase transformation from anatase to rutile is eliminated when the thermal energy can overcome the nucleation barrier during the dehydration process. In other words, the crystallite size of TiO<sub>2</sub> is suppressed by inserting dopants into the octahedral lattice structure of doped TiO<sub>2</sub>, enhancing its physicochemical characteristics. In addition, the smaller crystals reduce the recombination of the photogenerated charge carriers, hence, they are favoured over larger ones. Furthermore, smaller doped TiO<sub>2</sub> crystals induce a larger band gap due to the enhanced redox ability (Jongnavakit, 2012). In short, doped TiO<sub>2</sub> with a high anatase percentage, small crystallite size and large specific surface area, assists high photocatalytic activity.

## **2.8 Doping processes**

In the doping process, the rapid charge recombination is retarded and visible light absorption is enabled by defect states created in the band gap. In the first case, recombination is inhibited and the interfacial charge transfer is enhanced by the trapping of VB holes or CB electrons in the defect sites. In the second case, electronic transitions from the defect states to the CB or from the VB to the defect states are allowed under sub-band gap irradiation. Metal ions (transition metals and noble metals) and non-metal ions are the two main categories of dopants. Generally, selective metals are preferred since they have the potential to transfer electrons and decrease the band gap energy level. For doped catalysts, metal ions are activated in the presence of a light source, generating electron holes. Therefore, the presence of metal ion dopant in the photocatalyst matrix significantly improves the interfacial electron transfer and charge carrier recombination rates, which is followed by greater photoreactivity. Among different metallic doping elements, copper has proven to be an effective dopant in enhancing visible light absorption. For example, Park et al. (Park,Choi et al., 2013)

modified TiO<sub>2</sub> by incorporating Ni<sup>2+</sup>, Co<sup>2+</sup>, Zn<sup>2+</sup> and Cu<sup>2+</sup> and reported that Cu-doped TiO<sub>2</sub> was a promising photocatalyst in the photo-decomposition of methylene blue. Sangpour et al. (Sangpour, Hashemi et al. 2010) modified TiO<sub>2</sub> by doping with Ag, Au, and Cu and found that doping increased the probability of radical formation. The photoactivity levels of the investigated photocatalysts were reported to be in the following order: Cu:TiO<sub>2</sub> > Au:TiO<sub>2</sub> > Ag:TiO<sub>2</sub> > TiO<sub>2</sub>.

However, in the heterojunction process, the synergic effects of two semiconductors with similar band gaps can result in low recombination rate and increased electron-hole pair lifetime. The TiO<sub>2</sub> photocatalyst can be potentially coupled with other semiconductors, e.g. SiO<sub>2</sub>, MoO<sub>3</sub>, CdS, MgO, WO<sub>3</sub>, SnO<sub>2</sub>, Cu<sub>2</sub>O, In<sub>2</sub>O<sub>3</sub> and ZnO (Wu, Yu et al. 2006). Among different semiconductors, the photocatalytic activity of ZnO is quite similar to TiO<sub>2</sub> and appears to be as reactive as TiO<sub>2</sub> under sunlight. Basically, the band gap of ZnO (around 3.37 eV) is close to the energy level of titanium dioxide (Hadj Benhebal & Ange'lique Leonard 2013). According to the literature, the energy level and surface area of TiO<sub>2</sub> increase when it is mixed with another photocatalyst. Besides, the light absorption range shifts towards visible light due to the narrowing band gap energy level as TiO<sub>2</sub> is doped with a semiconductor catalyst (Chin-Chuan Liu, 2006).

TiO<sub>2</sub>/ZnO has been investigated by a number of researchers for improving the photodegradation efficiency of TiO<sub>2</sub> catalyst (Zhu et al., 2004; Lakshminarayana, Qiu et al., 2008). The ability of copper in modifying the photoactivity of TiO<sub>2</sub> (Kim, Shin et al. 2013, Pham and Lee 2014, Wang, Duan et al. 2014) and ZnO (Wu, Shen et al. 2012, Ahmad et al., 2013) has been separately investigated in various works. The hybrid photocatalyst of TiO<sub>2</sub>/ZnO with other metals has also been investigated in some studies (Wang, Li et al., 2010; Pant et al., 2013). However, to the best of our knowledge, the hybrid Cu-ZnO/TiO<sub>2</sub> photocatalyst has not been studied yet.

### 2.8.1 Effect of metal doping

Photocatalytic efficiency generally depends on the generation of electron-hole pairs that react with the species adsorbed on the photocatalyst's surface. For doped catalysts, the metal ions are activated in the presence of a light source, generating electron holes. Therefore, the presence of metal ion dopants in the photocatalyst matrix significantly improves the interfacial electron transfer rates and charge carrier recombination rates, which is followed by greater photoreactivity. Metal dopants are also able to improve the morphology of doped TiO<sub>2</sub>. To date, different metal dopants, including iron (Fe) (Pang & Abdullah 2013), zinc (Zn) (Zhao et al., 2008), copper (Cu) (Xin et al., 2008), platinum (Pt) (Yu et al. 2013), nickel (Ni) (Jing et al., 2005), manganese (Mn) (Denga et al., 2011), barium (Ba) (Son et al., 2010) and cobalt (Co) (Mugundan et al., 2015) have been analysed for their ability to enhance the photocatalytic performance of nano-doped TiO<sub>2</sub>. They improve doped TiO<sub>2</sub> performance and increase its industrial applications by shifting the light absorption wavelength from the UV to the visible light irradiation spectrum. The properties of various metal dopants of TiO<sub>2</sub> are summarized in Table 2.3.

**Table 2.3:** Properties of various metal dopants of TiO<sub>2</sub>

Metal Dopant	Metal/TiO <sub>2</sub> (molarratio)	Synthesis method	Starting material of TiO <sub>2</sub>	Starting material of metal dopants	Crystallite size (nm)	Phase	BET Surface area (m <sup>2</sup> /g)	Ref
Fe	0.090	Hydrothermal	TTB	FeCl <sub>3</sub> , FeCl <sub>2</sub>	11.40	Anatase	101.40	(M. Asilturk 2009)
Fe	0.100	Hydrothermal	(Ti(OC <sub>4</sub> H <sub>9</sub> - <i>n</i> ) <sub>4</sub> )	Fe(NO <sub>3</sub> ) <sub>3</sub> •9H <sub>2</sub> O	14.50	Anatase	102.00	(T. Tong 2008)
Fe	1.200	Hydrothermal	TiCl <sub>3</sub>	FeCl <sub>3</sub> •6H <sub>2</sub> O	23.70	Anatase	55.50	(Z. Ambrus 2008)
Fe	0.007	Sol gel	TTB	Fe(NO <sub>3</sub> ) <sub>3</sub>	—	Anatase	175.00	(W.C. Hung 2007)
Fe	0.007	Sol gel/ microemulsion	TTB	Fe(NO <sub>3</sub> ) <sub>3</sub>	12.70	Anatase	83.00	(C. Ad'an 2009)
Fe	0.980	Sol gel	Ti(OPri) <sub>4</sub>	Fe(NO <sub>3</sub> ) <sub>3</sub> •9H <sub>2</sub> O	9.00	Anatase	126.10	(M. Asilturk 2009)
Pt	0.800	Impregnation	TiO <sub>2</sub> Degussa P25	PtCl <sub>2</sub>	22.28	Anatase	29.17	(S. Sakthivel 2004)
Pt	1.000	Impregnation Photodeposition	TiO <sub>2</sub> Degussa P25	H <sub>2</sub> PtCl <sub>6</sub>	20.00	Anatase	107.00	(Vorontsov 2007)
Pt	1.500	Impregnation	TTIP	H <sub>2</sub> PtCl <sub>6</sub>	31.00	Anatase	19.10	(H. Abe 2006)
Pt	0.500	Photochemical deposition	TBOT	H <sub>2</sub> PtCl <sub>6</sub> •6H <sub>2</sub> O	9.15	Anatase	116.10	(W. Sun 2008)
Pt	1.500	Photochemical reduction	TNBT	H <sub>2</sub> PtCl <sub>6</sub> •6H <sub>2</sub> O	—	Anatase	118.70	(M. Huang 2008)
Ce	0.100	Sol gel	TiCl <sub>4</sub>	H <sub>2</sub> PtCl <sub>6</sub> •6H <sub>2</sub> O	14.00	Anatase	68.00	(Y. Ishibai 2008)
Ce	0.010	Hydrothermal	Ti(SO <sub>4</sub> ) <sub>2</sub>	Ce(NO <sub>3</sub> ) <sub>4</sub>	—	Anatase	454.00	(J. R. Xiao 2006)
Ce	4.000	Reflux	Ti(OBu) <sub>4</sub>	Ce(NO <sub>3</sub> ) <sub>4</sub>	8.30	Anatase	—	(C. Wang 2010)
V	1.000	Sol gel	Ti(OBu) <sub>4</sub>	VO(OPr) <sub>3</sub>	12.00	Anatase	107.00	(M. Bettinelli 2007)

Among different transition metals such, as Cr, Fe, Ni, Zn, Co, (Zhu, Zheng et al. 2004, Zhu, Chen et al. 2006, Zhu, Deng et al. 2006; Schneider, Matsuoka et al., 2014) and Cu, copper with redox potentials of 0.52 V ( $\text{Cu}^{2+}/\text{Cu}$ ) and 0.16 V ( $\text{Cu}^{2+}/\text{Cu}^+$ ) has been used as a suitable modifier for various visible light-responsive photocatalysts (Sagar, 1996).  $\text{Cu}^{2+}$  (0.73Å),  $\text{Zn}^{2+}$  (0.83Å) and  $\text{Ti}^{4+}$  (0.64Å) have similar ionic radius parameters and therefore  $\text{Cu}^{2+}$  can easily penetrate into  $\text{TiO}_2$  and ZnO matrices as deep acceptors in conjunction with neighbouring oxygen vacancy or substituting the positions of  $\text{Zn}^{2+}$  or  $\text{Ti}^{4+}$ . In addition, Cu doping shifts the absorption edges of both photocatalysts towards the visible region (Mohan et al., 2012).  $\text{Cu}^{2+}$  directly traps the electrons generated from the photocatalyst excitation in Cu- $\text{TiO}_2$  or Cu-ZnO. As such, doping reduces the electron-hole recombination rate during photocatalysis by generating charge trapping sites.

Copper has been utilized more extensively as a dopant than other transition metals. Sreethawong and Yoshikawa (Sreethawong & Yoshikawa 2005) compared the photocatalytic activity of Au-, Pd- and Cu-loaded mesoporous  $\text{TiO}_2$  in a single-step sol-gel process with a surfactant template. Zhou et al. (Zhou, Ji et al. 2012) investigated the photocatalytic activity of meso-tetraphenylporphyrin with different metal centres (Fe, Co, Mn and Cu) on the surface of  $\text{TiO}_2$  (Degussa P25) and reported that CuP- $\text{TiO}_2$  presented the highest activity. In another work, Kaneco et al. (Dalai Ajay, 2012) investigated the photocatalytic hydrogen production of aqueous alcohol solution with  $\text{ZnO}/\text{TiO}_2$ ,  $\text{SnO}/\text{TiO}_2$ ,  $\text{CuO}/\text{TiO}_2$  and  $\text{CuO}/\text{Al}_2\text{O}_3/\text{TiO}_2$ , where the maximal hydrogen production was obtained by using the latter. A few studies have also been conducted on co-doping of  $\text{TiO}_2$  with copper and another metal/non-metal dopant (Morikawa, Irokawa et al. 2006, Song, Zhou et al. 2008, Trejo-Tzab, Alvarado-Gil et al. 2012). Although incorporating a dopant into the integrated structure of  $\text{ZnO}/\text{TiO}_2$  may yield improved physical and chemical properties, very few studies have focused on this. To the best of

the author's knowledge, no study has been conducted on the integration of copper into the TiO<sub>2</sub>/ZnO structure to further support semiconductors. .

Normally, metal-doped TiO<sub>2</sub> products induce a greater anatase phase presence, crystallite size of about 2.59-12.00 nm and specific surface area ranging from 100 to 500 m<sup>2</sup>/g. Among the mentioned metals, Cu has proven to improve the photocatalytic band gap of Cu-TiO<sub>2</sub> and Cu-ZnO separately. This is attributed to the presence of two electrons in the valence layer of Cu that enable electron transfer. Therefore, in this study copper (Cu) was selected for doping TiO<sub>2</sub>/ZnO, as it has not been extensively investigated so far.

### **2.8.2 Effect of non-metal doping**

Non-metal anion doping has been widely applied to hinder the recombination of photogenerated electron-hole pairs in nano-TiO<sub>2</sub>. This is attributed to the electronic states of non-metals, which are above the valence band edge of TiO<sub>2</sub>. Different nonmetal dopants like C-N-Codoped TiO<sub>2</sub> (Yu and Yu 2009), S,I-codoped mesoporous TiO<sub>2</sub> (Yu et al. 2010), WO<sub>3</sub> Coupled P-TiO<sub>2</sub> (Yu et al. 2010a), F-doped anatase TiO<sub>2</sub> (Yu et al. 2010b, Yu et al. 2012), sulphur (S) (Yu et al. 2010), nitrogen (N) (Wanqin et al. 2013) and carbon (C) (Fotiou et al. 2016) have been utilized owing to their ability to modify the photocatalytic activity and morphology of TiO<sub>2</sub>. The presence of non-metal anions generally enhances the specific surface area, restrains the growth of crystallite size and increases the anatase phase percentage in TiO<sub>2</sub> photocatalyst. In addition, non-metal anions influence the redshift in the absorption spectra of doped TiO<sub>2</sub> and broadens its band gap. Therefore, various photoelectrochemical, photochemical and photocatalytic activities of TiO<sub>2</sub> are improved by transferring its wavelength sensitivity from the ultraviolet region to the visible light region (Ansari et al. 2016).. A list of properties of various non-metal dopants of TiO<sub>2</sub> is summarized in Table 2.



**Table 2.4:** Properties of various non- metal dopants of TiO<sub>2</sub>

Metal Dopant	Metal/TiO <sub>2</sub> (molar ratio)	Synthesis method	Starting material of TiO <sub>2</sub>	Starting material of metal dopants	Crystallite size (nm)	Phase	BET surface area (m <sup>2</sup> /g)	Ref
P	0.020	Hydrothermal	TNBT	H <sub>3</sub> PO <sub>2</sub>	14.50	Anatase	104.00	(C. Jin 2009)
P	0.140	Sol gel	TiO <sub>2</sub> Degussa P25	H <sub>3</sub> PO <sub>4</sub>	8.60	Anatase/rutile	154.00	(K. J. A. Raj 2009)
N	0.265	Hydrothermal	TiO <sub>2</sub> Degussa P25	TEA	15.40	Anatase/rutile	—	(F. Peng 2008)
N	1.600	Hydrothermal	TTIP	CH <sub>3</sub> CH <sub>2</sub> NH <sub>2</sub>	25.40	Anatase	—	(Philip 2010)
S	1.500	Hydrothermal	TiCl <sub>4</sub>	CS(NH <sub>2</sub> ) <sub>2</sub>	30.00	Anatase	—	(H. Tian 2009)
S	2.800	Hydrothermal	TiS <sub>2</sub>	TiS <sub>2</sub>	2.80	Anatase	—	(W. K. Ho 2006)

### 2.8.3 Effect of metalloid and halogen doping

Recently, halogen doping techniques have attained much attention due to their ability to substitute in the  $\text{TiO}_2$  structure as well as to improve optical and surface properties. This technique is usually employed to hinder the transformation of anatase to rutile phase in  $\text{TiO}_2$ -doped photocatalysts. Accordingly, different halogen dopants, such as fluorine (F) (Yu et al., 2009a), bromine (Br) (Wang et al., 2017) and iodine (I) (Zhang et al., 2011) have been investigated in terms of modifying the morphology and photocatalytic activity of  $\text{TiO}_2$ . Boron (B) (Yu et al., 2013a) and silicon are two common metalloids used to dope  $\text{TiO}_2$ , which can be termed either non-metal or metal.

Boron dopants are proven to increase the surface area of B-doped  $\text{TiO}_2$ , inhibit the growth of  $\text{TiO}_2$  crystalline structure and induce the crystalline process. Some researchers contend that silicon dopants increase the thermal stability of anatase and suppress the transformation of anatase to rutile phase. A list of properties of various metalloid and halogen dopants of  $\text{TiO}_2$  is summarized in Table 2.5.

**Table 2.5:** Properties of various metalloids and halogen dopants of TiO<sub>2</sub>

Metal Dopant	Metal/TiO <sub>2</sub> (molar ratio)	Synthesis method	Starting material of TiO <sub>2</sub>	Starting material of metal dopants	Crystallite size (nm)	Phase	BET surface area (m <sup>2</sup> /g)	Ref
<b>Metalloid</b>								
B	0.001	Hydrothermal	Ti(OBu) <sub>4</sub>	NaBH <sub>4</sub>	2.59	Anatase	268.31	(J. R. Xiao 2006)
B	9.000	Sol gel	Ti(OBu) <sub>4</sub>	VO(OPr) <sub>3</sub>	6.00	Anatase	127.00	(J. J. Xu 2009)
B	0.040	Sol gel	TTIP	H <sub>3</sub> BO <sub>3</sub>	—	Anatase	219.00	(A. Zaleska 2008)
B	0.148	Sol gel	TiO <sub>2</sub>	(C <sub>2</sub> H <sub>5</sub> O) <sub>3</sub> B	7.00	Anatase	192.00	(E. Grabowska 2009)
Si	0.111	Destabilization	HFTA	HFSA	6.50	—	155.00	(M. Estruga 2010)
Si	0.030	Hydrothermal	Ti(OC <sub>4</sub> H <sub>9</sub> ) <sub>4</sub>	(C <sub>2</sub> H <sub>5</sub> ) <sub>4</sub> SiO <sub>4</sub>	8.20	Anatase	191.70	(R. Jin 2009)
Si	0.150	Templating	TBOT	TEOS	10.00	Anatase	120.00	(C. He 2010)
<b>Halogen</b>								
F	0.050	Hydrothermal	Ti(OC <sub>3</sub> H <sub>7</sub> ) <sub>4</sub>	NH <sub>4</sub> F	—	Anatas	48.00	(J. G. Yu 2009)
F	0.500	Hydrothermal	TBOT	NH <sub>4</sub> HF <sub>2</sub> -H <sub>2</sub> O	11.20	Anatas	122.00	(H. Sun 2010)
F	0.770	Hydrothermal	TIP	NaF	10.00	Anatas	148.00	(K. Mori 2008)
F	0.039	Sol gel	Ti(C <sub>2</sub> H <sub>5</sub> O) <sub>4</sub>	CF <sub>3</sub> COOH	13.20	Anatas	—	(N. Todorova 2008)
F	0.190	Spray pyrolysis	H <sub>2</sub> TiF <sub>6</sub>	H <sub>2</sub> TiF <sub>6</sub>	—	Anatas	27.10	(D. Li 2005)
F	0.001	Sol gel	Ti(OBu) <sub>4</sub>	NH <sub>4</sub> F	3.78	Anatas	169.48	(J. Xu 2008)
I	0.033	Hydrothermal	TTIP	HIO <sub>3</sub>	5.50	Anatase/brookite	137.60	(Q. Zhang 2011)
I	0.117	Hydrothermal	TNBT	KI	4.46	Anatase	184.87	(W.-A.Wang 2011)
I	0.025	Sol gel	Ti(OBu) <sub>4</sub>	HIO <sub>3</sub>	5.50	Anatase	259.10	(Y.Ma 2011)

#### **2.8.4 Effect of Co-doping**

The highest improvement in TiO<sub>2</sub> morphology is obtained by co-doping technique with double metal or double non-metal dopants or double metal/non-metal dopants. The co-doping technique shifts the wavelength absorption of TiO<sub>2</sub> from the ultraviolet to the visible light region, enhances the morphological properties of crystallite size and surface area, and withstands the anatase-to-rutile phase transformation. Although TiO<sub>2</sub> improvement is achievable under visible light and an optimal doping level, beyond this level the TiO<sub>2</sub> activity may deteriorate.

#### **2.8.5 Coupling of TiO<sub>2</sub> with other semi-conductors**

Different dopant categories for improving TiO<sub>2</sub> morphology, crystallinity, surface area and photocatalytic activity have been introduced and investigated. One technique of making TiO<sub>2</sub> suitable for receiving and utilizing visible light and improving its morphology is to couple it with another semi-conductor such as SiO<sub>2</sub>, MoO<sub>3</sub>, CdS, MgO, WO<sub>3</sub>, SnO<sub>2</sub>, Cu<sub>2</sub>O, In<sub>2</sub>O<sub>3</sub> or ZnO (Wu, 2006). According to the literature, the energy level and surface area of TiO<sub>2</sub> increase by mixing it with another photocatalyst. Besides, the light absorption range shifts towards visible light due to the reduction of band gap energy level when TiO<sub>2</sub> is doped with a semiconductor catalyst (Chin-Chuan Liu, 2006). Its photoactivity can then improve by reducing the recombination rate of the electron-hole pairs and by enhancing the interfacial charge transfer efficiency (Jongnavakit, 2012).

Among diverse semiconductors, ZnO is a suitable alternative for coupling with TiO<sub>2</sub> as it has similar band gap energy (around 3.37 eV) and hence similar photocatalytic activity. Moreover, it is low-cost and satisfies the performance in the degradation of several organic contaminants (Hadj Benhebal, 2013). It has additionally been found that ZnO is as reactive as TiO<sub>2</sub> under sunlight. Besides, these semi-conductors share

some advantages.  $\text{TiO}_2$  tends to have higher chemical stability while  $\text{ZnO}$  tends to have higher conductivity than  $\text{TiO}_2$ .  $\text{TiO}_2$  has a much higher dielectric constant and fewer defect states, which leads to less recombination, whereas  $\text{ZnO}$  can be easily nanostructured.

Heterojunction photocatalyst systems improve the photocatalytic behavior of doped photocatalysts. Heterojunction photocatalyst systems exhibit improved charge separations and increased lifetimes of the charge carriers (Fagan et al., 2016). In 2014 Rawal doped the W ions into the crystal lattice of  $\text{SnO}_2$  and conduction band was lowered position of  $\text{SnO}_2$ . Coupling of W-Doped  $\text{SnO}_2$  and  $\text{TiO}_2$  can absorb a considerable portion of visible light (Rawal et al., 2014). Coupling of W-Doped  $\text{SnO}_2$  and  $\text{TiO}_2$  heterojunction shows a significant activity of  $\text{TTO}_5/\text{TiO}_2$  which is mainly attributed to the inter-semiconductor hole transport mechanism (Rawal et al., 2014).

In the  $\text{TiO}_2/\text{ZnO}$  heterojunction, the conduction band (CB) of  $\text{ZnO}$  is positioned above the conduction band of  $\text{TiO}_2$  and valance band of  $\text{ZnO}$  is positioned between the valance band and conduction band of  $\text{TiO}_2$ , which suppresses the recombination of electron hole pair and promotes the separation of this pair, improving the photocatalytic activity consequently (Khaki et al. 2016). The combination of  $\text{TiO}_2$  and  $\text{ZnO}$  offers a wide range of advantages and is the most suitable candidate for widespread environmental applications due to chemical and biochemical inertness, strong oxidation power, long-term stability against chemical and/or photo-corrosion and cost effectiveness. Doping of Cu in  $\text{TiO}_2/\text{ZnO}$  shifts the absorption edges to the visible region. Copper directly traps the electrons generated from the excitation of doped Cu- $\text{ZnO}$  or Cu- $\text{TiO}_2$  catalyst. The doping process with the generation of charge trapping sites reduces the electron-hole recombination rate during photocatalysis.

## **2.9 Operational factors effecting the photocatalytic degradation**

Doping of TiO<sub>2</sub> with various types of transition metals can produce impurity states between the valance and conduction bands, which causes band gap narrowing and increased photo-efficiency of TiO<sub>2</sub>. The preparation methods influence the photocatalyst structure and activity. TiO<sub>2</sub> doped with metal ions used in the sol-gel technique offers many advantages, such as flexibility of introducing dopants in large concentrations, homogeneity and ease of processing. Dopant concentration and calcination temperature affect the photocatalyst structure by changing the crystal size, particle size, surface area and band gap energy level.

In general, the doping technique is an effective method of improving the morphology and activity of TiO<sub>2</sub>. However, different parameters may affect the efficiency of this method and are explained subsequently.

### **2.9.1 Effect of calcination temperature of nano-doped-TiO<sub>2</sub>**

Calcination is a thermal process in the presence of oxygen or air that is commonly applied in the formation of photocatalysts in order to facilitate phase transition, thermal decomposition, or the removal of a volatile fraction. Accordingly, applying calcination to doped-TiO<sub>2</sub> formation can also improve its photocatalytic activity, morphology, surface area and crystallinity properties as well as the photocatalyst's optical absorption. However, there is an optimal temperature for calcination, beyond which the photocatalytic activity may be reduced due to the agglomeration of particles that decrease the specific surface area of the photocatalyst. High calcination temperature induces the replacement of nitrogen by oxygen in the air. Therefore, photocatalyst absorption in the visible light region decreases, followed by a decrease in TiO<sub>2</sub> activity.

### **2.9.2 Effect of dopant concentration**

The photocatalytic activity of photocatalysts has been found to be directly and extremely proportional to dopant concentration. However, beyond an optimal amount of dopant in the photocatalyst structure, the photocatalytic performance decreases.

### **2.9.3 Effect of initial concentration**

The effect of the initial reactant concentration is a determining factor in the photocatalytic activity of doped TiO<sub>2</sub> in pollutant degradation. The relationship between the photocatalytic activity of TiO<sub>2</sub> and initial reactant concentration is affiliated with the adsorption of reactant on the photocatalyst surface and the screening effect due to reactant overloading. The photocatalytic activity of TiO<sub>2</sub> normally decreases as the initial reactant concentration increases. This may be attributed to the limited number of active sites available on the photocatalyst surface.

### **2.9.4 Effect of photocatalyst concentration**

Employing an optimum photocatalyst concentration minimizes cost and energy while maximizing photocatalytic performance. However, it has frequently been reported that increasing the photocatalyst concentration enhances the number of photons absorbed on the photocatalyst surface, subsequently increasing the generation of electron-hole pairs and the number of hydroxyl radicals. Nonetheless, the amount of organic pollutants adsorbed on the photocatalyst surface increases, which contributes to higher degradation efficiency (Kaur & Kansal 2016). Table 2.6 presents the effects of photocatalyst concentration and operational conditions on the degradation of industrial pollutants.

**Table 2.6:** Effect of photocatalyst concentration and operational condition on degradation of industrial pollutant

No	Doped catalyst	Target pollutant	Operational condition					Out come		Ref
			UV	pH	T (°C)	concentration	TOC	COD	Photocatalytic degradation	
1	Co-TiO <sub>2</sub>	2-chlorophenol	228 420 nm		22 °C	10–50 mg/L	–	–	Highest degradation at 600 °C	(C. Ad'an 2009)
2	Mn-dopdTiO <sub>2</sub>	methylene blue	310-400 nm		24–27 °C	100mg	–	–	99% reduction rate	(H. Abe 2006)
3	V- TiO <sub>2</sub> 2.8g/l	methylene blue	420	5.5	25 °C	2.8 g/l	–	–	Decrease 15-30%	(W. Sun 2008)
4	B- TiO <sub>2</sub> 2.8 g/l	methylene blue	420	5.5	25 °C	2.8 g/l	–	–	Decrease 2–3%	(W. Sun 2008)
5	TiO <sub>2</sub> -Cu	methylene blue	665	6.5	25 °C	10 mg	–	–	degradation >95%	(Liu 2005, Carvalho 2013)
6	Pr- TiO <sub>2</sub>	phenol	365 577	6.5 6.8	25 °C	0.2–1.0 g/L	–	–	99 -50% degradation	(M. Huang 2008)
7	TiO <sub>2</sub> -Cu	phenol	365	–	25 °C	1 g/l	–	–	Best photocatalytic activity calcined at 600 °C	(W.C.Hung 2007)
8	V <sup>5+</sup> -TiO <sub>2</sub>	chlorpyrifos	350-400	5.89	25 °C	0.1%	–	–	least activity	(Y. Ishibai 2008)
9	Th <sup>4+</sup> -TiO <sub>2</sub>	chlorpyrifos	350-400	5.89	25 °C	0.06%	–	–	highest activity	(Y. Ishibai 2008)
10	Mo <sup>6+</sup> -TiO <sub>2</sub>	chlorpyrifos	350-400	5.89	25 °C	0.06%	–	–	highest activity	(Y. Ishibai 2008)
11	Zn <sup>2+</sup> -TiO <sub>2</sub>	Congo Red (CR)	456	–	25 °C	100 mg	–	–	78 %	(J. R. Xiao 2006)
12	V <sup>5+</sup> -TiO <sub>2</sub>	Congo Red (CR)	456	–	25 °C	100 mg	–	–	44 %	(J. R. Xiao 2006)
13	N- TiO <sub>2</sub>	methylene blue	400	–	25 °C	100mg	–	–	87%, 93% and 95%	(C. Wang 2010)
14	Cu-ZnO	methylene blue	200-800	–	25 °C	0.5% mol	–	–	highest photocatalytic activity	(M. Bettinelli 2007)
15	Er <sup>3+</sup> -TiO <sub>2</sub>	methylene blue	365	–	25 °C	0.1 g	–	–	50%	(C. Jin 2009)
16	Sn- TiO <sub>2</sub>	penicillin solution	365	–	25 °C	0.1 g	–	–	3mol.% mol of photocatalyst have a high activity	(K. J. A. Raj 2009)

(continued on next page)



Table Continue 2.6

No	Doped catalyst	Target pollutant	Operational condition						Out come	Ref
			UV	pH	T (°C)	concentration	TOC	COD		
17	N- TiO <sub>2</sub>	Azo Dyes	250-450	–	25 °C	10 mg l <sup>-1</sup>	60%	–	95%	(Liu 2005)
18	ZrO <sub>2</sub> - TiO <sub>2</sub>	phenol	365	6.2	25 °C	–	–	–	54%, 61% and 62%	(Philip 2010)
19	Fe <sup>3+</sup> -TiO <sub>2</sub>	phenol	365	5	25 °C	0.5 mol%	–	–	55.2% to 65.68%	(H. Tian 2009)
20	Fe <sup>3+</sup> -TiO <sub>2</sub>	real textile wastewater	35 kHz	3-11	25 °C	6 g/L	49.8%	59.4%	79.9%	(W. K. Ho 2006)
21	Bi <sup>3+</sup> - TiO <sub>2</sub>	methylparathion	365	–	25 °C	0.25 g	–	–	97%	(J. J. Xu 2009)
22	Zn- TiO <sub>2</sub>	Methylene blue	352	–	25 °C	–	–	–	46.3 to 91.4%	(A. Zaleska 2008)
23	Fe-TiO <sub>2</sub>	Azo Dyes	400	6.5	35°C	0.5 g L <sup>-1</sup>	–	–	60%	(E. Grabowska 2009)
24	Yttrium-TiO <sub>2</sub>	methyl orange	365	<3->4	25 °C	50 ml	–	–	20%	(M. Estruga 2010)
25	Sm <sup>3+</sup> - TiO <sub>2</sub>	Methylene blue	664	–	25 °C	200 mg	–	–	73.90%	(R. Jin 2009)
26	Pd- ZnO	Methyl orange	365	7	25 °C	50 mg	–	–	48.2%	(C. He 2010)
27	Fe-TiO <sub>2</sub>	Dye	–	–	25 °C	–	–	33%	–	(Li 2010)
28	Ag/F-TiO <sub>2</sub>	phenol	420 nm	–	25 °C	–	–	–	0.50Ag/F-TiO <sub>2</sub> highest activity	(F. Peng 2008)

For a photocatalyst to be highly efficient in pollutant degradation, it should possess a low band gap energy level and high specific surface area. The best way to increase the adsorption capacity of zinc oxide and titanium dioxide is to use a support with reduced energy, high porosity and high surface area. According to Table 2.6, Bi<sup>3+</sup>, Mn and Cu-doped TiO<sub>2</sub> and ZnO display high photocatalytic efficiency. Degradation results showed that copper-doped TiO<sub>2</sub> enhanced the photoactivity. Moreover, incorporating Cu<sup>2+</sup> into the TiO<sub>2</sub> crystal structure as Cu-doped TiO<sub>2</sub> demonstrated high activity under visible light. Nanocrystal Mn-doped TiO<sub>2</sub> displayed high photocatalytic activity under UV and visible light, where the range of methylene blue degradation was 99%. Bi<sup>3+</sup>-doped TiO<sub>2</sub> with the sol-gel process boosted methyl parathion degradation under UV light by 97%. In the case of copper-doped TiO<sub>2</sub>, results indicated that Cu/TiO<sub>2</sub> boosted methylene blue degradation by over 95% under visible light. Cu-doped ZnO calcined at 600°C achieved the highest photoactivity under UV and visible light..

### **2.9.5 Preparation methods of doped-photocatalysts**

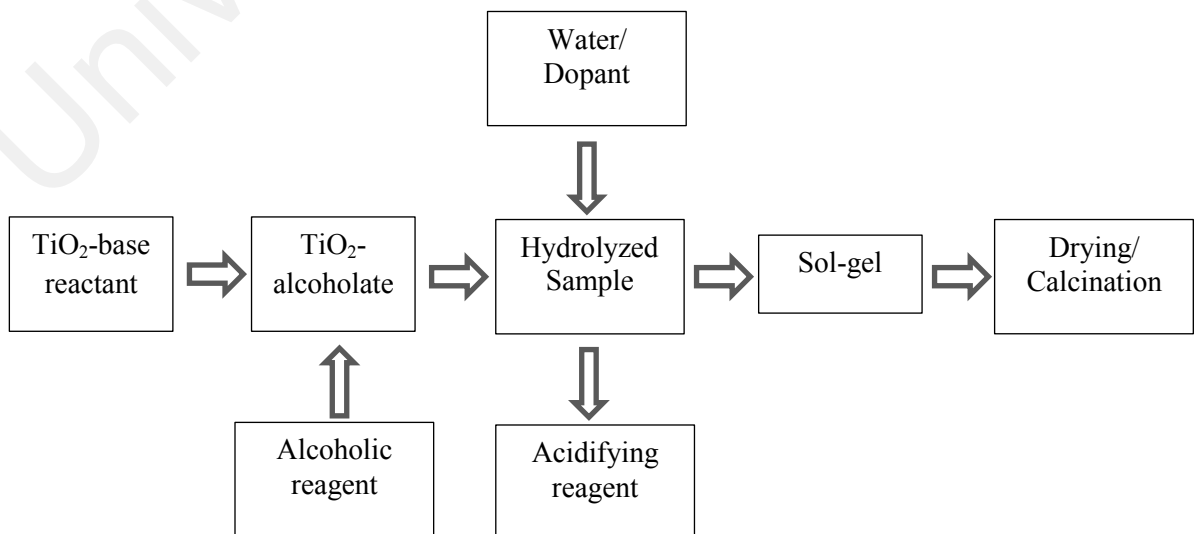
The effect of doping on photocatalytic activity depends on the type of compound as well as method employed (Colon, 2006) Preparation methods used for catalyst doping include sol-gel (Barakat, 2005), microemulsion (Adan, 2007), co-precipitation (Anandan, Vinu et al., 2007), hydrothermal process (Asilturk, 2009) and solvothermal synthesis (He, 2013).

Nevertheless, the advantages derived from synthesis of TiO<sub>2</sub>-based-photocatalyst by sol-gel method, which include synthesis of nano-sized crystallized powder of high purity at atmospheric pressure, relatively low temperature, possibility of stoichiometry controlling process have suggested by many researchers.

### 2.9.6 Sol-gel method

A lot of research has reported the use of the sol-gel method for catalyst doping. The sol-gel process has been successfully employed in preparing glassy materials, ceramic powders, and dense or porous ceramic pieces, as well as for thin film deposition and biosensor construction. The materials obtained from these processes can also be used in selective heterogeneous catalysis, which represents an area of great economical interest. Nowadays, sol-gel methods are well-established, as they allow the preparation of a broad variety of supported metals, metal oxides, coatings and composite materials with tailored properties. The sol-gel process has been applied in preparing supported metal catalysts and catalyst supports with higher thermal stability and resistance to deactivation while providing better flexibility in controlling catalyst properties, such as particle size, surface area and pore size distribution. Many authors have suggested sol-gel as the best means of dispersing catalytic metals in gels with fine texture (Gonçalves, 2006).

Sol-gel is a wet-chemical technique and one of the most widely used means of photocatalysts preparation. This method is mainly used to produce catalyst powders or thin films. A brief schematic diagram of this process is presented for TiO<sub>2</sub>-based photocatalysts in Figure 2.5.



**Figure 2.5:** Process of Sol-gel method

Generally, the sol-gel method is inexpensive, easy to operate and often achievable at low operational temperatures. This process can easily be used for the deposition of substrates that have large surface areas or complex surfaces. The sol-gel method is usually started with a chemical solution that behaves as a precursor for an integrated gel (or network) of either network polymers or discrete particles. Metal alkoxides such as  $\text{TiO}_2$  can be precursors. In fact, a gel-like diphasic system prepared with this method contains both solid and liquid phases. In the last step, the solvent should be removed from the produced structure through a drying process, which is accompanied by notable densification and shrinkage. The distribution of porosity in the gel is a determinant factor in the drying process. The final microstructure is prominently affected by changes imposed upon the structural template during drying. Afterwards, a firing process, or thermal treatment, is applied in order to enhance the structural stability and mechanical properties. Different types of sol-gel and related methods of  $\text{TiO}_2$  doping include co-doping, alkaline earth metal ions, rare earth metal ions, transition metal ions and other metal/non-metal ions. A brief list of applications and efficiency of  $\text{TiO}_2$ -based photocatalysts prepared through the sol-gel method is presented in Table 2.7.

As observed, co-doping of  $\text{TiO}_2$  improves the catalyst's photocatalytic activity in most cases. Doping  $\text{TiO}_2$  with alkaline earth metals through the sol-gel method also provides better photocatalysis for  $\text{TiO}_2$  than through the co-precipitation method. On the contrary,  $\text{TiO}_2$  doping with transition metals is not useful for photocatalytic efficiency, except in very few cases.

Coupled semiconductor photocatalyst of  $\text{TiO}_2/\text{ZnO}$  has been investigated by a number of researchers for improving the photodegradation efficiency of  $\text{TiO}_2$  catalyst. Besides, the triple complex of  $\text{TiO}_2/\text{ZnO}$  with some metals has also been investigated in a few studies. However, based on the knowledge of the author, the triple complex of Cu-

TiO<sub>2</sub>/ZnO has not yet been studied. Cu appears to improve the photocatalytic band gap of Cu-TiO<sub>2</sub> and Cu-ZnO separately. This is attributed to the presence of two electrons in the valence layer of Cu, which enables electron transfer. Therefore, TiO<sub>2</sub> is doped with both ZnO and Cu in parallel in the present study. The main aim is to reduce the band gap energy of Cu-TiO<sub>2</sub>/ZnO in order to improve its activity. Therefore, a new hybrid photocatalyst, namely Cu-doped TiO<sub>2</sub>/ZnO nano-catalyst is fabricated by entrapping copper ions in the crystalline matrix of TiO<sub>2</sub> and ZnO through the sol-gel synthesis method. The new doped photocatalyst is calcined at two different temperatures of 500°C and 700°C. The photoactivity of Cu-doped TiO<sub>2</sub>/ZnO is then evaluated through the degradation of methyl orange (MO) and methylene blue (MB) under visible light irradiation.

**Table 2.7:** Sol gel method for preparation doped catalyst

Doped catalyst	Material and conc		Parameter			Catalyst characteristics			Ref
			T (°C)	pH	SA m <sup>2</sup> g <sup>-1</sup>	BG	CS nm	PS nm	
Co-TiO <sub>2</sub>	Co(III)0.0040.14mol%	TiCl <sub>4</sub> 98%	200 -900	-	39.7	-	-	25	(Barakat 2005)
Mn-dopdTiO <sub>2</sub>	Mn (II) 0.1 M	Ti(OCH(CH <sub>3</sub> ) <sub>2</sub> ) <sub>4</sub>	700	7	38	-	20–30	-	(Binas 2012)
V- TiO <sub>2</sub>	Ti(OBu) <sub>4</sub>	6.0 ml	500	-	139	-	10.5	-	(Bettinelli 2007)
B- TiO <sub>2</sub>	Ti(OBu) <sub>4</sub>	17.0 ml	450	-	107	-	12	-	(Bettinelli 2007)
TiO <sub>2</sub> -Cu	Ti(O-Pr) <sub>4</sub>	5ml CuSO <sub>4</sub> ·5H <sub>2</sub> O 170 mg	400 500	-	-	-	107	-	(Carvalho 2013)
Pr- TiO <sub>2</sub>	(Ti[ <i>iso</i> -OC <sub>3</sub> H <sub>7</sub> ] <sub>4</sub> )	0.12 mol	100 800	1.8	40	2.80 and 3.10 eV	-	10–50	(Chiou 2007)
TiO <sub>2</sub> -Cu	TTIP	10 ml, Cu(NO <sub>3</sub> ) <sub>2</sub> 0.5 M%	400 800	-	2	3.00	34	-	(Colon 2006)
V <sup>5+</sup> -TiO <sub>2</sub>	TiCl <sub>4</sub>	25 ml [NH <sub>4</sub> VO <sub>3</sub> ]	550	7-8	24	2.7	28.42	-	(Devi 2009)
Th <sup>4+</sup> -TiO <sub>2</sub>	TiCl <sub>4</sub>	25 ml [Th(NO <sub>3</sub> ) <sub>4</sub> ]	550	7-8	32	3.00	30.28	-	(Devi 2009)
Mo <sup>6+</sup> -TiO <sub>2</sub>	TiCl <sub>4</sub>	25 ml (NH <sub>4</sub> ) <sub>6</sub> Mo <sub>7</sub> O <sub>24</sub> ·4H <sub>2</sub> O	550	7-8	22	2.7	29.38	-	(Devi 2009)
Zn <sup>2+</sup> -TiO <sub>2</sub>	TiCl <sub>4</sub>	25ml	550	7-8	31	2.8	15.6	-	(Devi 2010)
V <sup>5+</sup> -TiO <sub>2</sub>	TiCl <sub>4</sub>	25ml	550	7-8	24	2.8	28.4	-	(Devi 2010)
N- TiO <sub>2</sub>	Titanium (IV)	Na <sub>2</sub> EDTA	500	-	58	3.06	-	9.6	(Elghniji 2012)

(continued on next page)

Table 2.7, continued

Doped catalyst	Material and conc	Parameter		Catalyst characteristics				Ref
		T (°C)	pH	SA m <sup>2</sup> g <sup>-1</sup>	BG	CS nm	PS nm	
Cu-ZnO	Zn(CH <sub>3</sub> COO) <sub>2</sub> ·2H <sub>2</sub> O 0.3 M Cu(CH <sub>3</sub> COO) <sub>2</sub> ·H <sub>2</sub> O	400	-	-	-	3.294	-	(Jongnavakit 2012)
Er <sup>3+</sup> -TiO <sub>2</sub>	Ti[O(CH <sub>2</sub> ) <sub>3</sub> CH <sub>3</sub> ] <sub>4</sub> 3.5 g ErCl <sub>3</sub>	500	-	-	3.09	10.0	-	(Lee 2012)
Sn- TiO <sub>2</sub>	Ti(OC <sub>4</sub> H <sub>9</sub> ) <sub>4</sub> (AR) 5 ml	450	9	399	3.6	-	-	(Li 2009)
Fe-TiO <sub>2</sub>	Ti(OC <sub>4</sub> H <sub>9</sub> ) <sub>4</sub> Fe(NO <sub>3</sub> ) <sub>3</sub>	500	7-8	338.7	-	-	-	(Li 2010)
Ag/F-TiO <sub>2</sub>	Ti(OBu) <sub>4</sub> Ag(NO <sub>3</sub> )	623 K	-	179.6	2.35	5.2	-	(Lin 2012)
N- TiO <sub>2</sub>	Ti[OCH (CH <sub>3</sub> ) <sub>2</sub> ] <sub>4</sub> 9ml	400	-	-	-	-	10	(Liu 2005)
ZrO <sub>2</sub> - TiO <sub>2</sub>	Ti(OCH <sub>2</sub> CH <sub>2</sub> CH <sub>2</sub> CH <sub>3</sub> ) <sub>4</sub> 14ml Ti:acac, (Zr(acac) <sub>4</sub> )	400 1000	-	- 140.4	-	- 1.8	-	(McManamon 2011)
Fe <sup>3+</sup> -TiO <sub>2</sub>	TBOT 0.1 mol Fe(NO <sub>3</sub> ) <sub>3</sub> ·9H <sub>2</sub> O	450	-	-	-	8.3	-	(Naeem 2010)
Fe <sup>3+</sup> -TiO <sub>2</sub>	Ti(OBu) <sub>4</sub> Fe(NO <sub>3</sub> ) <sub>3</sub> ·9H <sub>2</sub> O	500	3	167.6	2.70	-	10	(Pang and Abdullah 2013)
Bi <sup>3+</sup> - TiO <sub>2</sub>	Ti(O-Bu) <sub>4</sub> 21 ml	500	-	-	-	16-22	-	(Rengaraj 2006)
Zn- TiO <sub>2</sub>	TTIP ZnSO <sub>4</sub> ·7H <sub>2</sub> O	450	-	101.27	-	14.03	-	(Ryu 2011)
Fe-TiO <sub>2</sub>	(Fe(NO <sub>3</sub> ) <sub>3</sub> ·9H <sub>2</sub> O TTIP 8.87 mL	200	-	118	3.06	8.91	-	(Vargas 2012)
Yttrium-TiO <sub>2</sub>	(Y(NO <sub>3</sub> ) <sub>3</sub> ·6H <sub>2</sub> O) Ti(OBu) <sub>4</sub> 10ml	823 K	-	69.0	-	11.5	-	(Wang 2011)
Sm <sup>3+</sup> - TiO <sub>2</sub>	(Ti (OPri) <sub>4</sub> ) Sm (NO <sub>3</sub> ) <sub>3</sub>	600	6-7	82.94	-	12.80	-	(Xiao 2008)
Pd- ZnO	Zn(O <sub>2</sub> CCH <sub>3</sub> ) <sub>2</sub> Pd(NO <sub>3</sub> ) <sub>2</sub>	773 K	-	6.49	-	33	-	(Zhong 2012)

## 2.10 Summary of literature review

Non-biodegradable organic waste entails compounds that cannot be naturally recycled into the life cycle, as they cannot break down into natural components. Advanced Oxidation Technology (AOT) is a robust treatment process for wastewater including non-biodegradable compounds. Four different methods are employed with AOTs to generate hydroxyl radicals and treat wastewater, which include (i) ozone treatment, (ii) electrochemical processes, (iii) direct decomposition of water, and (iv) photocatalysis. Among the various AOPs, heterogeneous photocatalytic processes are suitable for eliminating a broad range of pollutants at ambient temperatures and pressures without generating harmful intermediates. In the introduction section, the photocatalysis reaction was presented and  $\text{TiO}_2$  was introduced as one of the most efficient photocatalysts. Subsequently, the effects of different parameters (e.g. dopants and operational parameters) on  $\text{TiO}_2$  were investigated. Furthermore, different types of dopant (e.g. metal, non-metal, metalloid and halogen, co-doping) and coupling of  $\text{TiO}_2$  with other semi-conductors were investigated. In terms of operational parameters, the effects of calcination temperature on nano-doped  $\text{TiO}_2$ , dopant concentration, initial reactant concentration, and photocatalyst concentration, and preparation methods of doped photocatalysts were outlined.  $\text{TiO}_2$  and  $\text{ZnO}$  have wide band gaps of around 3.2eV and 3.3 eV at room temperature, hence they are mainly used under ultraviolet (UV) irradiation.  $\text{TiO}_2$  and  $\text{ZnO}$  photocatalysts also have the potential to be employed under visible light for greater energy efficiency. The photocatalytic activity of  $\text{TiO}_2$  and  $\text{ZnO}$  can be improved by reducing the band gap energy level. According to Table 2.7 metal-doped  $\text{TiO}_2/\text{ZnO}$  nano-size particles such as Ag, Fe, Mo and Cu can enhance photocatalytic activity. Especially copper was considered as one of the most effective doping elements for improving the activity of photocatalyst.



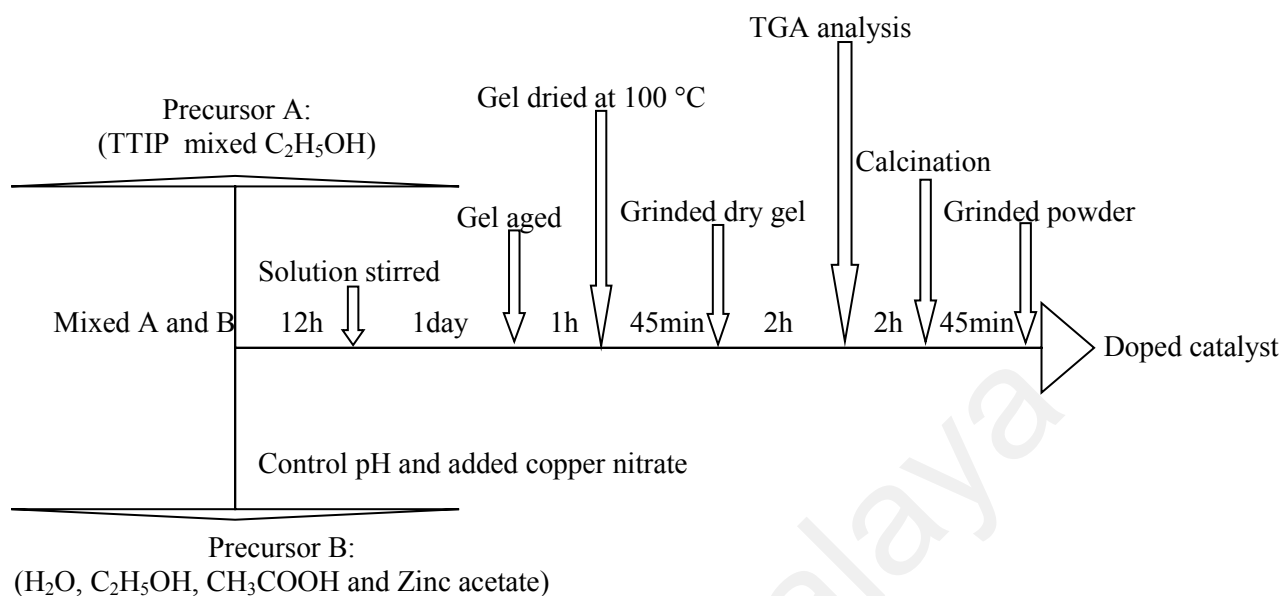
## CHAPTER 3: METHODOLOGY

### 3.1 Material

Titanium (IV) isopropoxide (TTIP,  $\text{Ti}[\text{OCH}(\text{CH}_3)_2]_4$ , 97%) used to synthesize titanium dioxide was purchased from Sigma Aldrich .U.S. Zinc acetate dihydrate ( $\text{Zn}(\text{CH}_3\text{COO})_2 \cdot 2\text{H}_2\text{O}$ , >98%) and Copper(II) nitrate trihydrate ( $\text{Cu}(\text{NO}_3)_2 \cdot 3\text{H}_2\text{O}$ , 99%) were purchased from Chemical U.K. Ethanol ( $\text{C}_2\text{H}_5\text{OH}$ >99.8%) for catalyst synthesis were purchased from Sigma Aldrich and Chemical .U.K. Acetic acid ( $\text{CH}_3\text{COOH}$ ,  $M=60.051\text{g/mol}$  and Purity=98%) and hydrochloric acid ( $\text{HCl}$ ,  $M=36.45\text{g/mol}$ , Purity=fuming 37%) used to control the ambient pH was also supplied by the same company, and sodium hydroxide ( $\text{NaOH}$ ,  $M=40.0\text{g/mol}$ , Purity= 99.99%) that were used to control the ambient pH were supplied by Merck. Methyl orange (MO,  $\text{C}_{14}\text{H}_{14}\text{N}_3\text{NaO}_3\text{S}$ ) and methylene blue (MB,  $\text{C}_{16}\text{H}_{18}\text{N}_3\text{SCl}$ ) employed for photocatalytic activity of the synthesised catalyst were purchased from Merck. All the chemicals were directly used as received without further purification.

### 3.2 Photocatalyst preparation

In the present study, Cu-ZnO/TiO<sub>2</sub> was synthesized using sol-gel method (Gao, Luan et al. 2011, Jongnavakit, Amornpitoksuk et al. 2012). Fig 3.1 shows a simplified diagram of the synthesis. The process includes three main steps, which are gel preparation, drying and calcination. In this study, the synthesis started with preparation of precursor A and B. For precursor A predetermined amount of TTIP was mixed with ethanol and stirred for an hour at room temperature to get a precursor solution. Then, a 30ml solution of distilled water, ethanol, acetic acid and zinc acetate (according to the weight ratio of TiO<sub>2</sub>: ZnO=70:30) were mixed together by continuous and tempestuous agitation to form a homogeneous solution (precursor B). Meanwhile, the solution pH



**Figure 3.1:** Diagram of catalyst synthesis process

value was controlled between 2.0 and 3.0 by adding a certain quantity of hydrochloric acid solution next a certain amount of Copper (II) nitrate trihydrate was added to precursor B with vigorous stirring for metal doping. Then, precursor B was dropped into precursor A at a speed of one drop per second under strong stirring. The produced mixture was continuously stirred for about 12 h to complete the sol-gel process and a transparent sol was then created. It was aged for one day to finish the sol-gel transition and evaporate excess alcohol. After that, it was thermally-treated in an electric oven at 100°C for 1h. In the next step, the catalysts went through the calcination process which was carried out in a Furnace (Thermconcept KL 15/11) with a heating rate of 10°C/min to almost the maximum temperature determined by the TGA process. Thermal process was conducted and analysed by a Thermo-Gravimetric Analyser (TGA) (TG-Q500, Research instrument, USA) in order to determine the calcination temperature. The synthesised catalysts were subjected to a heating process starting from the room temperature to the maximum temperature of 1000°C.

Calcination continued for 2 hours to regulate the molecular network and structure of the photocatalyst and to remove excess solvent. It should be noted that heating process was conducted before calcination and the results were analysed in order to determine the thermal resistance of the synthesised samples and the calcination temperature. The calcination continued for 2 hours with two desirable temperatures to make the molecular network and structure of the photocatalyst regular and remove excess solvent.

The nano-sized Cu-TiO<sub>2</sub>/ZnO was then obtained through ball milling process. It should be noted that, 5 different concentrations of Cu (1 to 5 wt%) and the TiO<sub>2</sub> to ZnO ratio of 7:3(wt%) were investigated. The effects of two different calcination temperatures of 500 and 700°C were considered as well. Cu content of 3wt% along with calcination temperature of 500°C provided the best characteristics for Cu-TiO<sub>2</sub>/ZnO.

Accordingly, Cu (3wt%)-TiO<sub>2</sub>/ZnO calcined at 500°C was synthesised, characterised and evaluated in this study. In order to evaluate and compare the photocatalytic activity of Cu-ZnO/TiO<sub>2</sub>, pure TiO<sub>2</sub> and ZnO/TiO<sub>2</sub> were also synthesized separately. In order to obtain the optimum result, two groups of samples were prepared. In the first group, the compositions of ZnO and Cu were varied while the amount of TiO<sub>2</sub> was constant. In the second group, the compositions of TiO<sub>2</sub> and Cu were varied while the amount of ZnO was constant. The details of sample preparation are presented in Table 3.1.

**Table 3.1:** Amount of Titanium Oxide, Copper Nitrate and Zinc Sulphate in two groups of synthesised catalyst.

(a)				
No	Wt.%	Ti(gm)	Zn(Ac) <sub>2</sub> .H <sub>2</sub> O(gm)	Cu(NO <sub>3</sub> ) <sub>2</sub> (gm)
1	1%	21.251	8.441	0.320
2	2%	21.251	8.150	0.641
3	3%	21.251	7.859	0.961
4	4%	21.251	7.568	1.282
5	5%	21.251	7.277	1.602
(b)				
No	Wt.%	Ti(gm)	Zn(Ac) <sub>2</sub> .H <sub>2</sub> O(gm)	Cu(NO <sub>3</sub> ) <sub>2</sub> (gm)
6	1%	20.947	8.732	0.320
7	2%	20.644	8.732	0.641
8	3%	20.340	8.732	0.961
9	4%	20.037	8.732	1.282
10	5%	19.733	8.732	1.602

### 3.3 Characterization of Photocatalyst

Thermo-Gravimetric Analyser (TG-Q500, Research instrument, USA) was employed to analyse the thermal stability of the synthesized photocatalysts. Quantity of the synthesized catalysts was subjected to heating process starting from the room temperature to the maximum temperature of 1000°C, under a dynamic nitrogen atmosphere. After that, the structural identifications and the phase purity of Cu-TiO<sub>2</sub>/ZnO samples were carried out by X-Ray Diffractometer (XRD) using an advanced X-ray diffraction (7602 EA Almelo, analytical Empyrean, Netherlands). It employed a scanning rate of 0.026° s<sup>-1</sup> in 2θ ranging from 20° to 80°. The morphology analysis was performed by Field Emission Scanning Electron Microscope (FESEM, model Quanta FEG 450, EDX-OXFORD). It operated at beam energy level of 10.00 kV under high vacuum level and spot size of 3.0. Transmission electron microscope (TEM) images were used to observe the internal structure of sample (ORIOUS SC1000). The microscope had accelerating voltage from 20 to 200kV and standard magnification from 22X to 930KX. The surface area of the sample was determined using Brunauer-Emmett-Teller BET method (micromeritics tristar 3020, analyser) using N<sub>2</sub> adsorption at 77K. Particle

size of the samples was approximated using a particle size analyser (Mss+Hydromu, Malvern instrument, U.K) operating in a range lens of 300 RF mm. The UV-vis (diffuse reflectance) spectra in the wave length range of 200-800 nm was obtained using a spectrophotometer equipped with an integrated sphere (UV-Vis-NIR spectrophotometer Uv-3600, Shimadzu, Japan). Accordingly, the band gap was determined through the Kubelka-Munk's model. The results were further compared with that estimated through Planck's equation.

### **3.4 Experimental design and statistical analysis**

The factorial design of experiments (DOE) along with statistical analysis of obtained results, is able to analyse the individual and interactive effects of parameters with a minimum number of experiments while eliminating systematic errors at the same time. In this study, a response surface methodology based on a 3-level, 5-factor central composite design was performed to investigate the effects of five independent numerical factors, develop of regression models and optimize conditions for photocatalytic degradation using the software Design Expert (Version 9.0.3, Stat-Ease Inc., USA). Initial dye concentration ranging from 20 to 50ppm, initial pH from 4 to 10, catalyst concentration from 0.3 to 0.7g/L, light irradiation intensity from 14 to 23Watt and reaction time from 40 to 120min were selected to evaluate the photocatalytic activity of synthesised Cu-TiO<sub>2</sub>/ZnO on degradation of two types of dye: Methyl Orange (MO) as an anionic- and Methylene Blue (MB) as a cationic-dye. These levels were selected according to available literature of similar works considering TiO<sub>2</sub> and ZnO properties as well as Cu dopant (Zhang et al. 2016). The degradation responses, photocatalytic efficiency (%), were investigated in terms of Color (YC), COD (YCOD) and TOC (YTOC) removals. The independent variables, X<sub>i</sub>, were converted to coded form  $\underline{x}_i$  for statistical calculations by Equation (3-1):

$$x_i = \frac{X_i - X_0}{\delta X} \quad (3-1)$$

where,  $X_0$  refers the value of  $X_i$  at the center of the domain and  $dX$  refers to the step change. Total 100 tests were conducted for both categorical variables in which 16 replications were at center points: [Catalyst]: 0.5g/L, [dye]: 35ppm, intensity of light irradiation: 18Watt, pH: 7 and reaction time of 80min; to determine the experimental error. The experimental conditions along with responses obtained for both MO and MB degradations were summarized in Table 3.4, respectively.

Afterwards, a second order polynomial equation correlating the effect of variables in terms of linear, quadratic and cross product terms was used to evaluate the efficiency of synthesised photocatalyst by illustrating the behaviour of selected responses as a function of individual and interactive effects of independent variables.

$$Y = b_0 + \sum_{i=1}^n b_i x_i + \sum_{i=1}^n b_{ii} x_i^2 + \sum_{j>i}^n \sum_{i=1}^n b_{ij} x_i x_j + \varepsilon \quad (3-2)$$

In this equation,  $Y$  is the predicted response,  $b_0$  is a constant term,  $b_i$ ,  $b_{ii}$  and  $b_{ij}$  are the coefficients for the linear, quadratic and cross product terms, respectively.  $x_i$  also denotes the coded variables and  $n$  refers to the number of variables. The models significance and adequacy were further evaluated by ANOVA (Analysis of Variance) and their fitness's were expressed by the coefficients of determination,  $R^2$ ,  $R_{adj}^2$  and  $R_{prod}^2$ . Fisher variation ratio (F-value), probability value (Prob>F) with 95% confidence level and adequate precision were also employed as the main indicators of the models.

$$Adequate\ precision = \frac{Y_{Max} - Y_{Min}}{\sqrt{\bar{V}(Y)}} \quad (3-3)$$

$$\bar{V}(Y) = \frac{1}{n} \sum_{i=1}^n \bar{V}(Y) = \frac{p\sigma^2}{n} \quad (3-4)$$

Here,  $Y$  is predicted response,  $\sigma^2$  is the residual mean square,  $p$  and  $n$  also refer the number of model parameters and experiments. The regression models for each categorical variable will be presented in Table 4.4, removal of color, COD and TOC were obtained after elimination of insignificant terms. In these models, positive coefficients indicate a synergistic effect, while negative coefficients, an antagonistic effect between or among the variables. Moreover, the three-dimensional plots were obtained based on the effect of the levels of the two factors. Finally, the operating parameters were optimized on the basis of the obtained models in order to achieve the maximum degradation level of the photocatalyst and extra experiments were conducted to assess the optimal conditions.

### **3.5 Adaptive neuro-fuzzy inference (ANFIS)**

Adaptive Neuro-Fuzzy Inference (ANFIS) was used to determine the performance of Cu-TiO<sub>2</sub>/ZnO in advanced oxidation reaction for water treatment by using the data obtained from the experiments. In short, ANFIS was used for variable search at first, known as “variable selection”; and then the same network was used to examine how the mentioned operating parameters influenced the photoactivity of copper-ZnO/TiO<sub>2</sub>.

The photo-degradation of both MO and MB using Cu-TiO<sub>2</sub>/ZnO was designed using Response Surface Methodology (RSM) provided by Design-Expert software Version 9.0.4.1 (Stat-Ease Inc., USA). A standard RSM design matrix, Central Composite Design (CCD) was employed to evaluate the dependency of photo-activity of the synthesised photocatalyst on operating conditions. Five independent operating parameters were identified including A: Initial dye concentration (20 to 50ppm), B: initial pH (4 to 10), C: catalyst loading (0.3 to 0.7g/L), D: light irradiation intensity (14 to 23Watt) and E: reaction time (40 to 120min). The responses chosen were color, COD and TOC removal. In this study,  $\alpha$  value, which is the distance of the axial point from

the center was fixed at 1. Accordingly, a face central composite which is not rotatable but easier to work with was used. The independent variables were coded at three levels:

1 (maximum), 0 (center), -1 (minimum). Eventually, a three-level-five-factor central composite design was employed to fit a third-order response surface model which required 50 experiments for degradation of each dye, including 32 factorial, 10 axial and one central point. The center point with the conditions of [Catalyst]: 0.5g/L, [dye]: 35ppm, intensity of light irradiation: 18Watt, pH: 7 and reaction time of 80 min were repeated 8 times to determine the experimental error and reproducibility of the data. The experiments were run randomly in order to minimize the errors from the systematic trends in the variables.

### 3.5.1 Variable selection methodology

In order to analyse the sensitivity of the photo-activity of Cu-TiO<sub>2</sub>/ZnO on the five independent operating parameters and to determine the influence of these 5 parameters on the efficiency of advanced oxidation reaction, ANFIS was employed.

#### 3.5.1.1 Input and output variable

Table 3.2 shows the 5 input parameters selected for the analysis and Table 3.3 lists the complete design matrix along with the responses of advanced oxidation reaction for MO and MB reduction.

**Table 3.2:** Independent numerical variables and their levels. (Input parameters For ANFIS)

Inputs	Parameters description	Symbol	Parameters characterization		
			Minimum Value	Middle Value	Maximum Value
input 1	PH	A-PH	4	7	10
input 2	Light Irradiation Intensity	B-LII	14	18.5	23
input 3	Dye Concentration(ppm)	C-[Dye]	20	35	50
input 4	Cu-TiO <sub>2</sub> /ZnO (mg)	D-[Cat]	0.3	0.5	0.7
input 5	Reaction Time	E-t	40	80	120



**Table 3.3:** Experimental design matrix and the final results of Methyl Orange & Methylene Blue removals. Using Response Surface Methodology (RSM) based on a 3 level and 5 factor.

Run No.	Experimental design					MO Removal (%)			MB Removal (%)		
	pH	Light	Dyes	Catalyst	Time	UV	COD	TOC	UV	COD	TOC
1	4	14	20	0.3	40	33.00	25.90	18.32	24.50	16.00	9.47
2	10	14	20	0.3	40	25.95	18.63	13.91	31.00	24.00	14.13
3	4	23	20	0.3	40	40.00	31.54	18.92	33.25	18.00	5.26
4	10	23	20	0.3	40	35.00	24.27	18.84	38.75	24.00	16.22
5	4	14	50	0.3	40	13.66	11.00	3.30	13.82	7.09	4.63
6	10	14	50	0.3	40	17.60	14.83	4.96	21.76	17.00	5.31
7	4	23	50	0.3	40	24.88	15.83	6.79	21.00	10.00	4.95
8	10	23	50	0.3	40	20.46	15.00	5.64	24.84	20.90	6.44
9	4	14	20	0.7	40	57.00	44.72	29.59	34.85	28.00	9.85
10	10	14	20	0.7	40	42.50	32.00	17.79	49.95	44.00	31.84
11	4	23	20	0.7	40	63.00	52.18	31.38	38.90	32.00	11.62
12	10	23	20	0.7	40	47.00	37.63	19.18	56.00	48.00	33.23
13	4	14	50	0.7	40	36.40	33.00	23.43	19.34	18.00	2.75
14	10	14	50	0.7	40	19.20	16.33	6.89	36.80	25.63	12.16
15	4	23	50	0.7	40	45.60	39.83	26.50	26.20	23.00	6.70
16	10	23	50	0.7	40	28.80	23.16	10.88	42.94	31.45	14.20

(continued on next page)

Table 3.3, continued

Run No.	Experimental design					MO Removal (%)			MB Removal (%)		
	pH	Light	Dyes	Catalyst	time	UV	COD	TOC	UV	COD	TOC
17	4	14	20	0.3	120	45.95	32.27	25.24	33.45	26.00	14.17
18	10	14	20	0.3	120	41.55	28.09	22.66	37.50	28.00	19.32
19	4	23	20	0.3	120	59.00	49.09	35.09	41.00	22.00	7.49
20	10	23	20	0.3	120	49.50	39.72	25.92	46.35	34.00	19.33
21	4	14	50	0.3	120	36.44	30.16	20.23	18.80	12.00	7.66
22	10	14	50	0.3	120	22.50	16.83	13.28	30.46	26.36	20.57
23	4	23	50	0.3	120	52.60	41.36	25.40	29.88	16.90	8.95
24	10	23	50	0.3	120	39.76	31.33	22.56	38.86	31.45	24.89
25	4	14	20	0.7	120	79.80	69.72	53.26	44.15	36.00	19.41
26	10	14	20	0.7	120	58.00	49.09	30.09	71.00	66.00	45.64
27	4	23	20	0.7	120	83.35	73.54	54.46	59.00	48.00	27.24
28	10	23	20	0.7	120	64.55	52.90	31.40	75.50	68.00	46.41
29	4	14	50	0.7	120	55.68	43.00	30.56	25.98	16.90	3.12
30	10	14	50	0.7	120	33.20	24.66	16.96	48.00	38.72	25.98
31	4	23	50	0.7	120	56.80	43.83	29.66	32.00	21.81	5.22
32	10	23	50	0.7	120	34.88	25.50	16.16	54.20	43.63	28.20

(continued on next page)

Table 3.3, continued

Run No.	Experimental design					MO Removal (%)			MB Removal (%)		
	pH	Light	Dyes	Catalyst	Time	UV	COD	TOC	UV	COD	TOC
33	4	18.5	35	0.5	80	68.00	53.15	37.45	28.00	19.25	7.16
34	10	18.5	35	0.5	80	47.00	35.57	25.34	42.14	31.75	19.90
35	7	14	35	0.5	80	59.40	48.63	42.88	51.51	38.00	21.95
36	7	14	35	0.5	80	81.57	64.68	50.95	54.77	41.25	23.08
37	7	18.5	20	0.5	80	70.85	50.81	40.12	57.00	40.00	17.83
38	7	18.5	50	0.5	80	48.00	38.83	28.05	39.80	27.72	12.70
39	7	18.5	35	0.3	80	48.00	41.07	38.88	45.00	36.75	22.12
40	7	18.5	35	0.7	80	64.00	51.84	41.29	50.00	28.25	18.22
41	7	18.5	35	0.5	40	60.97	50.68	43.02	50.28	33.50	21.15
42	7	18.5	35	0.5	120	78.91	64.73	51.19	57.37	42.50	32.18
43	7	18.5	35	0.5	80	69.54	58.68	47.99	53.80	34.50	27.38
44	7	18.5	35	0.5	80	68.62	57.57	48.22	53.00	34.45	27.95
45	7	18.5	35	0.5	80	68.02	56.78	47.92	53.14	35.00	27.98
46	7	18.5	35	0.5	80	67.17	55.68	48.12	52.71	34.25	27.02
47	7	18.5	35	0.5	80	66.94	56.73	48.29	52.91	35.75	28.57
48	7	18.5	35	0.5	80	67.17	56.89	47.85	52.65	35.50	28.08
49	7	18.5	35	0.5	80	68.65	57.84	47.82	53.48	34.52	27.32
50	7	18.5	35	0.5	80	68.31	59.94	47.95	53.37	35.55	26.15

Table 3.4 and 3.5 also summaries the minimum and maximum colour, COD and TOC removal of MO and MB.

**Table 3.4:** Output parameters (MO)

Output	Parameters description	Parameters characterization	
		Minimum Value	Maximum Value
output 1	UV	13.66	83.35
output 2	COD	11.00	73.54
output 3	TOC	3.30	54.46

**Table 3.5:** Output parameters (MB)

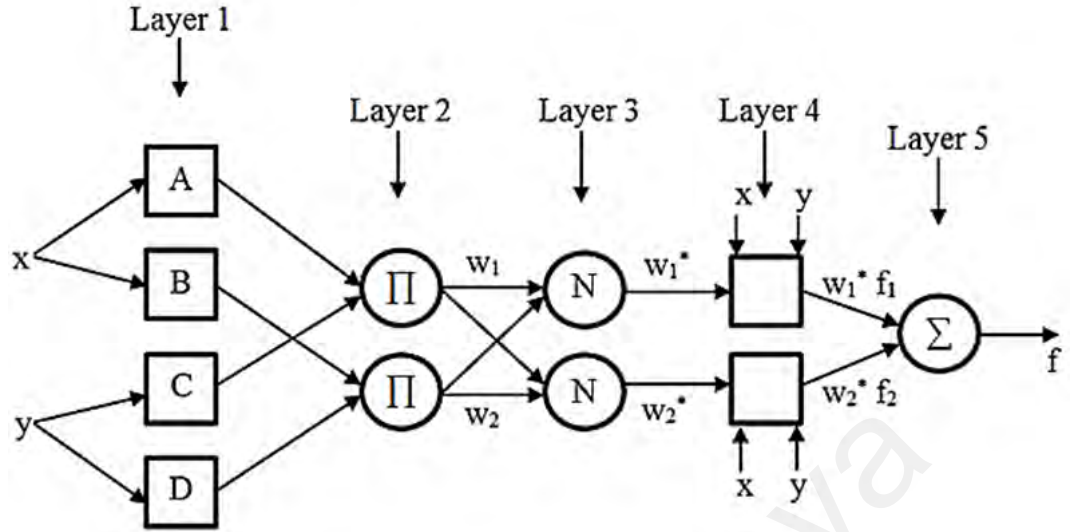
Output	Parameters description	Parameters characterization	
		Minimum Value	Maximum Value
output 1	UV	13.82	75.5
output 2	COD	7.09	68
output 3	TOC	2.75	46.41

In order to better analyze system performance and design a system with the best characteristics, it is necessary to select a subset of the most relevant and influential parameters and to predict which covariates have the strongest effects on the response of interest. This process of selection is named as “variable selection”. Neural networks can be defined as architectures that consist of a large parallel adaptive processing elements interconnected via structured networks (Kwong, Wong et al. 2009, Chan, Ling et al. 2011). Essentially, with neural network as the foundation, the complex system’s architecture in the function of approximation and regression can be modelled. Accordingly, variable selection process is crucial to generate a model capable of estimating a special process output. Therefore, in order to build a model capable of predicting a specific process output, it is essential to find a subset of variables that are relevant to the respective output (Buyukbingol, Sisman et al. 2007, Singh, Kainthola et al. 2012). Parameters that are irrelevant can be separated and removed prior to variable

selection' based on the existing literature information. Otherwise, an optimization procedure can be applied by using the Genetic algorithms. Herein, the objective is to select proper explanatory (input) parameters and thereby minimize error that exists among the observed and the predicted values. In this study, adaptive neuro-fuzzy inference system (ANFIS) was used for variable selection (Geethanjali & Raja Slochanal 2008). Aiming at organizing fuzzy inference system, ANFIS analyses the input/output data pairs. It gives fuzzy logic the ability to determine how the main parameters affect the final result.

### **3.5.1.2 Variable selection using ANFIS**

Constructing sets of 'IF THEN' fuzzy rules alongside suitable membership functions (MFs) is required to generate predetermined input-output subsets. ANFIS can serve as the foundation for such a construction. The input-output data are converted into membership functions. ANFIS takes the initial FIS and adjusts it through a back propagation algorithm according to the collection of input-output data. FIS consists of three components - (i) a database, (ii) a rule base and (iii) a reasoning mechanism. The database assigns MFs which are employed in the fuzzy rules. The rule base comprises a choice of fuzzy rules. Reasoning mechanism is inferred from the rules and input data, giving a feasible outcome. The intelligent combination of knowledge, methods and techniques from a variety of different sources adapts well to the changing environment. MATLAB employs FIS in the whole process of training and evaluation. FIS integrates human comprehension, does interfacing and makes decisions. Based on the ANFIS results, 2 input variables, as depicted in Fig 3.2 were the most influential operating parameters on the photoactivity of Cu-TiO<sub>2</sub>/ZnO in advanced oxidation reaction for water treatment.



**Figure 3.2:** ANFIS structure.

In this study, the rules of fuzzy IF-THEN from the Takagi and Sugeno's class and two inputs for the first-order Sugeno were employed, as shown below:

$$\text{if } A \text{ is for } x \text{ and } C \text{ is for } y \text{ then } f_1 = p_1x + q_1y + r_1 \quad (3-5)$$

In Fig 3.2 the first layer consists of input variable membership functions (MFs) that only supplies the input values to the next layer. Each node here is considered as an adaptive node having a node function  $O = \mu_{AB}(x)$  and  $O = \mu_{CD}(x)$  where  $\mu_{AB}(x)$  and  $\mu_{CD}(x)$  are membership functions. Bell-shaped membership functions having the minimum and maximum values of (0.0) and (1.0) were chosen.

$$\mu(x) = \text{bell}(x; a_i, b_i, c_i, d_i) = \frac{1}{1 + \left[ \frac{(x - c_i)}{a_i} \right]^{2b_i}} \quad (3-6)$$

Here, the set  $\{a_i, b_i, c_i, d_i\}$  consists of parameter sets. These sets are designated as the premise parameters. Besides,  $x$  and  $y$  are the inputs to nodes. They represent a

combined version of the two most influential variables on the photoreduction of MO and MB in the presence Cu-TiO<sub>2</sub>/ZnO photocatalyst.

The membership layer (second layer) searches for the weights of each membership function. This layer receives the input values from the preceding layer (first layer) and acts as a membership function to represent the respective fuzzy sets of input variables. All nodes in the second layer are non-adaptive. This layer acts as a multiplier for the receiving signals and sends out the outcome in equation (3-7):

$$w_i = \mu_{AB}(x) * \mu_{CD}(y) \quad (3-7)$$

Every output node exhibits the firing strength of a rule. Each node at third layer calculates the normalized weights. This layer is also non-adaptive and each node computes the ratio of the rule's firing strength to the sum of all rules' firing strengths in the form of below equation.

$$w_i^* = \frac{w_i}{w_1 + w_2}, i = 1, 2 \quad (3-8)$$

The outcomes are referred to as the normalized firing strengths. The fourth one, defuzzification layer, provides the output values resulting from the inference of rules. Each node in this layer is adaptive and having the node function.

$$O_i^4 = w_i^* x f = w_i^* (p_i x + q_i y + r_i) \quad (3-9)$$

In this layer,  $\{p_i, q_i, r\}$  is the variable set. The variable set is designated as the consequent parameter.

The final layer is known as the output layer (fifth layer) that adds up all the receiving inputs from the preceding layer and converts the fuzzy classification outcomes into a binary (crisp). This layer considers the single node in the output layer as non-adaptive. The single node computes the total output as total of the entire receiving signals.

$$O_i^5 = \sum_i w_i^* x f = \frac{\sum_i w_i f}{\sum_i w_i} \quad (3-10)$$

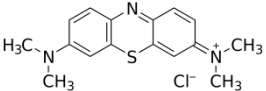
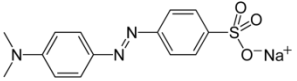
The hybrid learning algorithms are applied for identifying the variables in the ANFIS architectures. The functional signals progress until the 4<sup>th</sup> layer whereby the hybrid learning algorithm passes. Then, the consequent variables are determined by the least square estimation. In the backward pass, gradient decline order synchronizes the premise variables since the error rates circulate backwards.

### 3.6 Photocatalytic activity

To the best of our knowledge, no study has been done to integrate the benefits of copper in a hybrid matrix including two semiconductors of TiO<sub>2</sub> and ZnO in order to gain the advantages of copper in supporting two semiconductors at the same time. As such its behavior and effects in such systems is unclear. Accordingly, in this study, a hybrid of Cu-TiO<sub>2</sub>/ZnO was synthesized, characterized and evaluate in term of its photocatalytic activity through the decomposition of Methylene blue (MB) and Methyl orange (MO). Herein, the effects of five main process parameters: dye concentration, catalyst load, initial pH, intensity of visible light irradiation and reaction time was investigated using central composite design (CCD). Table 3.6. Presents the main properties of the investigated dyes.



**Table 3.6:** The main properties of the investigated dyes

Investigated Dye	Formula	Molecular structure	$M_w$ (g.mol <sup>-1</sup> )	$\lambda_{max}$ (nm)	pKa	Colour index
Methylene Blue	C <sub>16</sub> H <sub>18</sub> N <sub>3</sub> SCl		319.852	664	9.0	52.015
Methyl Orange	C <sub>14</sub> H <sub>14</sub> N <sub>3</sub> NaO <sub>3</sub> S		327.33	508	6.0	13025

The photocatalytic activity of the synthesized photocatalyst was evaluated through photodegradation of both methylene blue and methyl orange under visible light irradiation.

**Figure 3.3.** Shows the photoreactor set-up.



**Figure 3.3.** The photoreactor set-up (a) before experiment (b) during experiment.

The experiments were conducted in Pyrex cylindrical photoreactor (ID=8cm, H=13cm), as a batch photoreactor, covered with aluminum foil and equipped with a magnetic stirrer to maintain the photocatalyst suspended in the aqueous solution and an air distributor device. The photoreactor was irradiated with a fluorescent lamp (light intensity: 18-23Watt) with wavelength emission in the range 400–550 nm, positioned at the center of the photoreactor. First a specific value of catalyst was suspended in a predetermined concentration of MB or MO. The pH of the solution was then adjusted at selected value by hydrochloric acid (HCl, 1.0M) or sodium hydroxide (NaOH, 1.0M) using pH-meter (EUTECH, CyberScan pH

300). Prior to irradiation, the suspension was magnetically stirred in the dark for 60 min to reach sorption equilibrium. The photocatalytic reaction was then initiated when exposed to visible light. Liquid samples were taken out at regular time intervals and filtered by a membrane filter with a disposable syringe to remove the remaining catalyst particle from the aqueous solution. The photoactivity of the synthesized photocatalyst was then analyzed in terms of color, COD and TOC removals. The absorbance of the dye solution was measured by a UV-Vis spectrophotometer (Spectroquant-Pharo 300) on the basis of a calibration curve obtained using standard MB/MO solutions that represents a linear relationship between absorbance and dye concentration. *Chemical Oxygen Demand* (COD,  $\text{mg.L}^{-1}$ ) values were determined using COD test cell supplied by Merck in a thermoreactor (Spectroquant TR 420) according to the standard method (APHA, AWWA, and WFE, 1998). Total Organic carbon (TOC,  $\text{mg.L}^{-1}$ ) was measured with a solution of potassium phthalate as standard of calibration using (Shimadzu TOC-VCSH analyser). The degradation efficiency in terms of the percentages of color, COD and TOC removal was calculated by the following equation. Where,  $C_0$  and  $C_t$  are the initial and the retained values of Color, COD or TOC, respectively.

$$\text{Degradation Efficiency (\%)} = \frac{(C_0 - C_t)}{C_0} \times 100 \quad (3-11)$$

### 3.7 Safety Aspects

Throughout the experiments, care is taken to prevent the health, fire, reactivity, and contact hazards associated with all the chemicals and hazards associated with all the equipment and instruments used in the research project. Besides, normal laboratory safety precaution procedures including the use of appropriate personal protective equipment and use of standard operating procedures and waste disposal system is followed to eliminate and minimize the risk.

## CHAPTER 4: RESULTS AND DISCUSSION

### 4.1 Introduction

This chapter deals with the results obtained from TGA Thermo-Gravimetric analysis, XRD Identification of the structures and phase purity of Cu doped  $\text{TiO}_2/\text{ZnO}$  samples were carried out by an X-Ray Diffractometer, the crystal phase of all samples was identify by comparison with the Joint Committee on powder Diffraction Standard (JCPDS) files and the crystal size Calculated with scherrer's equation, the surface area of the sample was determined using Brunauer Emmett Teller, morphology studies of the samples were conducted using, scanning Electron Microscope (SEM) and Transmission electron microscope (TEM) image were used to observe the internal structure of samples, UV-vis diffuse reflectance was employed to determine the UV-vis diffuse reflectance spectra. The band gap energy level was determined through the Kubelka-Munk's model. The results indicated a significant improvement in the characteristics of Cu- $\text{TiO}_2/\text{ZnO}$  compared to  $\text{TiO}_2$  and ZnO.

photoactivity of new hybrid Cu doped  $\text{TiO}_2/\text{ZnO}$  investigated for photodegradation of two different dyes methyl orange MO and methylene blue MB under visible light irradiation. In addition, ANFIS (Adaptive Neuro Fuzzy Inference System) was employed to investigate the effects of five independent variables including dye and catalyst concentrations, pH, intensity of light irradiation and reaction time on the photocatalytic performance of Cu- $\text{TiO}_2/\text{ZnO}$ . The sensitivity analysis was performed to identify how the copper-  $\text{TiO}_2/\text{ZnO}$  is being affected by operating parameters.

## 4.2 Physico–chemical properties of new doped photocatalyst

The nanocrystalline Cu-doped TiO<sub>2</sub>/ZnO composite powder with TiO<sub>2</sub>/ZnO weight ratio of 7/3 and 1-5% copper concentration, calcinated at 500 °C and 700 °C was synthesized vis Sol-gel method, characterized and evaluated in this study.

### 4.2.1 Thermo-gravimetric analysis

In order to clarify the thermal stability of the Cu-TiO<sub>2</sub>/ZnO composite powder, the thermo-gravimetric analysis was conducted using the dried composite gel with Cu mass fraction of 1wt%, 3wt% and 5wt%. The results of weight loss due to decomposition and Derivative Thermogravimetric Analysis (DTG) are shown in Fig. 4.1.

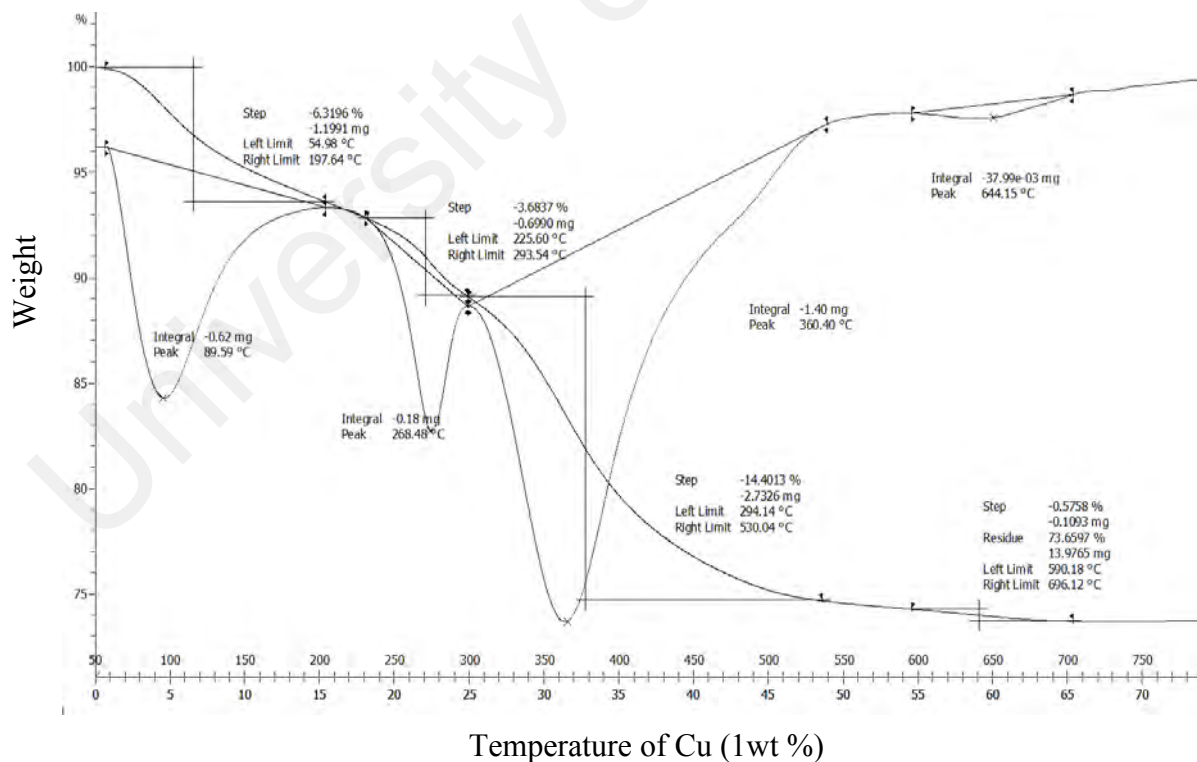


Figure 4.1, continued

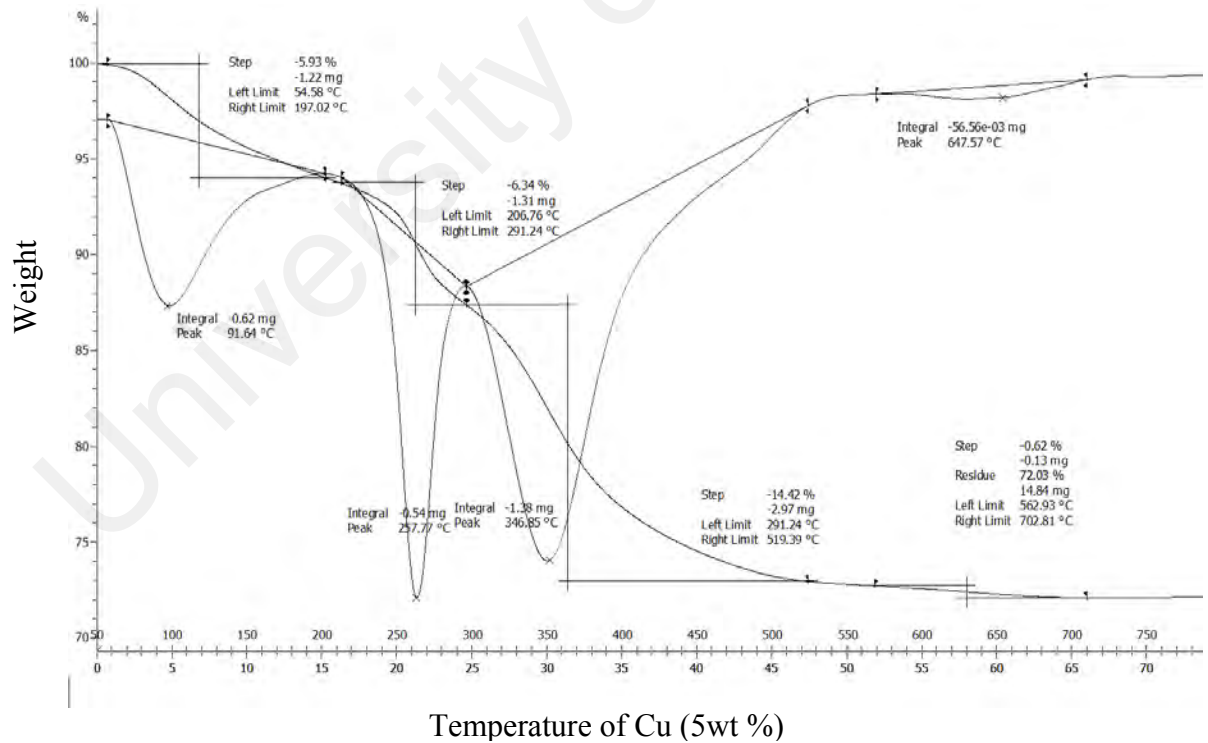
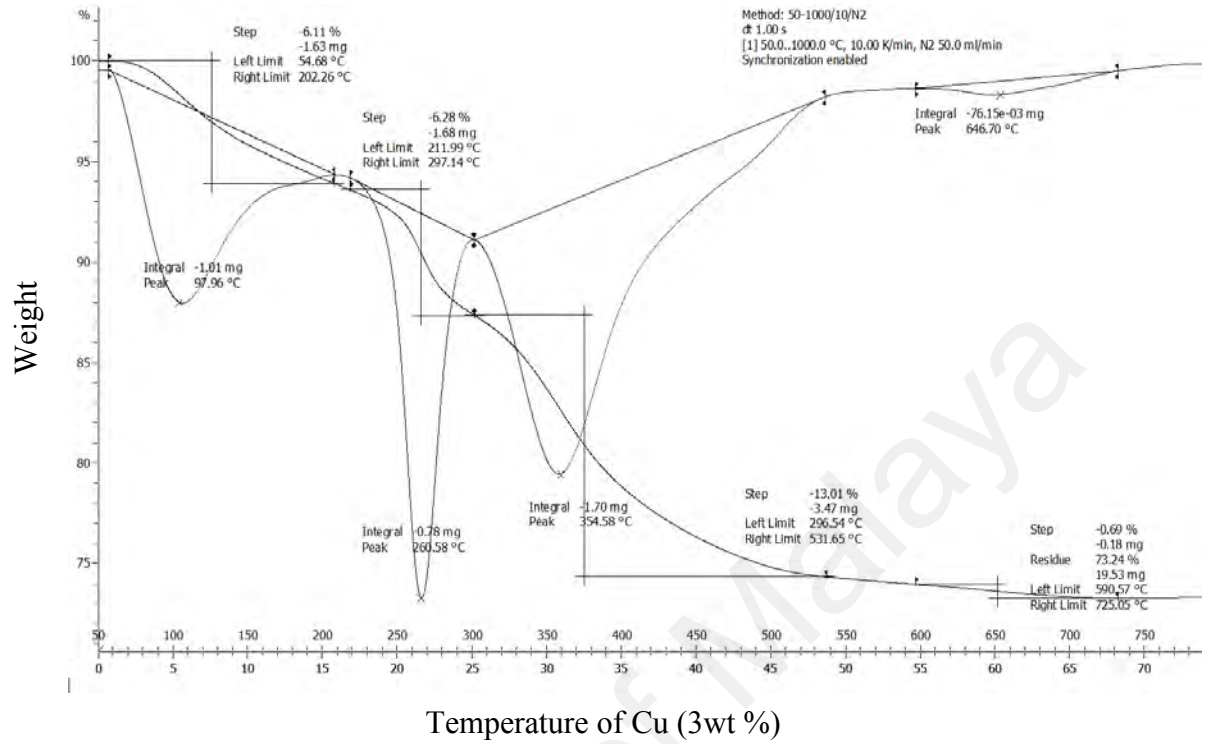


Figure 4.1: TGA curves of the Cu-ZnO/TiO<sub>2</sub> composite powder with Cu concentrations of —: Cu (1wt%), - - -: Cu (3wt%), —·—: Cu (5wt%). (Heating speed of 10°C/min).

Three main phases of mass loss during the whole thermal decomposition/combustion process were identified. The minor weight loss of 5.93 to 6.31wt%, as observed in all the graphs at the temperature below 115°C, was due to the loss of physically adsorbed water and solvent. This phase slightly decreased (around 1wt%) as the Cu concentration increased. The decomposition phase started after solvent evaporation. Based on Fig. 4.1, this phase happened from 200 to 260°C, resulting in a reduction of 3.68, 6.28 and 6.34wt% in the total mass. As observed, the mass reduction was dramatically lower at copper concentration of 1wt%. The third step, which occurred at about 270 to 380°C, was related to both the decomposition of the organic group's residuals and the condensation of the TiO<sub>2</sub> anatase phases. Similar results were also reported by (Ramimoghadam, Bagheri et al. 2014). From the analysis, the temperature assigned for this phase shifted to lower range with increasing Cu caused by compounds created by copper. Such results demonstrated the influence of copper and its corresponding compounds on the thermal stability of Cu-TiO<sub>2</sub>/ZnO.

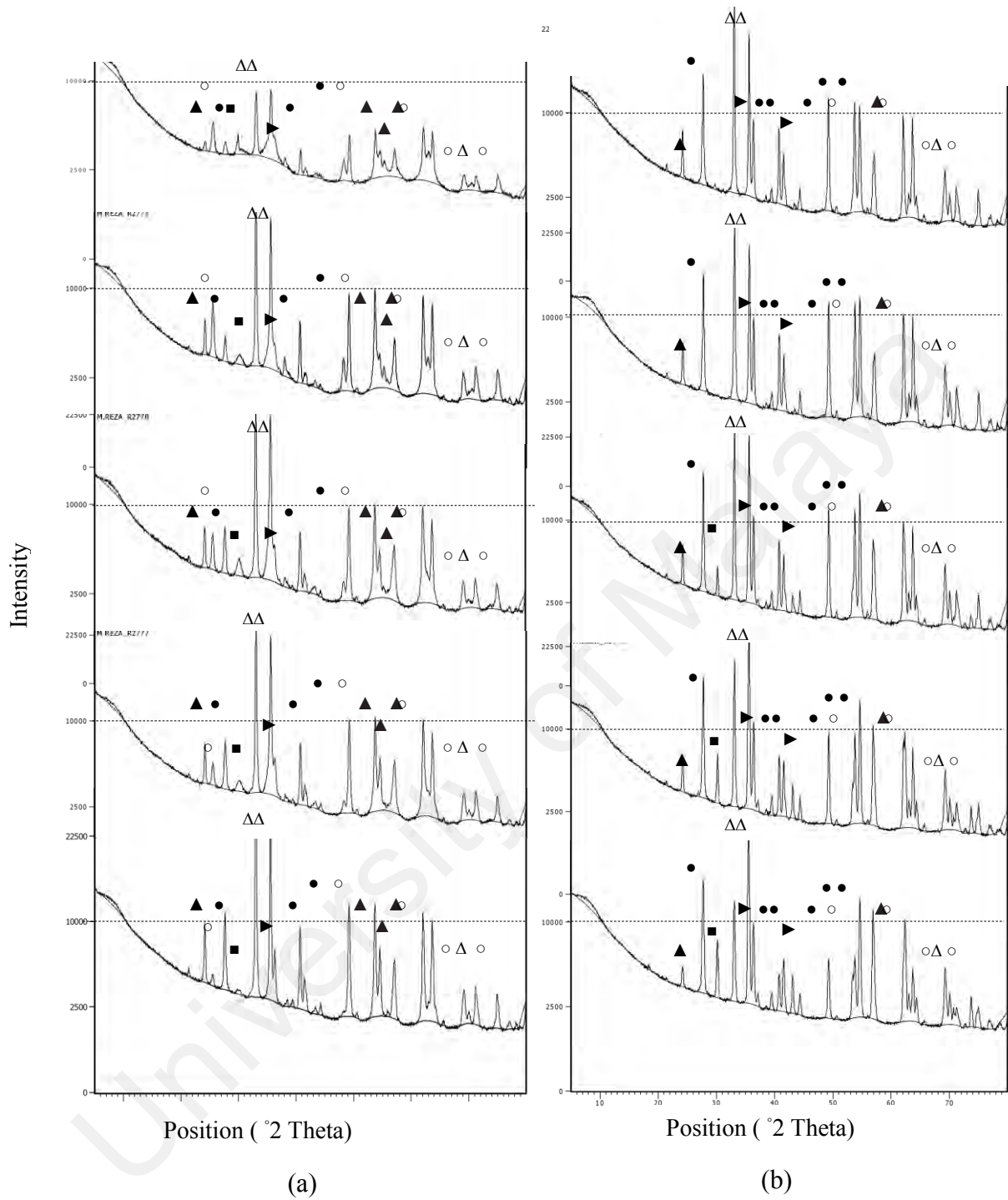
#### **4.2.2 Structure characterize of Cu-TiO<sub>2</sub>/ZnO**

In addition, TiO<sub>2</sub> has three main crystalline structures; anatase (tetragonal), rutile (tetragonal) and brookite (orthorombic). Anatase is the phase normally fabricated in the sol-gel process but brookite is mostly found as a by-product when precipitation is performed in an acidic medium at low temperature. Rutile is a stable structure while both brookite and anatase are metastable and usually transfigured to rutile when heated. Generally, brookite is more reactive than anatase. However, preparing pure brookite without rutile or anatase is rather difficult and therefore it has not been widely investigated (Paola et al. 2013). Besides, anatase has a higher photocatalytic activity compared to rutile because its higher E<sub>CB</sub> ( 0.2 eV) results in higher driving force for transferring electron to O<sub>2</sub>. It is because E<sub>CB</sub> position affects electron transfer rate and

subsequently, charge recombination rate. Therefore, it is a determining factor for efficiency of photocatalysis. It has always been reported that the photocatalytic activities of both anatase and rutile structures are highly influenced by the types of substrates applied (Serpone et al. 1996; Du and Rabani 2003; Ryu and Choi 2007; Tryba et al. 2007).

X-Ray Diffraction (XRD) explain the crystal structures of Cu- TiO<sub>2</sub>/ZnO in different TiO<sub>2</sub> and ZnO concentrations and calcination temperatures. Fig. 4.2 (a and b) displays the XRD patterns of the samples containing 1-5wt% Cu, calcined at 500°C (Fig. 4.2a) and 700°C (Fig. 4.2b), respectively.

University of Malaya



**Figure 4.2:** XRD patterns of synthesized Cu- TiO<sub>2</sub>/ZnO calcined at a) 500°C b) 700°C.  
 ○:Anatase, ●:Rutile, ▲:Brookite, △:ZnO, ►:ZnTiO<sub>3</sub>, ■:Cu<sub>2</sub>O, ▲:Cu<sub>2</sub>HNO<sub>3</sub>

The standard JCPDS patterns of Zinc Oxide (reference code 98-002-9272), crystal phases of TiO<sub>2</sub> including Anatase (00-021-1272), Rutile (01-075-1750) and Brookite (00-029-1360), Cu<sub>2</sub>O (00-05-0667) and CuO (00-48-1548) were used to analyse the



obtained patterns in this study. Generally, for Cu- TiO<sub>2</sub>/ZnO with copper loading of 1wt% which was calcined at 500°C, the crystal was rather amorphous. However, it crystallized well as the copper content increased in the matrix. Besides, as shown in Fig. 4.2a, among TiO<sub>2</sub> crystal structures, diffraction peaks of anatase and brookite showed the strongest intensities after calcination at 500°C, indicating their major phases within the photocatalyst at this stage. Meanwhile, traces of rutile has also detected in Cu-TiO<sub>2</sub>/ZnO calcined at 500°C. As the calcination temperature rose to 700°C, the crystalline phases changed accordingly. The strongest peaks in these samples were neither from brookite nor anatase, but rutile, indicating a crystal phase transfer towards rutile at the temperature of 700°C. These observations are in good agreement with those obtained in the literature (Bakardjieva, Stengl et al. 2006). As reported by Paola et al (Paola, Bellardita et al. 2013), anatase structure was normally generated in TiO<sub>2</sub> synthesis through sol-gel method whereas brookite was normally found as a by-product when the precipitation was performed in an acidic medium at low temperature. Rutile is the stable structure while brookite and anatase are metastable and can potentially transform to rutile when heated.

Besides TiO<sub>2</sub> crystals, ZnO with strong diffraction peak intensities were found in these photocatalysts. However, a number of ZnO peaks on the basis of standard peaks were not identifiable in this study. Meanwhile, more ZnO/TiO<sub>2</sub> were clearly detected, especially for those calcined at 700°C, indicating an extensive the below reaction (Batistella, Lerin et al., 2012).



The results confirmed that photodeposition modified the basic crystal structure of ZnO and transformed it into ZnO/TiO<sub>2</sub>. The phenomena may be due to the homogeneous dispersion of nanoscale copper deposits on the surface of ZnO. On the other hand,

presence of high quantity of zincite in samples calcined at 500°C indicated that the aforementioned transformation was not fully achieved for photocatalysis at that temperature.

In terms of copper quantity, according to the XRD patterns (Fig. 4.2), signal of Cu<sub>2</sub>O were clearly observed ( $2\theta$  of about 29.63°) and the intensity of these peaks increased with copper loading, which clarified that higher mass fraction of Cu<sub>2</sub>O was obtained with copper loading. Whereas, the diffraction pattern of CuO was not observed as CuO or small dimensions of Cu components were below the detection limit of XRD. The other possible reason might be high dispersion of CuO within the TiO<sub>2</sub> frameworks. Furthermore, by comparing the XRD patterns of Cu-TiO<sub>2</sub>/ZnO with that of pure TiO<sub>2</sub> (Zhu, Hartmann et al. 2000) and considering the Cu content in both the photocatalysts calcined at 500 and 700 °C, it was found that the anatase phase increased initially with the Cu content up to 2wt% and beyond that, the percentage of the anatase phase slightly reduced.

Meanwhile, the quantity of rutile phase was reinforced in both categories of the synthesised Cu-TiO<sub>2</sub>/ZnO. Accordingly, it can be suggested that the dopant content beyond 2%wt promoted the phase transformation from anatase to rutile. The reason was that the surface oxygen vacancy concentration of anatase grains is enhanced with Cu, rearranging the ions favourably and reorganizing the structure into the rutile structure (Rahman, Ahmed et al. 1995). In other words, since the synthesised photocatalysts were calcined at atmospheric condition, the chemical state of Cu is Cu<sup>+</sup> (on the basis of XRD pattern) which can be a substitute to Ti<sup>4+</sup> transformed TiO<sub>2</sub> into a denser rutile phase. The other possible reason was that the density of surface defects of the photocatalyst may increase as Cu content increased, resulting in phase transformation since the surface defects were considered as the rutile nucleation sites (Jongsomjit, Sakdamnusun et al. 2004). This finding was consistent with that of Fe-doped TiO<sub>2</sub> (Gennari &

Pasquevich, 1998) or Al-doped TiO<sub>2</sub> (Vemury & Pratsinis 1995). Besides, anatase phase percentage in Cu-TiO<sub>2</sub>/ZnO reduced with increasing the calcination temperature from 500 to 700 °C, which is opposite of the trend passed by rutile phase in those calcination temperatures. Therefore, the rutile phase dominated the TiO<sub>2</sub> structure when the calcinating temperature was 700°C (Fig. 4.2).

On the other hand, a number of anatase phase peaks appeared stable at both 500°C and 700°C. It was attributed to thermodynamic stability of anatase. High thermodynamic stability of anatase, compared to rutile phase, is a proven phenomenon in smaller crystallites (Hirano, Nakahara et al. 2002, Baiju, Shajesh et al. 2007, Hamadani, Reisi-Vanani et al. 2010). But the effect of doping should also be considered. During the sol-gel process, dopant significantly controls the crystallite growth (especially for crystallization of anatase phase). Although the dopant content increased the rutile nucleation sites or transferred TiO<sub>2</sub> into denser rutile, Cu<sub>2</sub>O and CuO molecules adsorbed on the surface of TiO<sub>2</sub> made crystal growth slow. Therefore, the key is the balance between the amount of dopant that behaves as the rutile nucleation sites and the amount of Cu<sub>2</sub>O or CuO which is adsorbed on the surface of the photo catalyst.

#### **4.2.3 Crystal size, specific surface area and particle size of Cu- TiO<sub>2</sub>/ZnO**

The average crystal size of nanoparticles were determined from the full-width of the half maximum (FWHM) of the most intense peaks of the respective crystals using the Scherrer's equation:

$$D = C_s \cdot k / \beta \cdot \cos \theta \quad (4-2)$$

where  $D$  is equal to or smaller than the grain crystallite size,  $C_s$  is the Scherrer constant, which has a value between 0.9 and 1.2, depending on the shape of the particles ( in this study,  $C_s=0.94$ ),  $k$  is the wave length of the incident X-ray,  $\theta$  is the Bragg diffraction

angle and  $\beta$  is the full-width of the half maximum (Binas, 2012). Accordingly, TiO<sub>2</sub> peaks of (105) (211) (204) for anatase phase, TiO<sub>2</sub> peaks of (110) (211) (220) for rutile phase and TiO<sub>2</sub> peaks of (320) (151) (052) for Brookite phase, ZnO peaks of (002), (101) and ZnTiO<sub>3</sub> peak of (103) were considered. However, brookite peaks of (320) (151) were only considered for calcination temperatures of 500 °C while rutile peaks of (211) (220) were only considered for calcination temperatures of 700 °C. The specific surface area of the synthesized photocatalysts was also estimated through Brunauer-Emmett-Teller, (BET) method. The results are presented in Table 4.1.

**Table 4.1:** Crystallite size and surface area of the Cu- TiO<sub>2</sub>/ZnO photocatalyst prepared at various calcination temperatures and compound concentrations

Photocatalyst	Cu (wt%)	Calcination Temperature	Crystal Size (nm)	Particle size (m <sup>2</sup> /g)	Surface Area (m <sup>2</sup> /g)	Ref
ZnO	-	500 °C	33.0	-	-	(S. Abedini Khorramia, G. Mahmoudzadeha et al. 2011)
ZnO	-	700 °C	30.0	-	-	(S. Abedini Khorramia, G. Mahmoudzadeha et al. 2011)
TiO <sub>2</sub>	-	500 °C	18.9	-	-	(Aguilar, Navas et al. 2013)
TiO <sub>2</sub>	-	700 °C	42.3	-	-	(Aguilar, Navas et al. 2013)
Cu-ZnO/TiO <sub>2</sub>	1	500 °C	28.2	5.58	29.1	Current
Cu-ZnO/TiO <sub>2</sub>	2	500 °C	37.1	2.94	-	Current
Cu-ZnO/TiO <sub>2</sub>	3	500 °C	37.6	4.13	71.2	Current
Cu-ZnO/TiO <sub>2</sub>	4	500 °C	38.2	3.40	-	Current
Cu-ZnO/TiO <sub>2</sub>	5	500 °C	39.9	3.89	117.9	Current
Cu-ZnO/TiO <sub>2</sub>	1	700 °C	36.1	36.35	37.4	Current
Cu-ZnO/TiO <sub>2</sub>	2	700 °C	42.4	18.97	-	Current
Cu-ZnO/TiO <sub>2</sub>	3	700 °C	50.8	9.08	80.1	Current
Cu-ZnO/TiO <sub>2</sub>	4	700 °C	53.3	18.11	-	Current
Cu-ZnO/TiO <sub>2</sub>	5	700 °C	54.9	16.06	126.6	Current

Generally, the mean crystallite size of Cu- TiO<sub>2</sub>/ZnO was highly influenced by calcination temperature and increasing crystal size improves the catalyst activity. As observed, when the calcination temperature rose from 500 to 700°C, the crystal size of Cu- TiO<sub>2</sub>/ZnO increased gradually. It was mainly attributed to phase transformation from anatase to rutile and ZnO to ZnTiO<sub>3</sub>. As shown in Table 1, the rutile phase and ZnTiO<sub>3</sub> content increased by about 20.24% and 3.74%, respectively. In other words, the increase in calcination temperature induced phase transformation and accelerated the growth of crystallites. Increase of crystal size with calcination temperature has also been reported by many other researchers (Ahn, Kim et al. 2003, Hamadani, Reisi-Vanani et al. 2009, Sahu, Hong et al. 2009, Hamadani, Reisi-Vanani et al. 2010, Shi, Chen et al. 2010).

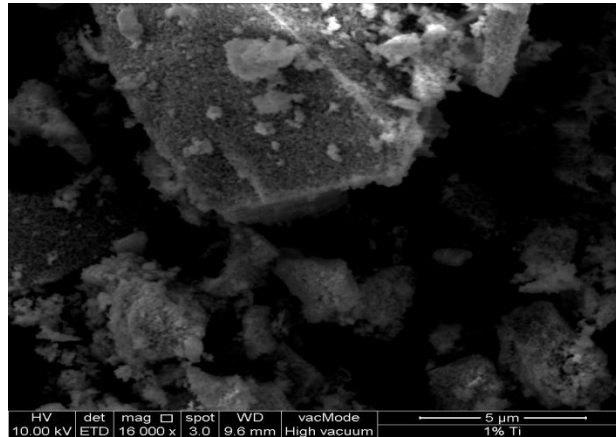
The XRD patterns showed that the most intense anatase peak with the width of (101) plane at  $2\theta = 25.6$  appeared at calcination temperature of 500°C and disappeared by increasing the calcination temperature to almost 700°C. The XRD patterns also showed that the rutile phase peaks became broader and more intense at 700°C (i.e. (2 0 0) plane at  $2\theta = 39.5$ , (111) plane at  $2\theta = 41.5$ , (210) plane at  $2\theta = 43$ , etc). To get a quantitative view, at 500°C the crystallite size of rutile phase reached a maximum of 35.04 nm, but it became 39.93nm as the temperature increased to 700°C at a copper concentration of 5wt%. At the same condition, the crystallite size of ZnO dropped from 33.17 to 28.73. Meanwhile, ZnTiO<sub>3</sub> monotonically increased from 30.99 to 34.08nm with calcination temperature, showing the transformation of ZnO to ZnTiO<sub>3</sub> through Eq. 16. From Table 4.1, it was observed that the average crystal size increased with dopant loading, which was attributed to phase transformation and in agreement with other published works. For example, Inturi et al. (Inturi, Boningari et al. 2014) who investigated the effect of different dopants on TiO<sub>2</sub> crystals reported that, Ce, Y, Zr and Mo reduced anatase crystal size while other metals, i.e. V, Cr, Fe, Co, Mn, Ni and Cu increased crystal size.

The specific surface areas of the synthesized Cu-TiO<sub>2</sub>/ZnO along with pure ZnO and TiO<sub>2</sub> are also listed in Table 4.1. As observed, the specific surface area for the synthesized photocatalyst was increased with the dopant content or calcination temperature, thus demonstrating higher ability to photoexcite the electron-hole pairs in the active sites and causing stronger absorption of reactants on the catalyst surface (Marci, Augugliaro et al. 2001). Therefore, the maximum crystal size along with the maximum surface area was observed in the samples with the Cu amount of 5wt%, calcined at 700°C. It can be suggested different concentrations of Cu led to certain degree of stability of the specific surface area of Cu-doped photocatalysts.

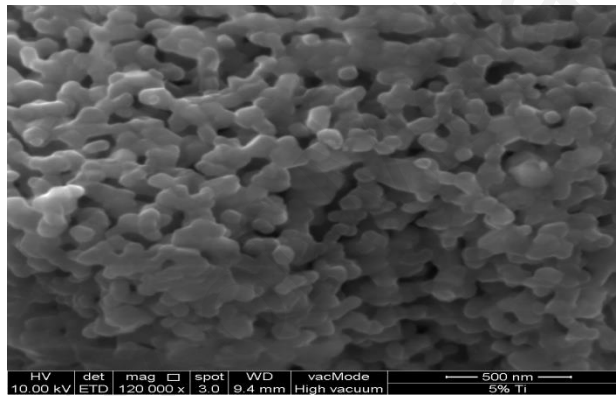
Moreover, it seems that the photocatalysts with greater TiO<sub>2</sub> concentrations tended to agglomerate into larger secondary particles during the synthesis processes, which led to lower surface areas. Particle size is the other important parameter that determines catalyst efficiency. Particle size can be analysed by scanning electron microscopy. Generally, the efficiency of a doped catalyst increases as its particle size reduces. However, it is reported that the photocatalytic activity is dependent on crystallinity rather than the particle size or surface area (Kanade, 2007). The details on particle sizes of the synthesised photo-catalysts are also listed in the same Table. As it can be observed, the values of particle sizes were within the range of 2.02 to 3.54nm indicating generation of a uniform powder of photocatalysts.

#### **4.2.4 Morphology of Cu- doped TiO<sub>2</sub>/ZnO**

Morphologies of the Cu-TiO<sub>2</sub>/ZnO photocatalyst were investigated by SEM and the results are shown in Figs. 4.3 and 4.4. Fig 4.3 shows the photocatalyst morphology as its copper doping increased (1wt, 2wt and 5wt%) whereas the effect of calcination temperature is demonstrated in Fig. 4.4.



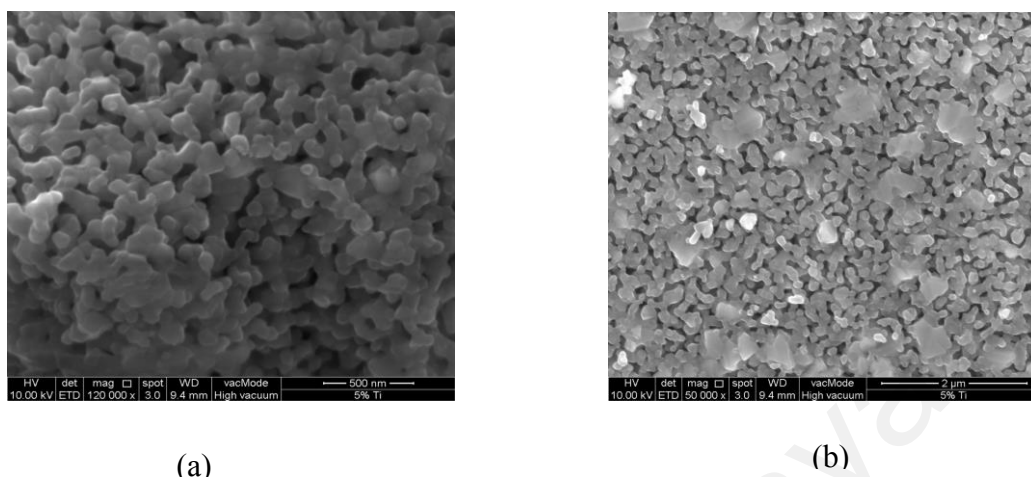
(a)



(c)

**Figure 4.3:** SEM images of Cu- TiO<sub>2</sub>/ZnO Calcined at 500°C, a) Cu=1wt%, b) Cu=5wt%

As discussed earlier (in the XRD analysis), the photocatalyst with 1.0wt% Cu synthesized at 500°C mainly comprised amorphous crystals. That observation was also confirmed by the SEM image in Fig 4.3 (a). As observed, the surface of the catalyst was smooth and crack free. Furthermore, according to the XRD analysis, the dopant concentration played a dominant role by either behaving as the rutile nucleation sites or being adsorbed on the surface of the photocatalyst. The SEM images also showed that the crystalline lattice improved by increasing the dopant content in the matrix of the photocatalyst matrix (Fig 4.3b). Fig 4.3c shows that the crystallinity was extended and improved notably as the dopant increased to 5wt%.



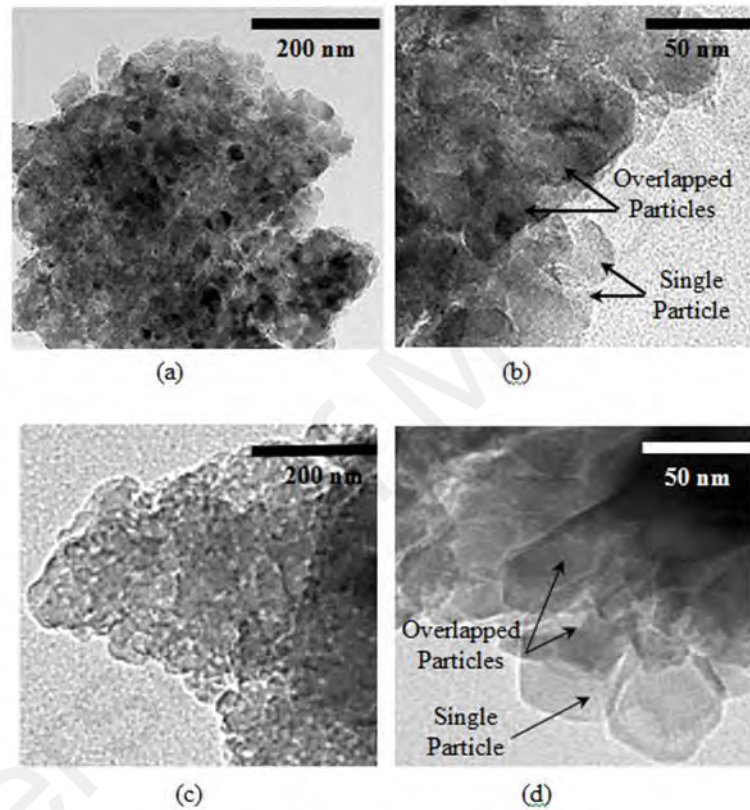
**Figure 4.4:** SEM images of Cu-TiO<sub>2</sub>/ZnO, a) Cu=5wt%, Calcined at 500°C, b) Calcined at 700°C.

Apart from the effects of the dopant content, the crystallinity became more regular as the calcination temperature increased to 700°C, as shown in Figs 4.4 (a and b). This result was also in line with that obtained by the XRD analysis. At this condition, Cu-TiO<sub>2</sub>/ZnO contained approximately 100% of specific monodisperse abundant dumbbell or ball shaped particles and nano-pores. As observed, calcination temperature favourably affected the growth of nanophase crystals due to crystal phase transformation.

For better analysis, the TEM images of Cu (3wt%)-TiO<sub>2</sub>/ZnO calcined at 500 °C and 700 °C are presented in Fig 4.5. As per images, the particles in the samples with dopant content of 3wt% calcined at either 500 °C or 700 °C, have distributed uniformly. Figure of 4.5b also depicts that the Cu-TiO<sub>2</sub>/ZnO consists of a large number of particulates with a size of around 30-40 nm which is consistent with the results of XRD. Both single and accumulated particles were clearly observed in Fig 4.5b. Corresponding results for the photocatalyst synthesized at 700°C were also presented in Fig 4.5d. In contrast, the samples calcined at 700°C showed a slight larger particle size than that calcined at



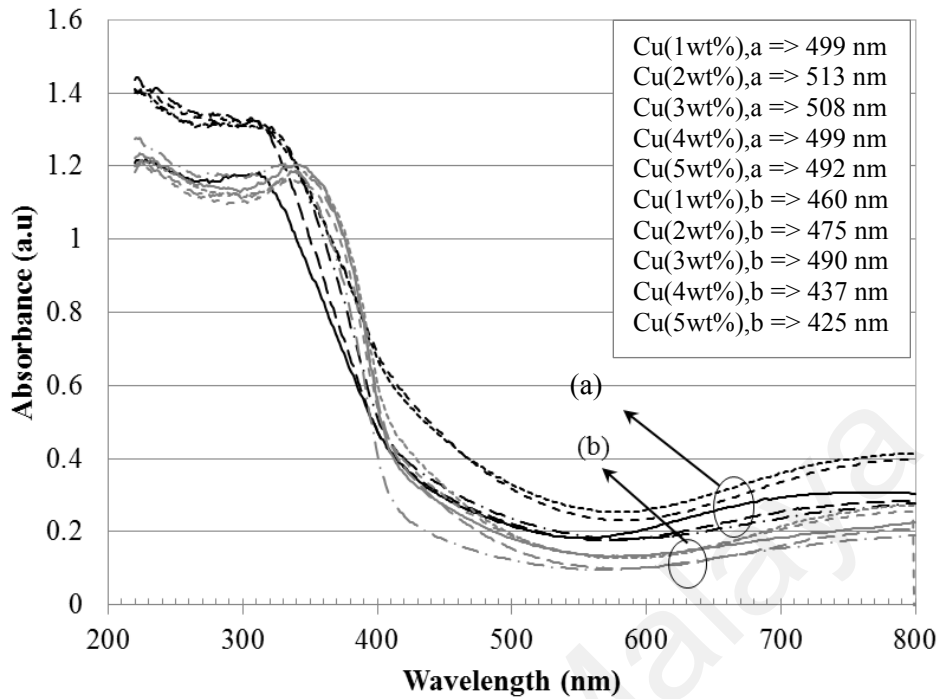
lower temperature, which is in agreement with the results obtained by XRD. Furthermore, it is observed that by increasing the calcination temperature, crystallinity have increased too, however, the impact of dopant should not be eliminated.



**Figure 4.5:** TEM images of Cu-TiO<sub>2</sub>/ZnO with Cu=3wt% calcined at 500 °C (a, b) and 700 °C (c, d).

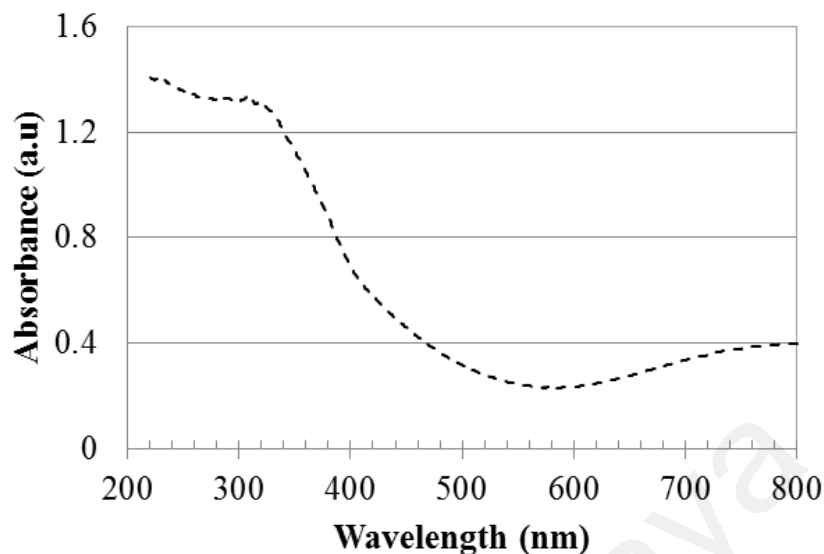
#### 4.2.5 Analysis of optical absorption of Cu-doped TiO<sub>2</sub>/ZnO

The analysis of UV–vis diffuse reflectance spectra (converted to absorbance) for Cu-TiO<sub>2</sub>/ZnO with different Cu content, calcined at 500°C and 700°C are shown in Fig. 4.6. Generally, incorporation of copper into TiO<sub>2</sub>/ZnO lattice induced an optical absorption with a steep edge in the visible light region.



**Figure 4.6:** The optical absorption curves of Cu- TiO<sub>2</sub>/ZnO, calcined at a) 500°C b) 700°C, with different copper content of —: 1wt%,----: 2wt%, - - -: 3wt%, — —: 4wt%, —·—: 5wt%.

It was that the absorption wave length of the new photocatalyst reached between 400 and 800 nm and hence the new photocatalyst have a considerable utilization of visible light for photocatalytic reactions. Besides, the visible light absorption of catalysts at both calcination temperatures improved by increasing Cu content till 3wt%. The rate of light absorption spectra of the synthesized Cu-TiO<sub>2</sub>/ZnO is presented in Fig. 4.7.



**Figure 4.7:** The rate of light absorption spectra of Cu (3wt%)-TiO<sub>2</sub>/ZnO calcined at 500°C.

The origin of the visible light sensitivity in Cu-doped TiO<sub>2</sub>/ZnO can be observed by the appearance of additional energy levels by the dopant orbitals (2p or 3d) and oxygen vacancies within the band gaps of TiO<sub>2</sub> and ZnO due to copper doping. The transition of excitation of 3d electrons from the Cu<sup>2+</sup> ions to the conduction band of TiO<sub>2</sub> plays an important role in this lattice. Apart from the Cu orbital levels, oxygen vacancies which are introduced into the lattice of TiO<sub>2</sub>/ZnO by doping enhances the visible light absorption of the lattice. The oxygen vacancy states are at 0.75–1.18 eV below the minimum conduction band of TiO<sub>2</sub> (Cronemeyer, 1959). The band gap narrowing due to the formation of localized states or oxygen vacancies induces the visible-light absorption.

Besides, among the samples, Cu- TiO<sub>2</sub>/ZnO with 2 and 3wt% Cu concentration showed the largest absorption intensity within the wavelength range of 400 to 800 nm in both groups of samples. In addition, as shown in Fig 4.6, higher absorption intensity and a shift to long wavelength were observed for the samples which were calcined at 500°C which might be caused by noticeable presence of anatase phase in the photocatalyst lattice since the band gap of anatase (3.2 eV) is wider than that of rutile (3.0 eV).

It should be noted that, the absorption at wavelength of about or less than 380-388 nm is caused by the intrinsic band gap absorption of TiO<sub>2</sub> (depend on its structures equilibrium) (Aguilar, Navas et al. 2013). On the other hand, ZnO has an absorption edge at approximately 370-380 nm (band gap: 3.35–3.26 eV) (Pawar, Choi et al. 2015). The strong absorption bands at around 400 nm contribute to the excitation of O 2p electron to the Ti 3d and/or Zn 3d level. The large absorption band between 400 and 800 nm is associated to the presence of Cu species. The visible light absorption bands might be due to metallic Cu absorption (225 to 590 nm), 3-d Cu<sup>3+</sup> clusters (400 to 500 nm) 25, excitation of CuO electron from the valance band to the excition level (<730 nm), d-d transition of Cu<sup>2+</sup> (600 to 800 nm) 25 and Zn<sup>2+</sup> 2p clusters (390 to 520 nm).

#### 4.2.6 Band gap energy level of Cu-doped TiO<sub>2</sub>/ZnO

In this study, the band gap was approximated through the model presented by (Johnson 1967).

$$(Fhv)^m = A(hv - E_g) \quad (4-3)$$

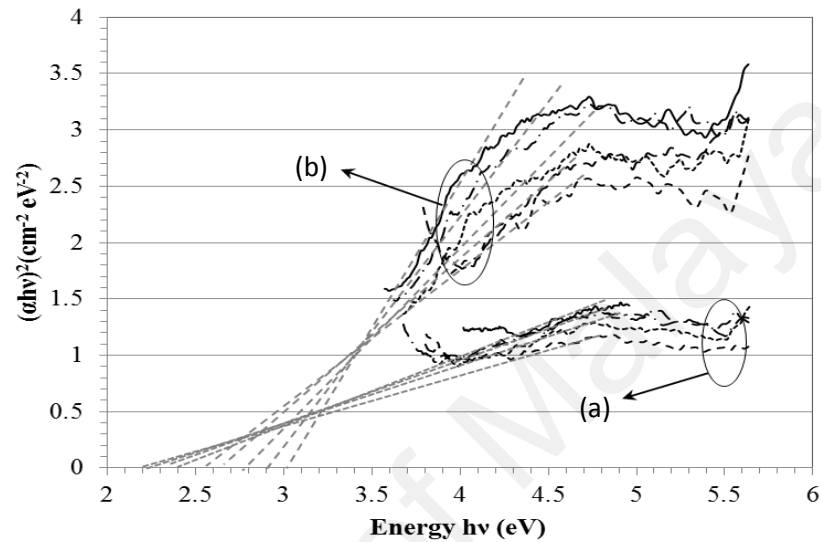
In this model,  $F$  is proportional to the absorption coefficient known as Kubelka-Munk value ( $F = (1-R)^2/2R$ ) where  $R$  is the reflectance of the semiconductor.  $A$  and  $E_g$  denote the constant parameter and band gap respectively.  $m$  represents the type of transition which is equal to 1/2 for direct band gap semiconductor and 2 for indirect band gap semiconductor.  $hv$  is calculated by:

$$hv = \frac{hc}{\lambda} \quad (4-4)$$

where,  $h$  is the Planck's constant ( $6.626 \times 10^{-34} \text{ Js}^{-1}$ ) and  $C$  is the speed of light ( $3.0 \times 10^8 \text{ m.s}^{-1}$ ). Therefore, band gap is calculated by extrapolating the rising portion of the absorption spectrum to the abscissa at zero absorption. In other words, the intersection between the linear fit and photon energy axis ( $hv$ ) gives the value of  $E_g$ .

$$A(h\nu - E_g)^m = 0 \Rightarrow h\nu = E_g \quad (4-5)$$

Eventually, the band gap of the synthesized photocatalysts is presented in Fig. 4.9. The results are also summarized in Table 4.2.

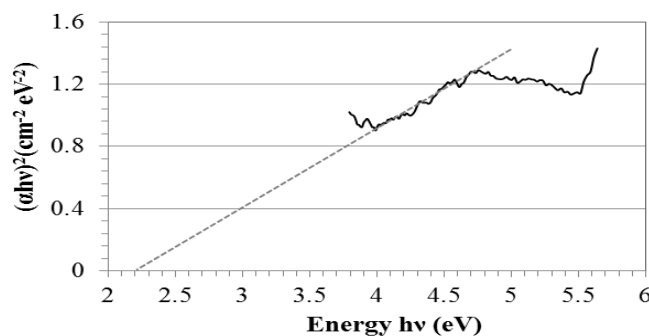


**Figure 4.8:**  $(\alpha h\nu)^2$  versus energy curve (Kubelka–Munk plots) to estimate the band gap energies of Cu- TiO<sub>2</sub>/ZnO with different copper content and Calcined at a) 500°C b) 700°C and copper content of —: 1wt%,----: 2wt%, - - -: 3wt%, — —: 4wt%, —·—: 5wt%.

**Table 4.2:** Band gap energies of Cu- TiO<sub>2</sub>/ZnO with different copper content and calcined at two different calcination temperatures through Plank’s Equation and Kubelka–Munk equation

Model	Kubelka–Munk equation		Plank’s Equation	
	500°C	700°C	500°C	700°C
Calcination Temperature				
Cu Content				
1 wt%	2.41	3.02	2.48	2.7
2 wt%	2.28	2.65	2.42	2.61
3 wt%	2.2	2.57	2.44	2.53
4 wt%	2.36	2.77	2.48	2.84
5 wt%	2.42	2.91	2.52	2.92
Pure TiO <sub>2</sub>	3.20	-	3.20	-
ZnO	3.30	-	3.30	-
TiO <sub>2</sub> /ZnO	2.90	-	2.90	-
Cu	1.50	-	1.50	-

Extrapolation of the linear part of the curve to the  $h\nu$ -axis yielded a band gap of about 2.2 and 2.5 eV for the samples calcined at 500 and 700°C, respectively. Undoped TiO<sub>2</sub> and ZnO have the band gap values of 3.2 and 3.37 eV, respectively. It can be suggested that, the band gap of the synthesized catalyst in this study was significantly less than that of TiO<sub>2</sub> or ZnO separately. Narrowing of the band gap indicated incorporation of Cu into the lattice of TiO<sub>2</sub>/ZnO. Hence, the band gap decreased, resulting in applicability of visible light in transferring electron between the bands. Furthermore, a significant red shift of 0.21-0.45 eV in the main band gap was observed as the dopant content increased to almost 3wt% under the temperature of 500 and 700°C, respectively. The band gap energy level of the Cu (3wt%)-TiO<sub>2</sub>/ZnO synthesized photocatalysts is presented in Fig. 4.9. As observed, the band gap of the synthesized photocatalyst was remarkably decreased compared to the pure TiO<sub>2</sub> (3.2 eV) and ZnO (3.37 eV). Its band gap was also smaller than that of Cu-TiO<sub>2</sub> (3.22 eV) (Colón, Maicu et al. 2006, Ganesh, Kumar et al. 2014), Cu-ZnO (3.34 eV) (Jongnavakit, Amornpitoksuk et al. 2012) and ZnO/TiO<sub>2</sub> (2.82~2.89 eV) (Pozan & Kambur 2014). The value of the band gap obtained for Cu-TiO<sub>2</sub>/ZnO warrants application of this photocatalyst under visible light irradiation.



**Figure 4.9:** Estimation of the band gap energy of Cu (3wt%)-TiO<sub>2</sub>/ZnO calcined at 500°C by Perkin Elmer.

In the most recent work, Ganesh et al (Ganesh, Kumar et al. 2014) investigated the Cu-doped TiO<sub>2</sub> (Cu=0-50wt%) powders and reported an initial increase in the band-gap energy with increase in copper content in TiO<sub>2</sub> from 0 to 0.1 wt.% and then a decrease upon further increase of the dopant content from 0.1 to 10 wt.% in both direct and indirect band gap. In another work performed by Sahu and Biswas (Sahu & Biswas 2011), the authors observed a band-gap energy reduction from 3.3eV to 2.51eV with the increase in Cu-doping concentration in TiO<sub>2</sub> from 0 to 15wt%.

For calcination at 500°C, the doped samples exhibited lower band gap energies which originated from either the presence of CuO and Cu<sub>2</sub>O at the surface of the photocatalyst and/or from residual copper due to incomplete pyrolysis. Cupric oxide, CuO possesses 1.4eV and cuprous oxide, Cu<sub>2</sub>O possesses 2.2eV. These results, combined with the XRD graphs and morphology pictures, confirmed that the crystallinity of Cu- TiO<sub>2</sub>/ZnO along with its band gap increased at calcination temperatures of 700°C and above. Band gap increment with calcination temperature in the systems containing TiO<sub>2</sub> and/or ZnO with a metal dopant has also been reported by other authors (Habibi, Talebian et al. 2007, Yang, Fan et al. 2008).

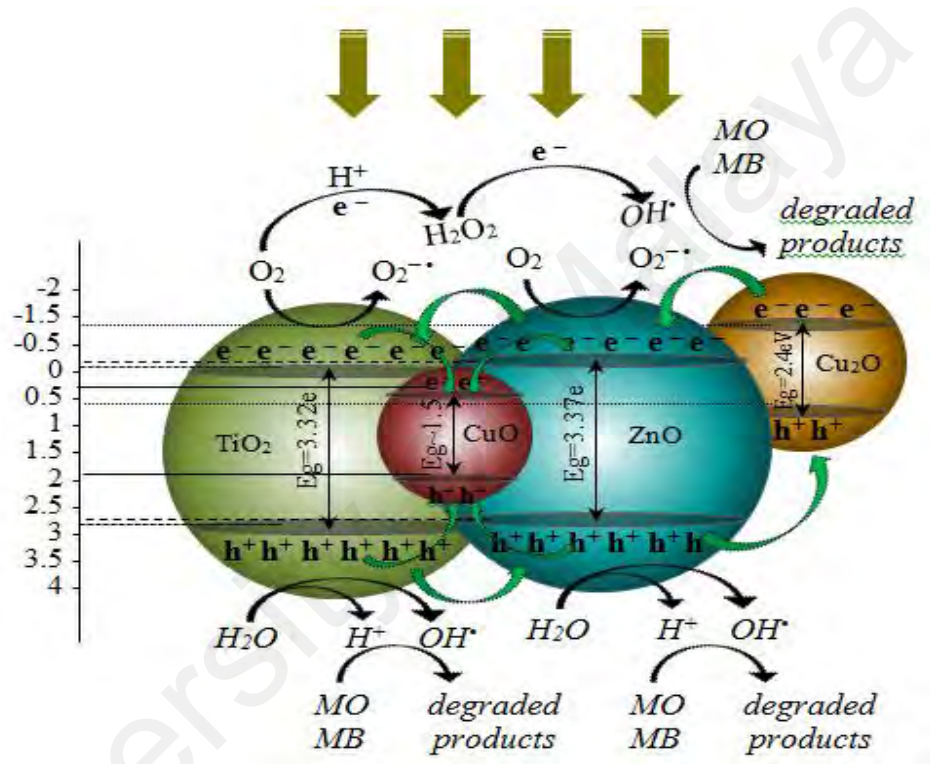
To quantitatively estimate the band gap energies ( $E_g$ ) and in order to compare the absorption onsets of the Cu- TiO<sub>2</sub>/ZnO samples, Planck's equation was used:

$$E_g = \frac{1240}{\lambda_g} \quad (4-6)$$

Where,  $\lambda_g$  is the wavelength at the overlap of the vertical and horizontal portions of the spectra. As per Table 4.2, the band gap estimated by Planck's equation was higher by about 0.3eV compared to the estimation by Kubelka-Munk's method. However, similar trend was produced by both models.

#### 4.2.7 The photocatalytic mechanism of Cu-doped TiO<sub>2</sub>/ZnO under visible light irradiation

The possible diagram for charge transfer and energy band positions of Cu-TiO<sub>2</sub>/ZnO is schematically illustrated in Figure 4.10.



**Figure 4.10:** Schematic diagram illustrating the charge-transfer process in Cu-doped TiO<sub>2</sub>/ZnO under simulated solar light irradiation.

Generally, the potential energy level of the conduction and valence band of Cu<sub>2</sub>O lie above than those of TiO<sub>2</sub> and ZnO semiconductors, which assist the transfer of electrons toward valence band of ZnO or TiO<sub>2</sub>. Besides, the potential energy level of the conduction and valence band of both TiO<sub>2</sub> and ZnO semiconductors, are more anodic and more cationic than those of CuO, respectively. This favors transfer of both e<sup>-</sup> and h<sup>+</sup> from TiO<sub>2</sub> and ZnO to CuO, hindering the partial recombination of e<sup>-</sup>/h<sup>+</sup> in the TiO<sub>2</sub> and



ZnO. Accordingly, the reactions occurring at the TiO<sub>2</sub>cb, CuOcb and ZnOcb are facilitated.

It should also be noted that, under visible light irradiation, Cu<sub>2</sub>O can reduce O<sub>2</sub> via a multi-electron process and be re-oxidized to CuO (Nozik, 1978). Therefore, although CuO was not detected in XRD analysis, it may be generated under visible light irradiation and so its activity should be considered in photo catalytic reaction. Considering this assumption it can be discussed that, the conduction band of CuO has a more negative potential than required for one-electron oxygen reduction:



Furthermore, Cu<sub>2</sub><sup>+</sup> can react with:



Cu<sup>+</sup> can reduce O<sub>2</sub> consuming electrons or be oxidized to Cu-ions by the photo-generated ZnO or TiO<sub>2</sub> holes to Cu<sub>2</sub><sup>+</sup> (Bandara, Guasaquillo et al. 2005). The ZnOvb or TiO<sub>2</sub>vb holes react with the surface <sup>-</sup>OH of the ZnO or TiO<sub>2</sub> releasing OH-radicals. On the other hand, the Cu<sub>2</sub>Ocb lies above the ZnO<sub>cb</sub> and TiO<sub>2</sub>cb. Accordingly, the excited photoelectrons may be transferred from the Cu<sub>2</sub>Ocb towards the ZnOcb and then to TiO<sub>2</sub>cb, whereas the photogenerated holes traverse the opposite direction. In such situation, ZnO as an intermediate stage favors the electron hole transfer between the bands of Cu<sub>2</sub>O and TiO<sub>2</sub> that would considerably reduces the charge recombination rate, increasing the photocatalytic activity of Cu-TiO<sub>2</sub>/ZnO.

According to the energy band structure of both TiO<sub>2</sub> and ZnO, the conduction band bottom and the valence band top correspond to mainly Ti/Zn 3d and O 2p states, respectively. The absorption edge of around 380 and 376 nm for un-doped TiO<sub>2</sub> and ZnO results from the band-to-band transition (O 2p → Ti/Zn 3d). In this study, the slight red shift in Cu- TiO<sub>2</sub>/ZnO can be mainly due to sp-d exchange interactions between the band electrons and the localized d-electrons of the Cu<sup>2+</sup>/Cu<sup>1+</sup> substituted titania and/or

zinc cations, resulting the formation of O-vacancies with concentration similar to that of added impurities. The sp-d exchange interactions causes an upward shifting of the valence band edge and a rise to downward shifting of the conduction band edge, eventuating a band gap narrowing.

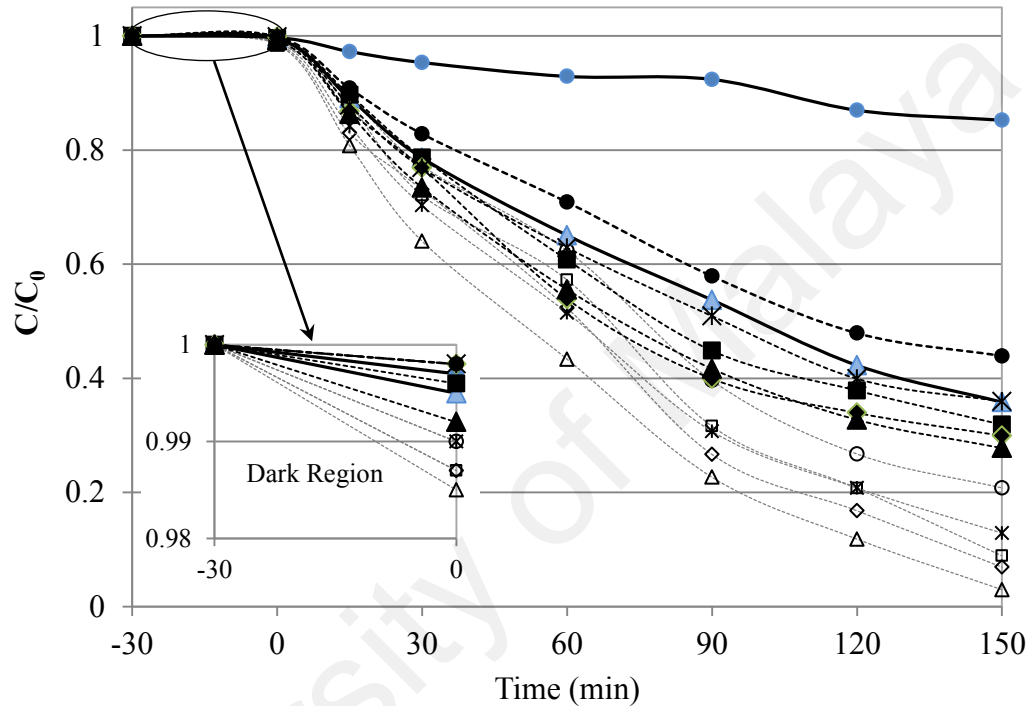
Zuo et al (Zuo, Wang et al. 2010) discussed that the presence of a mini band closely below the conduction band was related to  $O_v$  associated with  $Ti^{3+}$ , which narrowed the  $TiO_2$  band gap. A similar discussion related to  $O_v$ - induced band gap narrowing was presented by Wang et al (Wang, Wang et al. 2012) in a system containing ZnO.

Furthermore, as the valence and conduction band of  $TiO_2$  lie below than that of  $Cu_2O$  and ZnO (Yu, Low et al. 2014, Zhou, Yu et al. 2014), direct transfer of electron from both  $Cu_2O_{cb}$  and ZnO towards the  $TiO_2_{cb}$  in parallel with direct transfer of photogenerated holes from  $TiO_2_{vb}$  to  $ZnO_{vb}$  or  $Cu_2O_{vb}$ , may be the other charge transfer mechanism in Cu- $TiO_2/ZnO$ .

### **4.3 Photocatalytic activity of Cu-doped $TiO_2/ZnO$**

The capability of Cu-doped  $TiO_2/ZnO$  to degrade dye was evaluated through its application for degradation of methylene orange and methylene blue under visible light irradiation. Combinations of different levels of pH, light irradiation intensities, dye concentrations, catalyst loadings and reaction time were studied to evaluate the efficacy of the photocatalyst on color, COD and TOC removal. Among a total of 60 different 3-D graphs for the three responses (20 for each), 8 graphs were chosen to cover all important aspects while neglecting the similar ones. Moreover, since higher light irradiation highlights the impact of each factor, the combined synergistic or antagonistic effects of each factor with the intensity of light irradiation while the other factors kept at their middle values, are presented in Figs. 4.12(a-h).

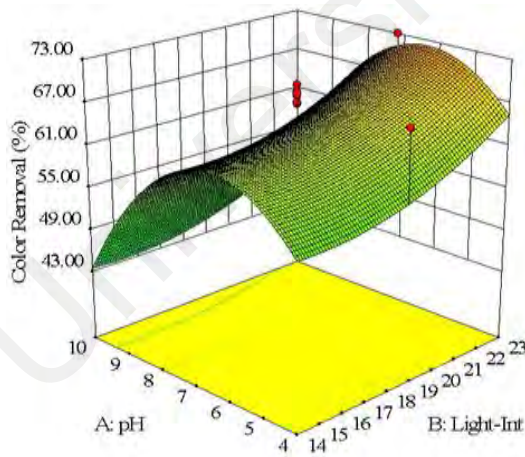
Fig 4.11 shows the photocatalytic degradation curves of 300 ml methyl orange 20 ppm with 0.5 g of photocatalyst at different durations. The degradation results were compared to that of pure TiO<sub>2</sub> and TiO<sub>2</sub>/ZnO calcined at 500°C.



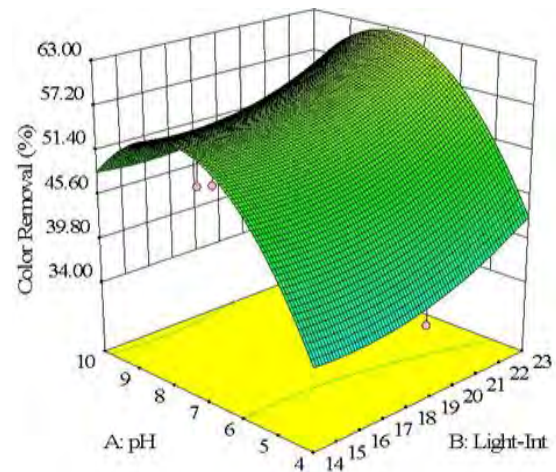
**Figure 4.11:** Photocatalytic degradation of methylene orange using different Cu-ZnO/TiO<sub>2</sub> with copper concentrations of □:Cu(1wt%), ◇:Cu(2wt%), △:Cu(3wt%), \*:Cu(4wt%), ○:Cu(5wt%). Empty bullets: Calcined at 500°C, Solid bullets: Calcined at 700°C, ●:Pure TiO<sub>2</sub>, ▲:TiO<sub>2</sub>/ZnO calcined at 500°C.

According to Fig 4.11 no significant degradation of MO solution was observed using pure TiO<sub>2</sub> under visible light. Compared to that, TiO<sub>2</sub>/ZnO photocatalyst calcined at 500 °C showed noticeable photodegradation of MO, giving a C/C<sub>0</sub> value of around 0.36 after 150 min under visible light irradiation. However, the figure indicated that Cu-TiO<sub>2</sub>/ZnO could improve the photoactivity of TiO<sub>2</sub>/ZnO, yielding lower C/C<sub>0</sub> values than that of TiO<sub>2</sub>/ZnO for almost all the reaction durations. TiO<sub>2</sub> Anatas crystal

structural give lesser band gap for photocatalyst activity. As observed, Cu- TiO<sub>2</sub>/ZnO with different Cu contents provided better results, except the one containing 5wt%, calcined at 700°C. Totally, the degradation efficiency was higher for the samples calcined at 500°C compared to that at 700°C, which should be attributed to the crystal structure of Cu- TiO<sub>2</sub>/ZnO and its band gap energy level. Accordingly, the average final degradation efficiency was around 87% for the former and 64% for the latter. On the other hand, the results clarified that the photocatalytic degradation of the dye increased with copper content up to 3wt%. After that, the degradation rate reduced noticeably. Therefore, among different photocatalysts, the one with copper content of 3wt% calcined at 500°C could reach the maximum degradation of 97% under visible light irradiation.



(a)



(b)

Figure 4.12, continued

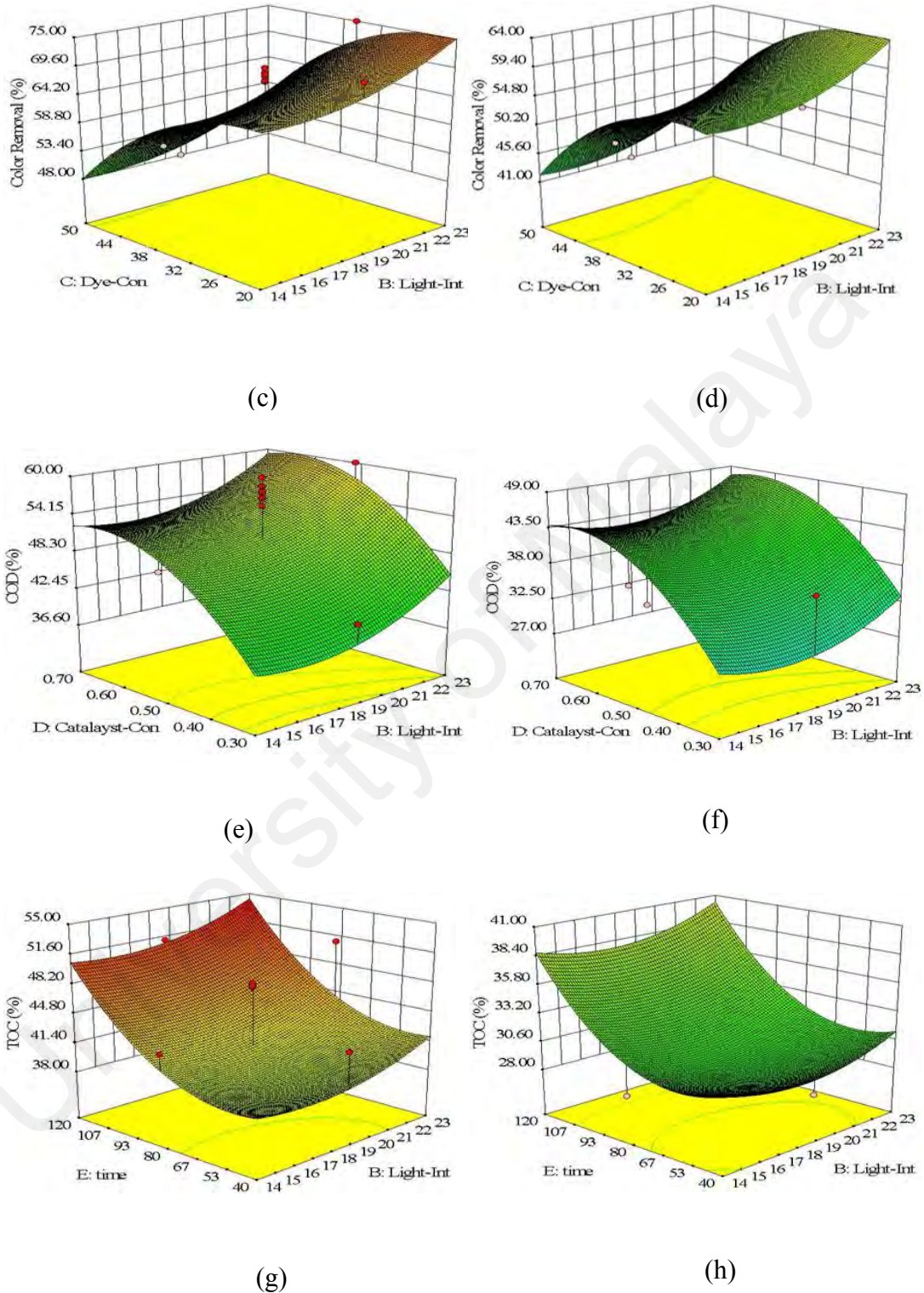


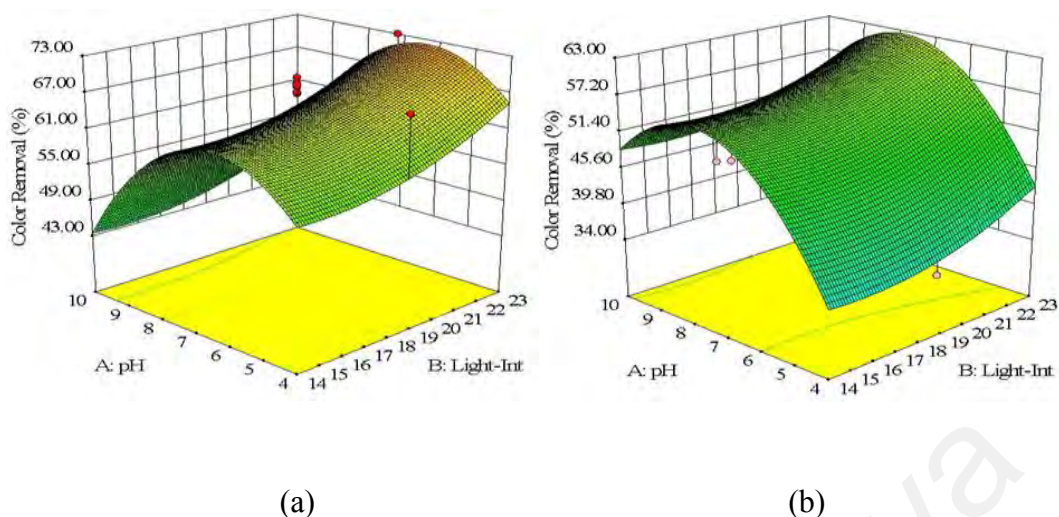
Figure 4.12: The response surface plot of Color, COD and TOC removal efficiency (%) as a function of BA, BC, BD and BE effects. (a)(c)(e)(g):MO and (b)(d)(f)(h):MB

### 4.3.1 Effect of light irradiation intensity

Fig 4.12(a-h) shows the interactive effects between light irradiation intensity and other operating parameters. The photocatalysis reaction was more efficient under more intensive light irradiation since more electron-hole pairs are activated, directly affecting the reaction efficiency. On average, the increment was about 8% for MO and 6.5% for MB within 80 min. Besides, the effect of light irradiation slightly reduced as the dye concentration increased. It was attributed to the darkness of the media that reduces the penetration depth of the photons.

### 4.3.2 Effect of solution acidity

The surface charge of a catalyst plays a vital role for photocatalytic reactions that take place on the surface of a catalyst. The surface charge is defined as the electrical potential difference between the surface of the catalyst and the media. It is dependent on the presence of hydroxyl groups on the catalyst surface. Basicity or acidity of the solution dictates the surface charge properties of the photocatalyst which directly affects its photoactivity. The point at which the surface charge of photocatalyst is null is known as zero charge point ( $\text{pH}_{\text{PZC}}$ ), making the catalyst less attractive to the dye molecules. According to the literature,  $\text{pH}_{\text{PZC}}$  is about 6.0 and 9.0 for  $\text{TiO}_2$  (Zhu, Wang et al. 2014) and  $\text{ZnO}$  (Benhebal, Chaib et al. 2013, Mohd Omar, Abdul Aziz et al. 2014), respectively. Therefore, at  $\text{pH} < \text{pH}_{\text{PZC}}$ , protonation reaction takes place and the catalyst surface is positively charged. On the other hand, deprotonation reaction occurs at  $\text{pH} > \text{pH}_{\text{PZC}}$  which makes the catalyst surface negatively charged. Accordingly, in this study, methyl orange as an anionic dye and methylene blue as a cationic dye were employed to determine the exact effect of pH on photoactivity of the synthesised  $\text{Cu-TiO}_2/\text{ZnO}$ . The results are demonstrated in Figs. 4.13a and 4.13b.

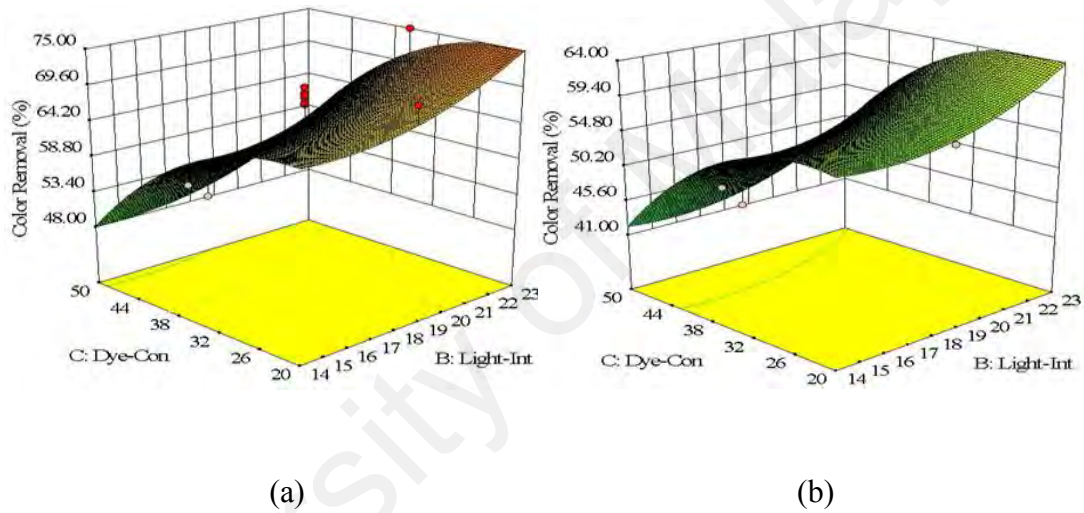


**Figure 4.13:** The response surface plot of Color removal (%) as a function of visible light irradiation intensity and pH effect. (a):MO and (b):MB.

As observed, higher degradation efficiency of methyl orange was observed at acidic pH, while the opposite was observed for methylene blue. According to the aforementioned information, Cu-TiO<sub>2</sub>/ZnO is negatively charged in alkaline solution and it adsorbed MB molecules by electrostatic attraction. In such conditions, the adsorption of MO becomes weaker due to repulsive forces in alkaline solution. The adsorption of MB molecules thus becomes stronger in alkaline condition. However, in this study, the desirable degradation values were obtained over a wide range of pH, which was observed in Fig. 4.13a and 4.13b, demonstrating the stability of copper species inside the catalyst structure. Similar results were observed by (Wang, Duan et al. 2014) when they evaluated the application of Cu doped TiO<sub>2</sub> for degradation of methyl orange within the pH range: 3.0–10.0. They reported the initial solution pH of 3.0 as the optimum value. The increase of methylene blue decomposition with an increase of pH value using nanoparticles of anatase TiO<sub>2</sub> was also perceived by Bubacz et al (Bubacz, Choina et al. 2010). The highest reactivity was obtained by basic reaction. Accordingly, the pH values ranging 4-6 and 7-10 were chosen as target values in the optimization process for MO and MB degradation, respectively.

### 4.3.3 Effect of dye and catalyst concentration

Figs. 4.14a and 4.14b illustrate the degradation percentage as a function of dye initial concentrations in the presence of 0.5g/L catalyst after 80min of light irradiation. It was observed that the reduction percentage of dye in aqueous solution depends dominantly on its initial concentration. In other words, higher absolute degradation ratio could be obtained at lower dye concentration or higher amount of catalyst.



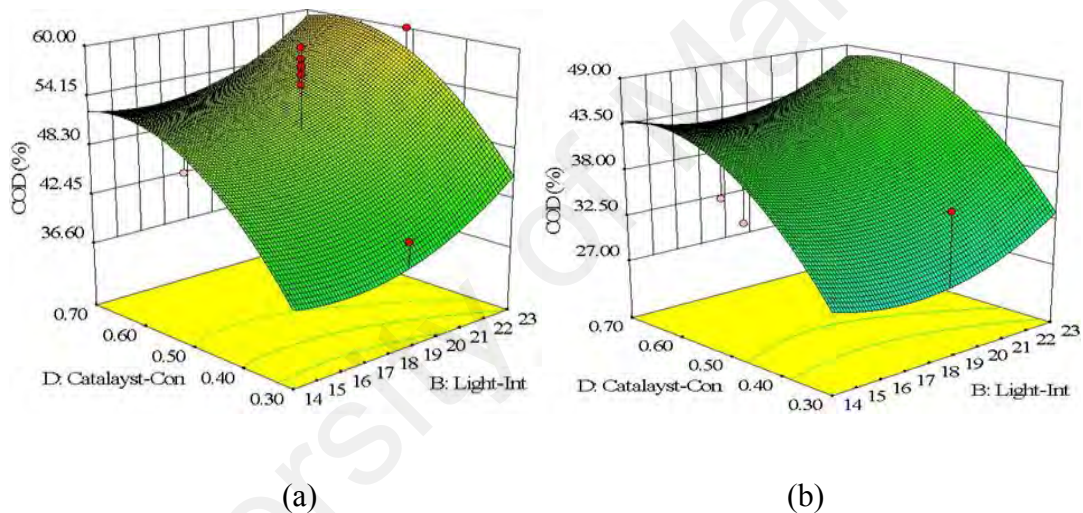
**Figure 4.14:** The response surface plot of COD removal (%) as a function of visible light irradiation intensity and dye concentration, (a):MO and (b):MB.

By increasing the initial concentration of dye, not only the surface of photocatalyst is saturated earlier but the photons also get intercepted before they can reach the surface of the catalyst. There are fewer active sites for adsorption of hydroxyl ions when the catalyst surface is saturated, reducing the efficiency of the catalyst. Interception of photons reduces the absorption of photons by the catalyst and thus the dye reduction percentage decreases. In this study, the colour removal efficiency (%) decreased by about 22.85% and 17.20% with the rise in the dye concentration of MO and MB from 20 to 50 ppm within 80min. The degradation efficiency reduced with increased dye



concentration for both MO and MB, especially for MB from 35 ppm to 50 ppm. In such condition, even higher intensity of light irradiation did not contribute to significant change in photocatalytic degradation, as shown in Fig. 4.14b.

It is important to employ an optimal catalyst amount to keep the treatment efficiency the maximum level. In order to determine the effect of the amount of Cu-TiO<sub>2</sub>/ZnO on the photocatalysis reaction under visible light irradiation, the catalyst amount in a range of 0.3g/L to 0.7g/L was studied. The corresponding results are depicted in Figs. 4.15a and 4.15 b.



**Figure 4.15:** The response surface plot of COD removal (%) as a function of visible light irradiation intensity and catalyst concentration, (a):MO and (b):MB.

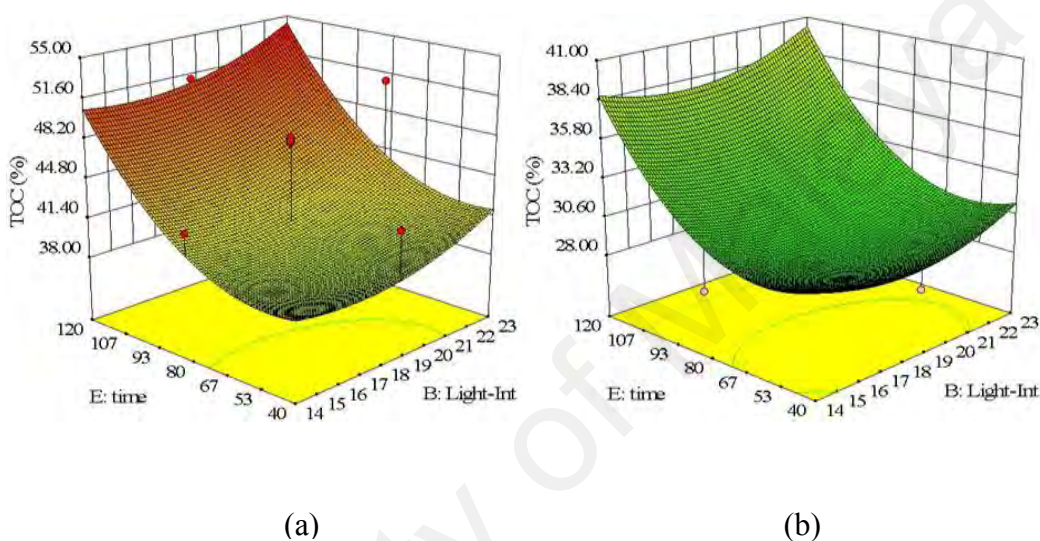
It revealed that the catalyst concentration of 0.6g/L was in synergistic interaction with higher levels of light irradiation and at the solution pH of 5.5 to 6, leading to the maximum photocatalytic degradation of methylene orange within 2h of reaction. Similar observation was obtained at pH 7.5 to 8 for methylene blue. Further increase of catalyst did not significantly improve the reaction and the reaction actually decreased slightly when the catalyst concentration was increased to above 0.6g/L. For instance,

reaction conditions of [catalyst]: 0.6 g/L, [dye]: 35 ppm, pH: 5.5, light irradiation intensity: 18.5 Watt and time: 120 min, brought about 78.45%, 63.68% and 51.81% removal of color, COD and TOC of the methyl orange solution. However, the corresponding removals only rose to 77.15%, 63.85% and 51.86% when the catalyst concentration rose to 0.7g/L. Similar conditions except for pH, which was equal to 7.5, brought about 66.13%, 51.90%, 40.41 removals of methylene blue that reached to the values of 64.72%, 51.67% and 40.30 at catalyst concentration of 0.7g/L. It can be concluded that increase of catalyst amount corresponds with availability of active sites on the catalyst surface till an optimum amount (Behnajady, Modirshahla et al. 2006). Catalyst loading which is beyond the optimum amount increases the turbidity of the suspension and is in antagonistic interaction with penetration of visible light, leading to decrease in photoactivation procedure. The other reason attributes to scavenging of OH radicals over the surface of the catalyst. The same observation was reported by (Daneshvar, Salari et al. 2004) for degradation of azo dye acid red 14 in water using ZnO. Wang et al. (Wang, Li et al. 2010) also obtained the same results for solar photocatalytic degradation of various dyes of methyl orange, rhodamine B, azo fuchsine, congo red and methyl blue, in the presence of  $\text{Er}^{3+}\text{-YAlO}_3/\text{ZnO-TiO}_2$  composite.

#### **4.3.4 Effect of irradiation time on photocatalysis reaction**

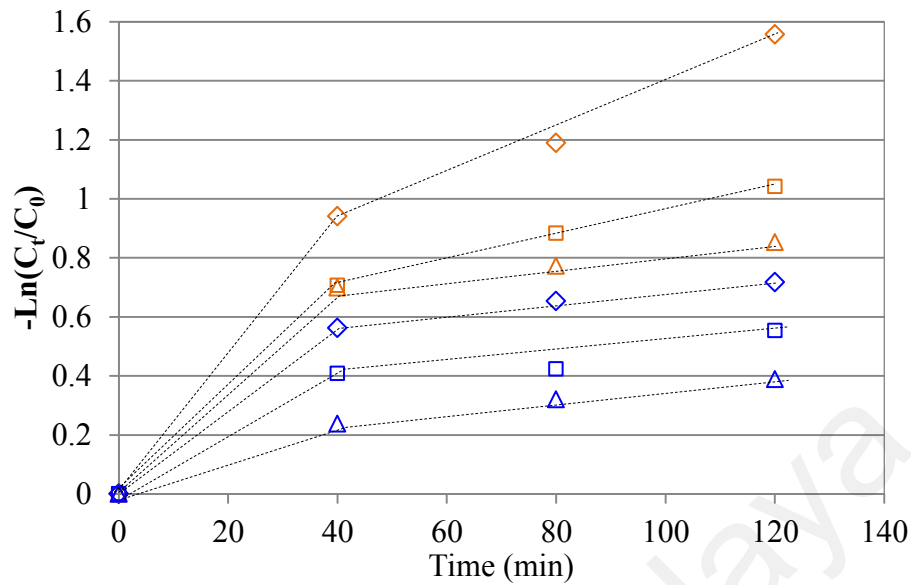
The trends of TOC removal over 120 min for both MO and MB ([dye]: 35 ppm) are presented in Figs. 4.16g and 4.16h which follow the same trend as color and COD removals. As observed, over 41% and 30% of TOC was removed within 40 min for MO and MB respectively and the removal percentage continued to increase to above 53% and 39% at 2 hours. Besides, the COD removal of MO using  $\text{Cu-TiO}_2/\text{ZnO}$  under visible light was found to be about 52%, 57% and 66% within 40, 80 and 120 min,

respectively. The COD removals of MB were 43%, 45% and 53% at the same times. The same trend was also observed for color removal with the values of 65%, 71% and 82% for MO and 58%, 61% and 68% for MB within 40, 80 and 120 min, respectively. All three responses followed a linear trend with time. Under visible light irradiation, the degradation rate of MO was found to be 7.75% (as the average value) higher compared to MB.



**Figure 4.16:** The response surface plot of TOC removal (%) as a function of visible light irradiation intensity and reaction time, (a):MO and (b):MB.

In order to assess the reaction kinetics of photocatalytic degradation using Cu-TiO<sub>2</sub>/ZnO the variation of  $-\ln C_t/C_0$  was plotted versus reaction time, as shown in Fig. 4.17. It was found that the degradation reactions of both MO and MB basically followed the second-order reaction kinetics. In other words, the degradation results implied a sharp increase as the reaction time increased to 40 min. After that, the degradation almost linearly increased with the reaction time with slower rate. This behavior indicates the effect of fresh catalyst with fresh activated sites. The results showed that that the reaction became slower as the activated sites became saturated.



**Figure 4.17:** Effect of irradiation time on ◇: Colour, □: COD △: TOC removals (%), Orange colour: MO, Blue Colour: MB.

#### 4.3.5 ANOVA analysis

Based on the obtained results from the photocatalysis reaction in the presence of Cu-TiO<sub>2</sub>/ZnO, a series of regression models were suggested by CCD analysis in which the reaction efficiency (Color, COD and TOC removals %) was illustrated as a function of independent variables: pH, light irradiation intensity, [Dye], [Catalyst] and reaction time. The equations were obtained according to Equation (3-2) which include a constant value, linear and quadratic terms, presenting the individual effect of each parameter and cross product terms that assess the interactive effects of the parameters on responses ( $Y$ ,  $Y_{COD}$ ,  $Y_{TOC}$ ). The regression models for each categorical variable were obtained after elimination of insignificant terms and the results presented in Tables 4.3 and the related their fitness versus coefficients of determination were presented in Table 4.4.

**Table 4.3:** Analysis of individual and interaction effects of operational parameters

Investigated Dye	Removal response	Final model in terms of coded forms	Eq.
Methyl Orange	$Y_{Color}$	$-62.11-3.57B+1.42C+259.14D-0.081E-1.42A^2-0.023C^2-183.63D^2-0.729CD$	(13)
	$Y_{COD}$	$-34.57-5.34B+1.86C+208.80D-0.14E-1.09A^2-0.988CD$	(14)
	$Y_{TOC}$	$-51.36+2.199C+120.58D-0.27E-1.18A^2-0.037C^2-0.699CD$	(15)
Methylene Blue	$Y_{Color}$	$-94.04-3.76B+1.55C+254.83D-0.157E-1.42A^2-0.023C^2-183.63D^2-0.729CD$	(16)
	$Y_{COD}$	$-66.10-5.70B+1.93C+208.94D-0.19E-1.09A^2-0.988CD$	(17)
	$Y_{TOC}$	$-83.50+2.67C+117.83D-0.31E-1.18A^2-0.037C^2-0.699CD$	(18)

**Table 4.4:** Fitness versus coefficients of determination

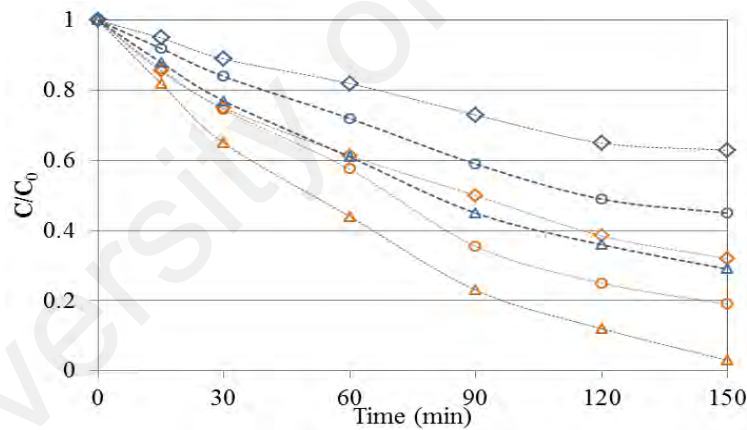
Removal response	Final model in terms of coded forms	$R^2$	$R_{adj}^2$	$R_{pred}^2$	$PV^a$	$AP^b$
$Y_{Color}$	$+59.84+3.96B-8.19C+7.33D+6.78E-4.34F-12.81A^2-5.18C^2-7.35D^2+6.55AF-2.19CD-1.50EF$	0.9285	0.9031	0.8555	<0.0001	27.900>4
$Y_{COD}$	$+45.50+2.78B-6.78C+7.25D+5.69E-5.06F-9.85A^2-5.44C^2+6.42AF-2.97CD$	0.8766	0.8326	0.7676	<0.0001	21.397>4
$Y_{TOC}$	$+35.43-5.13C+4.12D+5.16E-5.63F-10.61A^2-8.40C^2+5.81AF-2.10CD$	0.8502	0.7968	0.7056	<0.0001	16.642>4

<sup>a</sup> P value, Prob > F.

<sup>b</sup> Adequate precision.

In these models, positive coefficients indicate a synergistic effect, while negative coefficients indicate an antagonistic effect between or among the variables. Based on Table 4.3 and 4.4, it was observed that all parameters individually played effective roles during photocatalysis reaction in the presence of Cu-TiO<sub>2</sub>/ZnO while their interactive effects were negligible. Among the interactive effects, the interaction effect of catalyst and dye concentration played the most prominent antagonistic role in both systems containing methyl orange and methylene blue. In other words, visible light could hardly pass through the media as the dye concentration increased and therefore the photocatalysis efficiency reduced. On the other hand, higher concentration of

catalyst ( $>0.6\text{g/lit}$ ) was not as effective. The quality of the developed equations, presented in Table 4.6, also indicates the desirability of the suggested models. The adequate precision measures the signal to noise ratio. A signal to noise ratio greater than 4 indicates that the model is able to navigate the design space. As observed, the adequate precisions were 27.90, 21.39 and 16.64 ( $>>4$ ) for the studied responses. Aside from the photocatalytic activity, the photocatalyst stability is another determinant factor in practical application. In order to investigate the stability of Cu-TiO<sub>2</sub>/ZnO, three runs of cycling photodegradation of 300 ml methyl orange and methyl blue 20 ppm with 0.5 g of photocatalyst under the light intensity of 23 Watt and pH of 7 have been carried out. Accordingly more tests were performed and the results were presented in Fig. 4.18.



**Figure 4.18:** Cycling photocatalytic degradation of MO (Orange Colour) and MB (Blue Colour) using Cu (3wt%)-ZnO/TiO<sub>2</sub> calcined at 500°C. Δ: First Cycle, ○: Second Cycle, ◇: Third Cycle.

As observed, the photocatalytic performance of Cu- TiO<sub>2</sub>/ZnO decreases by about 15~20% for each repeated use. However, the performance reduction is more highlighted after second cycling degradation experiment under methyl blue. It may attributes to the impact of methyl blue on reduction of light absorption on the photocatalyst surface.

#### 4.4 Kinetic analysis of MO degradation

The kinetic or rate of MO degradation using the synthesized catalysts was studied to study the degradation process quantitatively. Accordingly, the experiments to analyse the activity of Cu-TiO<sub>2</sub>/ZnO were subjected to further analysis through the degradation kinetic models. In the most common approach, the experimental data were fitted against a series of popular models to find the most suitable model. In this study, the pseudo-zero-order, pseudo-first-order and pseudo-second-order kinetic models were chosen from similar studies. The linear forms of these models are as follows:

$$dC/dt = -k_0 \quad (4-9)$$

$$dC/dt = -k_1 C \quad (4-10)$$

$$dC/dt = -k_2 C^2 \quad (4-11)$$

Where,  $k_0$ ,  $k_1$  and  $k_2$  are the zero-order rate constant ( $\text{mg L}^{-1} \text{min}^{-1}$ ), pseudo-first-order rate constant ( $\text{min}^{-1}$ ), and pseudo-second-order rate constant ( $\text{mg}^{-1} \text{Lmin}^{-1}$ ), respectively. The  $k_0$ ,  $k_1$  and  $k_2$  constants were obtained from the slopes of the straight lines by plotting  $C_0 - C_t$ ,  $-\ln(C_t/C_0)$  and  $(C_0 - C_t)/C_t C_0$  as a function of time,  $t$ , through regression. Herein,  $C_t$  and  $C_0$  are the MO concentrations ( $\text{mg L}^{-1}$ ) at the reaction time,  $t$  and initial time ( $t=0$ ). The relative errors were estimated using the method below:

$$Err(\%) = \frac{1}{N} \sum_{i=1}^N \left| \frac{C_{cal} - C_{exp}}{C_{exp}} \right| \times 100 \quad (4-12)$$

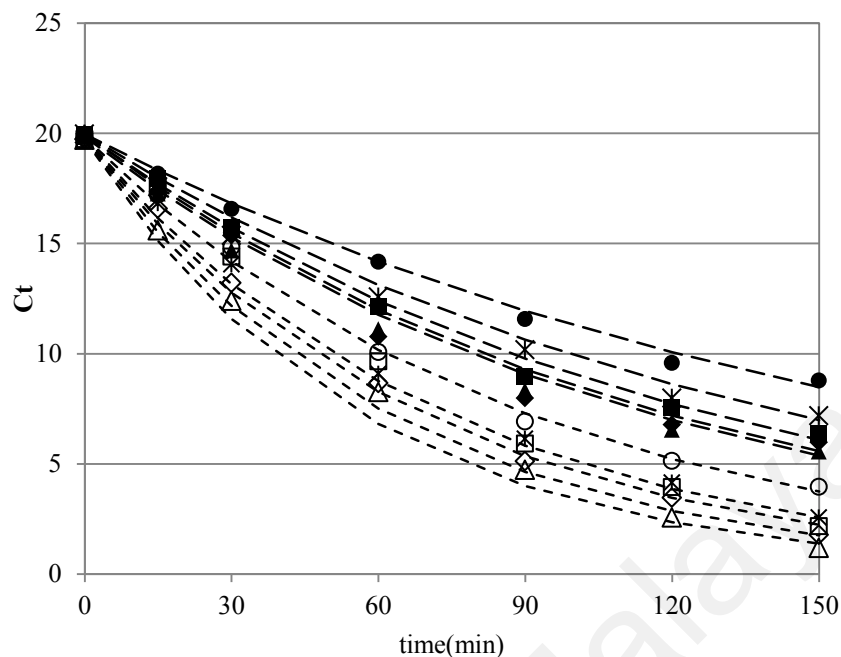
Data on the rate constants and regression values of both the studied models are presented in Table 4.5.

**Table 4.5:** The calculated parameters of the zero- and pseudo-first-order kinetic models for photocatalytic degradation of Methylene orange using different Cu-ZnO/TiO<sub>2</sub>

Sample	Kinetic model	Parameter
Cu(1wt%)-TiO <sub>2</sub> /ZnO calcined at 500°C	Pseudo-first order	k <sub>1</sub> :0.0145, R <sup>2</sup> :92.30
	Zero order	k <sub>1</sub> :0.1205, R <sup>2</sup> :77.71
Cu(2wt%)-TiO <sub>2</sub> /ZnO calcined at 500°C	Pseudo-first order	k <sub>1</sub> :0.0161, R <sup>2</sup> :92.04
	Zero order	k <sub>1</sub> :0.1192, R <sup>2</sup> :64.81
Cu(3wt%)-TiO <sub>2</sub> /ZnO calcined at 500°C	Pseudo-first order	k <sub>1</sub> :0.0186, R <sup>2</sup> :95.06
	Zero order	k <sub>1</sub> :0.1204, R <sup>2</sup> :55.49
Cu(4wt%)-TiO <sub>2</sub> /ZnO calcined at 500°C	Pseudo-first order	k <sub>1</sub> :0.0136, R <sup>2</sup> :96.26
	Zero order	k <sub>1</sub> :0.1151, R <sup>2</sup> :73.81
Cu(5wt%)-TiO <sub>2</sub> /ZnO calcined at 500°C	Pseudo-first order	k <sub>1</sub> :0.0111, R <sup>2</sup> :99.36
	Zero order	k <sub>1</sub> :0.1084, R <sup>2</sup> :84.06
Cu(1wt%)-TiO <sub>2</sub> /ZnO calcined at 700°C	Pseudo-first order	k <sub>1</sub> :0.0079, R <sup>2</sup> :98.96
	Zero order	k <sub>1</sub> :0.0928, R <sup>2</sup> :87.99
Cu(2wt%)-TiO <sub>2</sub> /ZnO calcined at 700°C	Pseudo-first order	k <sub>1</sub> :0.0085, R <sup>2</sup> :95.92
	Zero order	k <sub>1</sub> :0.0953, R <sup>2</sup> :82.12
Cu(3wt%)-TiO <sub>2</sub> /ZnO calcined at 700°C	Pseudo-first order	k <sub>1</sub> :0.0087, R <sup>2</sup> :96.67
	Zero order	k <sub>1</sub> :0.0956, R <sup>2</sup> :82.52
Cu(4wt%)-TiO <sub>2</sub> /ZnO calcined at 700°C	Pseudo-first order	k <sub>1</sub> :0.007, R <sup>2</sup> :96.94
	Zero order	k <sub>1</sub> :0.085, R <sup>2</sup> :88.02
Cu(5wt%)-TiO <sub>2</sub> /ZnO calcined at 700°C	Pseudo-first order	k <sub>1</sub> :0.0057, R <sup>2</sup> :98.93
	Zero order	k <sub>1</sub> :0.0762, R <sup>2</sup> :92.99

The R<sup>2</sup> values of the pseudo-second-order kinetic model were significantly lower than those of zero- and first-order. Accordingly, the results are not presented in Table 4.19 in Contrast, Err (%) values for the pseudo-first-order kinetic model were relatively smaller compared to those of the pseudo-zero-order kinetic model. This indicated that the photocatalytic degradation of MO using Cu-TiO<sub>2</sub>/ZnO followed the first-order kinetic model. Fig 4.19 demonstrates the theoretical and experimental MO degradation behavior during the reaction. It was observed that the degradation data were fitted well into the pseudo-first order model. The inter-comparison amongst the studied Cu-TiO<sub>2</sub>/ZnO synthesized under different calcination temperatures showed that the degradation rate decreased at higher calcination temperature. Besides, degradation rate increased with the copper loading in the synthesized photocatalyst till 3wt% and further increase of copper did not improve the MO degradation.

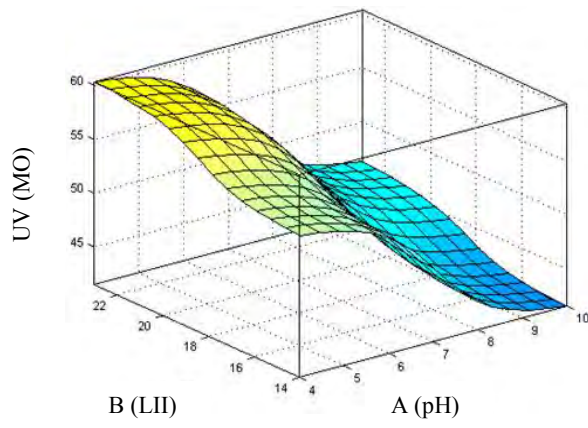




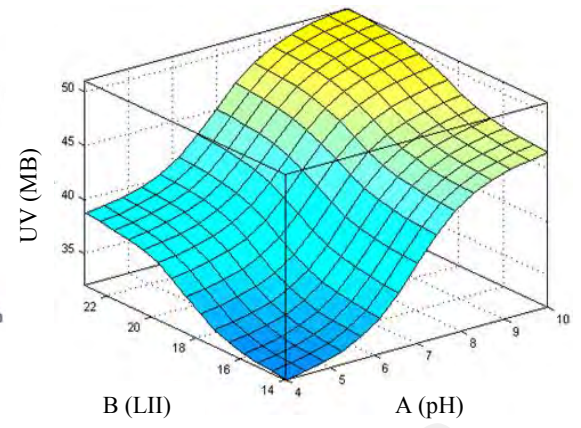
**Figure 4.19:** Pseudo-first-order kinetics for heterogeneous photocatalytic degradation of Methylene orange using different Cu-ZnO/TiO<sub>2</sub> with copper concentrations of □: 1wt%, ◇: 2wt%, △: 3wt%, \*: 4wt%, ○: 5wt%. Empty bullets: Calcined at 500°C, Solid bullets: Calcined at 700°C.

#### 4.5 Sensitivity using (ANFIS) methodology

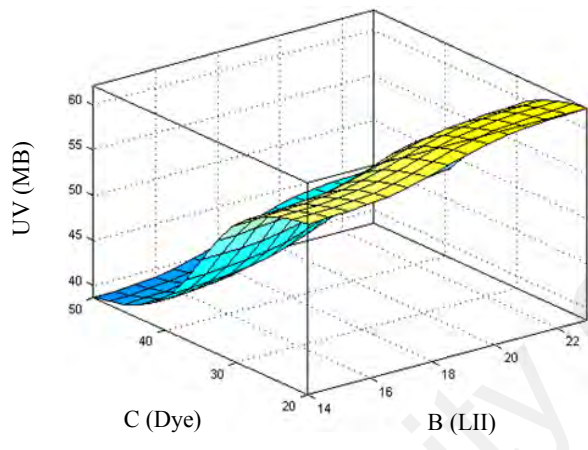
The photoactivity of Cu-TiO<sub>2</sub>/ZnO in terms of colour, COD and TOC removal of methyl orange and methylene blue for water treatment based on ANFIS analysis are presented in Fig. 4.20(a-h). Generally, the experimental results showed that greater light irradiation intensity increased the photoactivity of Cu-TiO<sub>2</sub>/ZnO due to activation of more electron-hole pairs. On average, the increment was about 6.5% and 8% for MB and MO within 80 min, respectively.



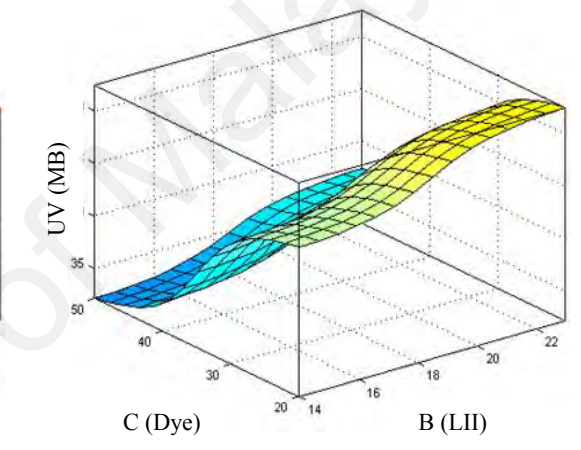
(a)



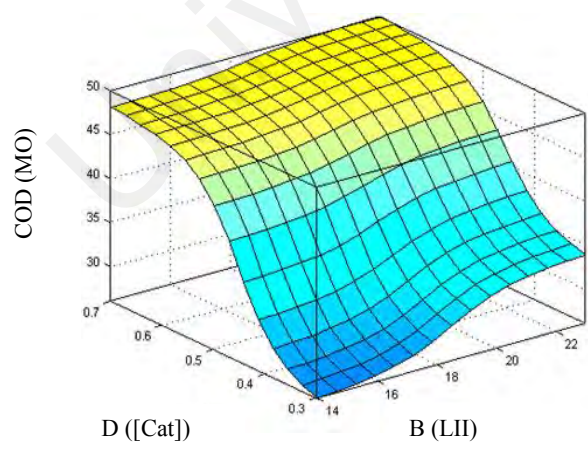
(b)



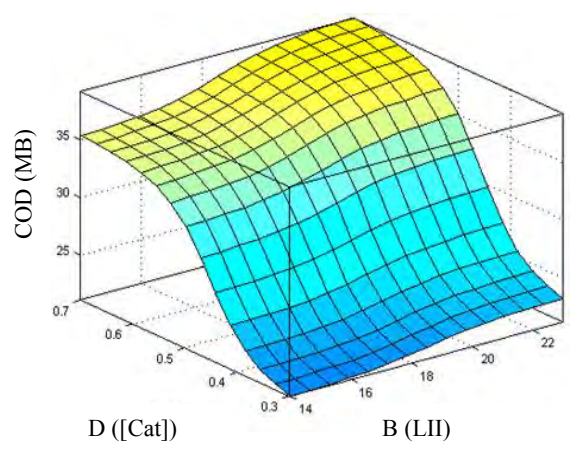
(c)



(d)

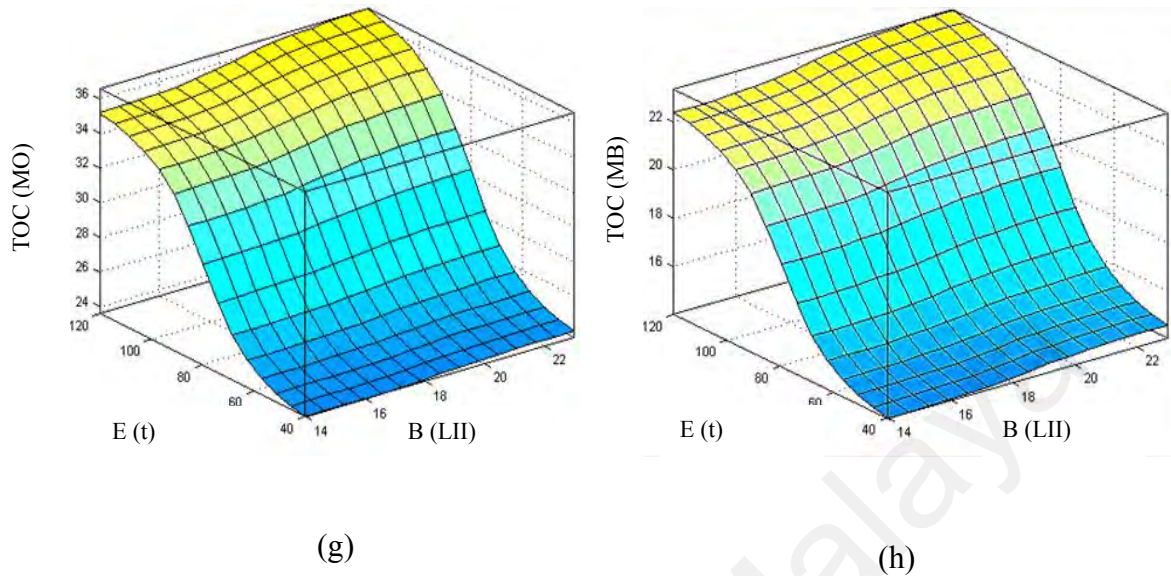


(e)



(f)

Figure 4.21, continued



**Figure 4.20:** ANFIS predicted relationship for Color, COD and TOC removal efficiency (%) as a function of BA, BC, BD and BE effects. (a)(c)(e)(g): MO and (b)(d)(f)(h):MB.

Accordingly, the combined synergistic or antagonistic effects of other parameters with the intensity of light irradiation are depicted in photoactivity of Cu-TiO<sub>2</sub>/ZnO. The colour removal of MO (an anionic dye) and MB (a cationic dye) versus acidity of the solution are shown in Fig. 4.20 (a-b). As observed, higher degradation efficiency of methyl orange was observed at acidic pH, while the opposite was observed for methylene blue. It was attributed to the zero charge point of the catalyst which is defined as the point at which surface charge of the catalyst is null (pH<sub>PZC</sub>). It has been reported that pH<sub>PZC</sub> is about 6.0 and 9.0 for TiO<sub>2</sub> and ZnO (Benhebal, Chaib et al. 2013, Mohd Omar, Abdul Aziz et al. 2014, Zhu, Wang et al. 2014), respectively. Therefore, at pH > pH<sub>PZC</sub>, deprotonation reaction that takes place makes the catalyst surface negatively charged. On the other hand, at pH < pH<sub>PZC</sub>, protonation reaction takes place and the catalyst surface is positively charged. Basicity or acidity of the solution

determines the surface charge properties of the photocatalyst. It can be suggested that Cu-TiO<sub>2</sub>/ZnO is positively charged in acidic solution and it adsorbs MO molecules by electrostatic attraction. In such conditions, adsorption of MB becomes weaker due to repulsive forces in alkaline solution. Similar results were observed by Wang et al. (Wang, Duan et al. 2014) and Bubacz et al. (Bubacz, Choina et al. 2010).

As shown in Fig. 4.20c and 4.20d, the photoactivity of Cu-TiO<sub>2</sub>/ZnO was critically affected by initial dye concentration. Greater dye concentration not only reduces the penetration depth of the photons but also saturates the surface charge of catalyst for adsorption of hydroxyl ions, reducing the efficiency of the catalyst. In this study, the colour removal efficiency (%) decreased by about 17.20% and 22.85% with increment in the concentration of MB and MO, respectively from 20 to 50 ppm in the presence of 0.5g/L catalyst within 80min.

The effect of catalyst concentration on COD degradation of MO and MB of 50ppm within 80 min are also presented in Fig. 4.20 (e) and (f). As observed, COD removal prominently increased with catalyst concentration to almost 0.6 g/L and then it reached a plateau. It can be suggested that, Cu-TiO<sub>2</sub>/ZnO concentration of 0.6g/L was in a synergistic interaction with light irradiation and at the solution pH of <6 for MO and >7.5 for MB, there was maximum and reasonable photocatalytic degradation of the dyes. For instance, the reaction conditions of [catalyst]: 0.6 g/L, [dye]: 35 ppm, pH: 5.5, light irradiation intensity: 18.5 Watt and time: 120 min yielded about 78.45%, 63.68% and 51.81% removal of color, COD and TOC of the methyl orange solution, respectively. However, the corresponding removals only rose to 77.15%, 63.85% and 51.86% when the catalyst concentration rose to 0.7g/L. Similar effect was observed for MB removal by increasing the catalyst concentration. The other reason was scavenging of OH radicals over the surface of the catalyst. The same observation was reported by

Wang et al. (Wang, Li et al. 2010) for degradation of methyl orange, rhodamine B, azo fuchsin, congo red and methyl blue in the presence of  $\text{Er}^{3+}\text{YAlO}_3/\text{ZnO-TiO}_2$  composite.

The trends of TOC removal over 120 min for both MO and MB ([dye]: 35 ppm) are presented in Fig. 4.20g and 4.20h. The same trend was also observed for color and COD removal. It was observed that the photocatalytic degradation increased sharply as the reaction time increased to 90 min and then it significantly reduced. Based on the calculation, the degradation rate within 40min from the starting time ( $t=0\text{min}$ ) was much higher compared to that of  $40\text{min}<t<120\text{min}$ . On the basis of the details of the analysis, the degradation reactions of both MO and MB followed the second-order reaction kinetics. Moreover, Table 3.4 shows that by increasing the reaction time from 40 to 120 min, the averaged colour, COD and TOC removal increased from 39.19 to 58.70, 31.75 to 47.87 and 19.78 to 34.23, respectively for MO at pH 4. For MB removal, the averaged colour, COD and TOC removal changed from 37.75 to 50.23, 29.37 to 42.02 and 16.69 to 28.79 at pH10.

After evaluating the overall effect of different operating variables on photoactivity of the synthesized  $\text{Cu-TiO}_2/\text{ZnO}$ , a comprehensive searching from the given inputs was performed by ANFIS to choose the set of the ultimate optimal combination inputs which has the highest influence on the output parameter (Colour, COD, TOC removal). Accordingly, an ANFIS was model built by the functions of each combination and the functions were then trained for single epoch. Since, a simple model is always preferred; the use of more than two inputs to construct an ANFIS model is not advisable. Therefore, the two-input ANFIS was the basis for further examination. Input parameters were chosen from the initial training and the checking datasets were then extracted. To enable ANFIS to find the right inputs quickly, the used function for all variables only

trained each function for a single epoch. Once the inputs were fixed, the quantity of epoch on ANFIS training was increased.

Subsequently, the achieved performance was reported in Tables 4.6-4.8 and Figs. 4.21 and 4.22 (a-f). From the outset, the input that had the highest impact on the prediction of the output was identified and determined, as depicted in Figs. 4.21 and 4.22(a-f). The left-most input variables had the lowest number of errors and were the most relevant to the outcome.

**Table 4.6:** ANFIS regression errors for (a) COD (MO) and (b) COD (MB) prediction

<b>(a)</b>					
	A	B	C	D	E
A	trn=13.5788, chk=39.5953	trn=12.9884, chk=21.0814	trn=11.8725, chk=14.1942	trn=10.2664, chk=41.6486	trn=11.6586, chk=26.6697
B		trn=13.1975, chk=15.2822	trn=11.4721, chk=13.3005	trn=9.7388, chk=14.5786	trn=11.2546, chk=28.0656
C			trn=11.8903, chk=13.0000	trn=8.0218, chk=13.0796	trn=9.9401, chk=44.4019
D				trn=10.4922, chk=14.7359	trn=7.9459, chk=14.2732
E					trn=12.1929, chk=14.5034
<b>(b)</b>					
	A	B	C	D	E
A	trn=8.1257, chk=17.6228	trn=7.9404, chk=13.4524	trn=6.3140, chk=15.4134	trn=6.5434, chk=18.0497	trn=7.7340, chk=20.0278
B		trn=9.1685, chk=16.0595	trn=6.7466, chk=26.2550	trn=6.9417, chk=14.5628	trn=8.1765, chk=27.3865
C			trn=7.3443, chk=15.2469	trn=4.8595, chk=13.6452	trn=6.4309, chk=66.3315
D				trn=8.2355, chk=14.0243	trn=6.8426, chk=14.3543
E					trn=8.8049, chk=15.6607

**Table 4.7:** ANFIS regression errors for (a) TOC (MO) and (b) TOC (MB) prediction

<b>(a)</b>					
	A	B	C	D	E
A	trn=10.8394, chk=38.3261	trn=10.5725, chk=21.8870	trn=9.3418, chk=16.9875	trn=8.5134, chk=38.8058	trn=8.9344, chk=23.1855
B		trn=11.1558, chk=12.7111	trn=9.3714, chk=14.5617	trn=8.5229, chk=12.5232	trn=8.9506, chk=34.1983
C			trn=9.5428, chk=10.5240	trn=6.9257, chk=11.3991	trn=7.3784, chk=72.6985
D				trn=9.4093, chk=12.7736	trn=6.4158, chk=12.6455
E					trn=10.0470, chk=11.8429
<b>(b)</b>					
	A	B	C	D	E
A	trn=5.4325, chk=13.9648	trn=5.3844, chk=10.3864	trn=4.2751, chk=13.4206	trn=5.2694, chk=13.5342	trn=5.0276, chk=13.0826
B		trn=6.7627, chk=14.5613	trn=5.4159, chk=15.4851	trn=6.0617, chk=14.4486	trn=5.9961, chk=22.9495
C			trn=5.5215, chk=13.8583	trn=4.9256, chk=13.2302	trn=4.9194, chk=43.6577
D				trn=6.7585, chk=14.1394	trn=5.8706, chk=14.3237
E					trn=6.5806, chk=14.3668

**Table 4.8:** ANFIS regression errors for (a) UV (MO) and (b) UV (MB) prediction

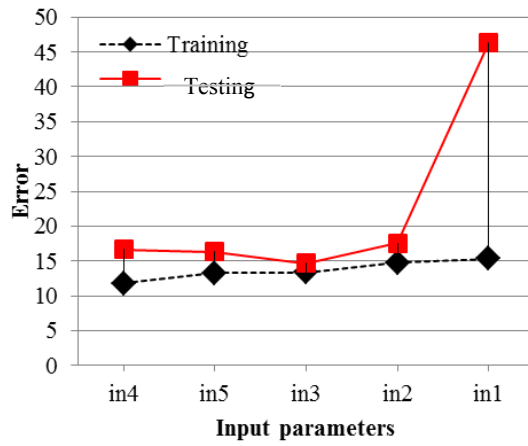
(a)					
	A	B	C	D	E
A	trn=15.3154, chk=46.3831	trn=14.4425, chk=23.3328	trn=13.0556, chk=22.4361	trn=11.6223, chk=50.0240	trn=12.6317, chk=31.6612
B		trn=14.7175, chk=17.5138	trn=12.6083, chk=22.6530	trn=10.9370, chk=16.6547	trn=12.1356, chk=31.9204
C			trn=13.3231, chk=14.6535	trn=9.0736, chk=14.2568	trn=10.4867, chk=78.5220
D				trn=11.7727, chk=16.6626	trn=8.5239, chk=16.0572
E					trn=13.2987, chk=16.2965

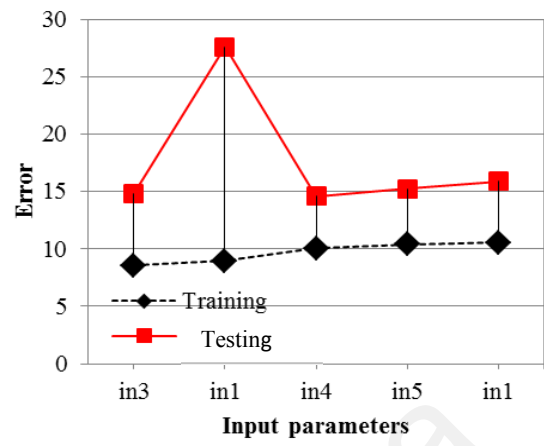
(b)					
	A	B	C	D	E
A	trn=8.9689, chk=27.5768	trn=8.3114, chk=15.0759	trn=6.4623, chk=17.3156	trn=8.2036, chk=27.7094	trn=8.1754, chk=25.9802
B		trn=10.5466, chk=15.8548	trn=7.0390, chk=34.9871	trn=8.8504, chk=14.7736	trn=8.7218, chk=39.2389
C			trn=8.5434, chk=14.8521	trn=6.9600, chk=14.0702	trn=6.8392, chk=108.8177
D				trn=10.0510, chk=14.6058	trn=8.7194, chk=14.7814
E					trn=10.3837, chk=15.2219

TiO<sub>2</sub>/ZnO concentration and reaction time (input variable 4 and 5) were the most influential on COD, TOC and UV removal of methyl orange. However, as shown in Figs. 4.21 and 4.22 (b, d, f), dye concentration and pH (input variable 1 and 3) were the most influential parameters for methylene blue removal. It may be due to the darkness of the media which significantly increased with MB concentration.

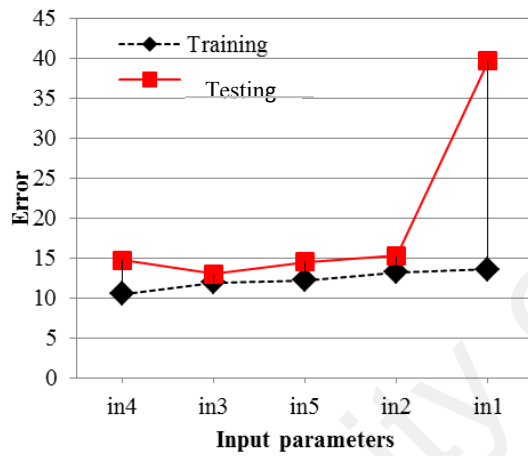




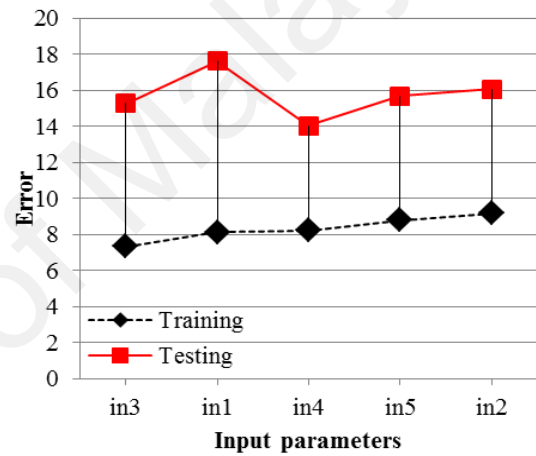
(a)



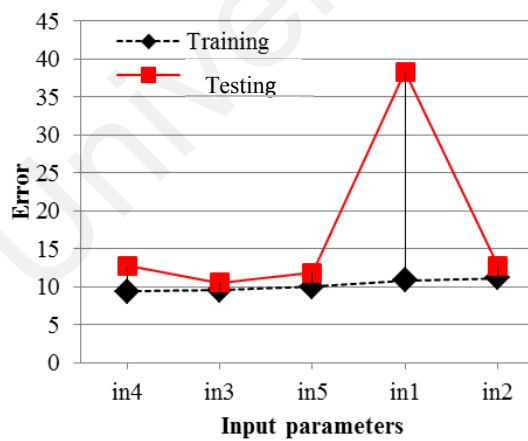
(b)



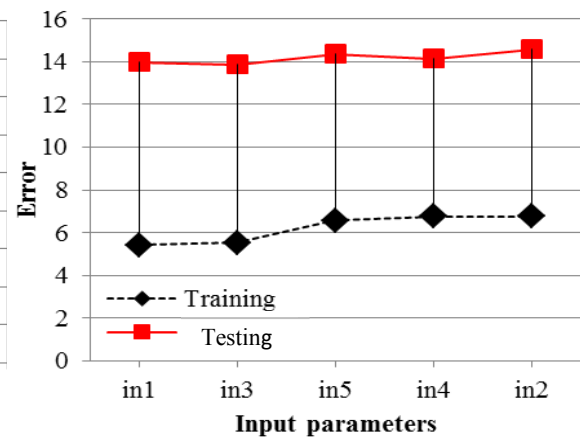
(c)



(d)

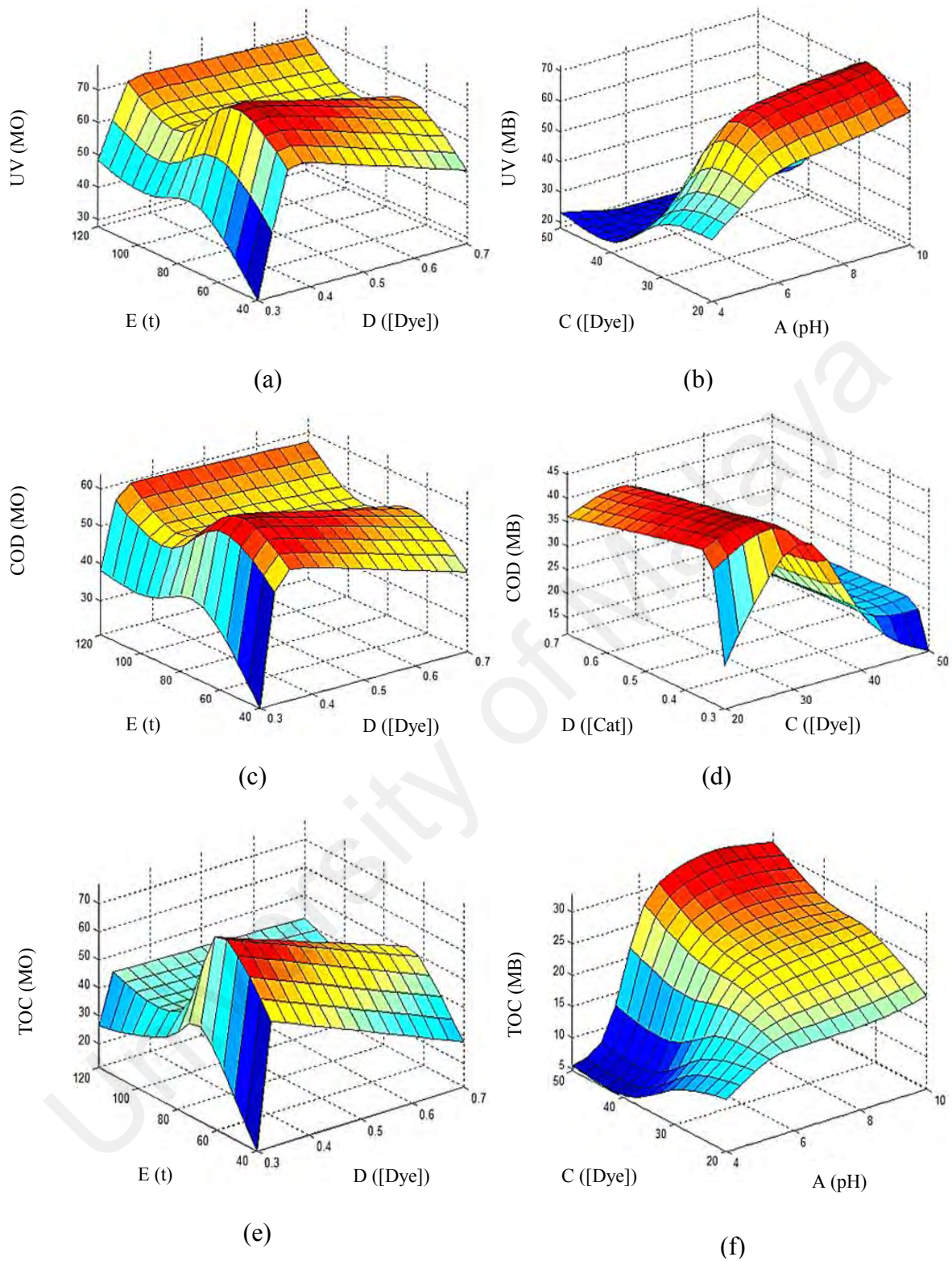


(e)



(f)

**Figure 4.21:** Every input parameter's influence on (a) UV (MO), (b) UV (MB), (c) COD (MO), (d) COD (MB), (e) TOC (MO), (f) TOC (MB).



**Figure 4.22:** ANFIS predicted relationship between the most influential parameters and (a) UV (MO), (b) UV (MB), (c) COD (MO), (d) COD (MB), (e) TOC (MO), (f) TOC (MB).

The fact that both the checking errors and training were comparable is an indirect indication that suggests that there was no over fitting. This means that the selection of more than one input parameter in the construction of the ANFIS model is feasible. Tables 4.6-4.8 show the optimal combinations of two inputs for prediction of COD, TOC and UV removal. The results indicated that the combination of D and E (Cu-TiO<sub>2</sub>/ZnO concentration and reaction time) was the most influential parameters on COD, TOC and UV removals of MO; while D, C and A (Cu-TiO<sub>2</sub>/ZnO and dye concentration and pH) were the most effective parameters for UV, COD and TOC removals of MB.

#### **4.6 Removal process optimization**

In order to identify the conditions at which Cu-TiO<sub>2</sub>/ZnO can demonstrate its highest removal efficiency or be more applicable/effective, optimization of operational factor levels was performed based on the experiments done for both MO and MB removals and the quadratic models obtained. Accordingly, the selected criteria to achieve the maximum desirability for photocatalyst efficiency (Color, COD and TOC), “within the range” for dye/catalyst concentrations, visible light irradiation and reaction time and pH value ranging 4-6 for MO and 7-10 for MB. Among 20 proposed solutions for each category, the one with the highest desirability was selected and two additional tests were conducted to evaluate the validity of the procedure. The identified optimum conditions for MO and MB were: [Cu-TiO<sub>2</sub>/ZnO]: 0.61 g/L, [Dye]: 20 ppm, pH: 7.8 (for MB); 4.5 (for MO), light intensity: 23 Watt and reaction time: 120 min, respectively. The values of the predicted and experimentally obtained color, COD and TOC removal along with the value of discrepancy among them are summarized in Table 4.9.

**Table 4.9:** Predicted and experimental values of the studied responses at optimum conditions

Response	Predicted Values		Experimental Results		Error%	
	MO	MB	MO	MB	MO	MB
Color removal efficiency (%)	87.43	76.08	85.45	73.20	2.27	2.78
COD removal efficiency (%)	73.15	60.96	70.56	59.92	3.54	1.7
TOC removal efficiency (%)	50.82	40.19	48.70	38.77	4.18	3.54

3% Cu doped TiO<sub>2</sub>/ZnO

As observed, the maximum deviation between the predicted and experimental values was 4.18% which confirmed the validity of the obtained regression models and desirable photoactivity of the synthesized Cu-TiO<sub>2</sub>/ZnO with respect to decolorization, degradation and mineralization of both methyl orange and methylene blue under visible light irradiation. Finally, the results obtained from this study can be compared with the available and similar literatures in Table 4.10.

**Table 4.10:** Available and similar literatures in terms of TiO<sub>2</sub> doped photocatalysts

Catalyst	Cu	surface area (m <sup>2</sup> /g)	Band gap	Crystal size(nm)	Calcination temperature	Comments	Ref
Cu-TiO <sub>2</sub>	0.0%	78.2	3.0	-	450 °C	•Cu(5.0%) presented the highest activity on...	(Aguilar, Navas et al. 2013)
	2.5%	90.9	2.1	-	450 °C		
	5.0%	99.1	1.7	-	450 °C		
	7.5%	104.2	1.6	-	450 °C		
Cu-TiO <sub>2</sub>	0.5%	81	3.15	13	400 °C	•The effect of Sulphoric Acid (SA) and Nitric Acid (NA) were investigated on photo catalyst.	(Colón, Maicu et al. 2006)
		13	3.14	20	500 °C		
		2	3.00	34	600 °C		
Cu-TiO <sub>2</sub>	1%	117	3.37	10	400 °C	•Sulphoric acid and calcination at greater temperature improved the catalyst	(Colón, Maicu et al. 2006)
		55	3.22	17	500 °C		
		<1	3.06	42	600 °C		
Cu-TiO <sub>2</sub> NA	0.5%	123	3.33	9	400 °C	•Cu(0.5%)-TiO <sub>2</sub> /S calcinated under 600 C presented the highest activity on...	(Colón, Maicu et al. 2006)
		11	3.27	19	500 °C		
		1	3.06	36	600 °C		
Cu-TiO <sub>2</sub> SA	1%	112	3.38	10	400 °C		(Colón, Maicu et al. 2006)
		47	3.38	21	500 °C		
		7	2.93	-	600 °C		

-eontinue on next pages”

Table 4.10: continued

Catalyst	Cu	surface area (m <sup>2</sup> /g)	Band gap	Crystal size(nm)	Calcination temperature	Comments	Ref
Cu-TiO <sub>2</sub>	1%	117	3.35	9	400 °C		(Colón, Maicu et al. 2006)
NA		21	3.28	19	500 °C		
		1	3.06	34	600 °C		
Cu-TiO <sub>2</sub>	0.5%	108	3.37	10	400 °C		
SA		43	3.38	20	500 °C		
		10	3.09	-	600 °C		
Cu-TiO <sub>2</sub>	0.1	54.42	3.254	17.01	550 °C	•Cu(0.1%) presented the highest activity on...	(Ganesh, Kumar et al. 2014)
	0.5	50.18	3.247	18.28	550 °C		
	1.0	17.96	3.265	18.80	550 °C		
	5	8.98	3.254	18.80	550 °C		
	10	8.24	3.247	19.05	550 °C		
Cu-ZnO	0.1	-	3.294	-	400 °C	•Cu(0.1%) presented the highest activity on...	(Jongnavakit, Amornpitoksuk et al. 2012)
	0.3	-	3.301	-	400 °C		
	0.5	-	3.315	-	400 °C		
	0.7	-	3.332	-	400 °C		
	1.0	-	3.342	-	400 °C		
ZnO/TiO <sub>2</sub>	20:80	32	2.82	24	450 °C	•ZnO(20)/TiO <sub>2</sub> (80) presented the highest activity on...	(Pozaan and Kambur 2014)
ZnO/TiO <sub>2</sub>	50:50	21	2,87	31	450 °C		
ZnO/TiO <sub>2</sub>	80:20	15	2.89	38	450 °C		

## CHAPTER 5: CONCLUSION AND RECOMMENDATION FOR FUTURE WORK

### 5.1 Conclusion

Objective 1:

In this study, a new photocatalyst, Cu-doped TiO<sub>2</sub>/ZnO with a titanium dioxide to zinc acetate weight ratio of 7:3 and copper content of 1-5wt%, was prepared with the sol-gel process and thermal calcination in air at temperatures of 500 and 700°C. The prepared photocatalyst powder was characterized in terms of thermal properties, crystalline structure, surface morphology, specific surface area, wavelength absorption, and band gap energy level. The characteristics of this new photocatalyst are influenced by both calcination temperatures of 500 and 700°C and ratios of Cu, TiO<sub>2</sub> and ZnO. Generally, the synthesized photocatalysts with greater ZnO content were calcined faster at lower temperature. These samples presented smaller crystal sizes (28.21 nm) and greater surface area (30.55m<sup>2</sup>/g). In terms of crystal morphology, it was found that Cu concentration as well as titanium dioxide to zinc acetate ratio could control the crystal size. This effect was more prominent in samples with higher ZnO content.

Objective 2:

The results indicate a significantly greater improvement in the characteristics of Cu-doped TiO<sub>2</sub>/ZnO compared to TiO<sub>2</sub> and ZnO, especially in band gap energy level, 2.2eV respectively. The objective of this work was to evaluate the photoactivity of Cu-doped TiO<sub>2</sub>/ZnO under visible light irradiation. Accordingly, this photocatalyst's performance in reducing and degrading two different dyes, namely methyl orange and methylene blue with different dye concentrations, catalyst loadings, pH of the medium, light irradiation intensities and reaction times was statistically investigated.

### Objective 3:

The photoactivity sensitivity of the synthesized Cu-doped TiO<sub>2</sub>/ZnO to the operational parameters (catalyst, dyes, pH, light irradiation intensity and time) during photocatalysis reaction was assessed. The results indicate that under optimum conditions ([Cu-doped TiO<sub>2</sub>/ZnO]: 0.6 g/lit, [Dye]: 20 ppm, pH: 4.5 for MO; 7.8 for MB, light intensity: 23 Watt and reaction time: 120 min), the photocatalyst presented the maximum removal efficiency (colour: 85.45%, COD: 70.56% and TOC: 48.70% for MO and colour: 73.20%, COD: 59.92% and TOC: 38.77% for MB). Cu-TiO<sub>2</sub>/ZnO displayed different characteristics depending on the dye molecules' charge. Cu-TiO<sub>2</sub>/ZnO was found to exhibit the highest photoactivity at pH~4.5 for methyl orange and pH~7.8 for methylene blue. Compared to the MB molecules, the negatively charged MO molecules were strongly adsorbed by the synthesised photocatalyst surface and therefore, the overall degradation of methyl orange was about 7.75% higher than methylene blue (on average). According to the results, the decomposition efficiency of the Cu-doped TiO<sub>2</sub>/ZnO photocatalyst also increased by about 8% and 6.5% with light intensity and reaction time for MO and MB, respectively. It was also observed that the new triple-doped photocatalyst, Cu-doped TiO<sub>2</sub>/ZnO complex, presented a lower band gap energy level than the double-doped photocatalysts, Cu doped TiO<sub>2</sub> and ZnO doped TiO<sub>2</sub> separately. Therefore, this new photocatalyst can be activated under visible light. The lowest band gap value about 2.2eV was observed for the Cu (3wt%)-doped TiO<sub>2</sub> (70wt %) / ZnO (27wt %) sample.

### Objective 4:

Finally, the photocatalysis evaluation revealed the superior photocatalytic activity of Cu-doped TiO<sub>2</sub>/ZnO over TiO<sub>2</sub>/ZnO and pure TiO<sub>2</sub> under visible light irradiation. It was noticed that the photoactivity of Cu-doped TiO<sub>2</sub>/ZnO was significantly influenced by



the key operational synthesis factors of calcination temperature and dopant content. Accordingly, the highest degradation of 97% was obtained by Cu-doped TiO<sub>2</sub>/ZnO with 3wt% copper calcined at 500°C.

## 5.2 Recommendation for future work

Based on the work done so far, the following recommendation for future work are suggested for their importance in improving the photocatalyst activity and photodegradation efficiency of the process:

1. Doping TiO<sub>2</sub>/ZnO with copper was investigated to achieve absorption from the visible region by reducing the band gap of the doped catalyst. The investigation of doping TiO<sub>2</sub>/ZnO with other materials for efficient of recalcitrant wastewaters are recommended.
2. Higher photocatalytic degradation of methylene blue MB and methyl Orange MO by Cu doped TiO<sub>2</sub>/ZnO is mainly triggered under visible light, more studies must be used of other pollutants from other sources or actual wastewater for photocatalytic degradation.
3. In this study Cu doped TiO<sub>2</sub>/ZnO was successfully synthesized by sol-gel. And future works are recommended to focus on other dopants.

## REFERENCES

- Abdollahi, Y., A. H. Abdullah, Z. Zainal and N. A. Yusof (2011). "Photodegradation of o-cresol by ZnO under UV irradiation." *Journal of American Science* **7**(8): 165-170.
- Abdollahi, Y., A. H. Abdullah, Z. Zainal and N. Yusof, A. (2011). "Photodegradation of m-cresol by Zinc Oxide under Visible-light Irradiation " *International Journal of Chemistry* **3**(3): 31-43.
- Abe, H. T. K., and M. Naito (2006). "Influence of NH<sub>3</sub>/Ar plasma irradiation on physical and photocatalytic properties of TiO<sub>2</sub> nanopowder." *Journal of Photochemistry and Photobiology A* **183**(1-2): 171-175.
- Abedini Khorramia, S. G. Mahmoudzadeha, S. S. Madania and F. Gharibb (2011). "Effect of calcination temperature on the particle sizes of zinc ferrite prepared by a combination of sol-gel auto combustion and ultrasonic irradiation techniques." *Journal of Ceramic Processing Research* **12**(5): 504-508.
- Adan, C., et al. (2007). "Structure and activity of nanosized iron-doped anatase TiO<sub>2</sub> catalysts for phenol photocatalytic degradation." *Applied Catalysis B: Environmental* **72**(1-2): 11-17.
- Adan, C. J. C., A. Bahamonde, and A. Mart'inez- Arias (2009). "Phenol photodegradation with oxygen and hydrogen peroxide over TiO<sub>2</sub> and Fe-doped TiO<sub>2</sub>." *Catalysis Today* **143**(3-4): 247-252.
- Aguilar, T., J. Navas, R. Alcántara, C. Fernández-Lorenzo, J. J. Gallardo, G. Blanco and J. Martín-Calleja (2013). "A route for the synthesis of Cu-doped TiO<sub>2</sub> nanoparticles with a very low band gap." *Chemical Physics Letters* **571**(0): 49-53.
- Ahmad, M., E. Ahmed, Z. L. Hong, X. L. Jiao, T. Abbas and N. R. Khalid (2013). "Enhancement in visible light-responsive photocatalytic activity by embedding Cu-doped ZnO nanoparticles on multi-walled carbon nanotubes." *Applied Surface Science* **285**, Part B(0): 702-712.
- Ahn, Y. U., E. J. Kim, H. T. Kim and S. H. Hahn (2003). "Variation of structural and optical properties of sol-gel TiO<sub>2</sub> thin films with catalyst concentration and calcination temperature." *Materials Letters* **57**(30): 4660-4666.
- Akpan, U. G. and B. H. Hameed (2011). "Enhancement of the photocatalytic activity of TiO<sub>2</sub> by doping it with calcium ions." *Journal of Colloid and Interface Science* **357**(1): 168-178.
- Alem, A. and H. Sarpoolaky (2010). "The effect of silver doping on photocatalytic properties of titania multilayer membranes." *Solid State Sciences* **12**(8): 1469-1472.

- Ambrus, Z. N. B. a., T. Alapi et al (2008). "Synthesis, structure and photocatalytic properties of Fe(III)-doped TiO<sub>2</sub> prepared from TiCl<sub>3</sub>." *Applied Catalysis B: Environmental* **81**(1-2): 27-37.
- Anandan, S., A. Vinu, K. L. P. Sheeja Lovely, N. Gokulakrishnan, P. Srinivasu, T. Mori, V. Murugesan, V. Sivamurugan and K. Ariga (2007). "Photocatalytic activity of La-doped ZnO for the degradation of monocrotophos in aqueous suspension." *Journal of Molecular Catalysis A: Chemical* **266**(1-2): 149-157.
- Ansari, S. A., Khan, M. M., Ansari, M. O., & Cho, M. H. (2016). Nitrogen-doped titanium dioxide (N-doped TiO<sub>2</sub>) for visible light photocatalysis. *New Journal of Chemistry*, **40**(4), 3000-3009.
- Arin, J., S. Thongtem and T. Thongtem (2013). "Single-step synthesis of ZnO/TiO<sub>2</sub> nanocomposites by microwave radiation and their photocatalytic activities." *Materials Letters* **96**(0): 78-81.
- Asilturk, M., F. Sayilkan, and E. Arpac (2009). "Effect of Fe<sup>3+</sup> ion doping to TiO<sub>2</sub> on the photocatalytic degradation of Malachite Green dye under UV and vis-irradiation." *Journal of Photochemistry and Photobiology A: Chemistry* **203**(1): 64-71.
- Asahi, R. Y. O. J. I., Morikawa, T. A. K. E. S. H. I., Ohwaki, T., Aoki, K., & Taga, Y. (2001). Visible-light photocatalysis in nitrogen-doped titanium oxides. *science*, **293**(5528): 269-271.
- Aviam, O., G. Bar-Nes, Y. Zeiri and A. Sivan (2004). "Accelerated biodegradation of cement by sulfur-oxidizing bacteria as a bioassay for evaluating immobilization of low-level radioactive waste." *Applied and environmental microbiology* **70**(10): 6031.
- Bahadur, N. M., T. Furusawa, M. Sato, F. Kurayama and N. Suzuki (2010). "Rapid synthesis, characterization and optical properties of TiO<sub>2</sub> coated ZnO nanocomposite particles by a novel microwave irradiation method." *Materials Research Bulletin* **45**(10): 1383-1388.
- Baiju, K. V., P. Shajesh, W. Wunderlich, P. Mukundan, S. R. Kumar and K. G. K. Warriar (2007). "Effect of tantalum addition on anatase phase stability and photoactivity of aqueous sol-gel derived mesoporous titania." *Journal of Molecular Catalysis A: Chemical* **276**(1-2): 41-46.
- Bakardjieva, S., V. Stengl, L. Szatmary, J. Subrt, J. Lukac, N. Murafa, D. Niznansky, K. Cizek, J. Jirkovsky and N. Petrova (2006). "Transformation of brookite-type TiO<sub>2</sub> nanocrystals to rutile: correlation between microstructure and photoactivity." *Journal of Materials Chemistry* **16**(18): 1709-1716.
- Bandara, J., I. Guasaquillo, P. Bowen, L. Soare, W. F. Jardim and J. Kiwi (2005). "Photocatalytic Storing of O<sub>2</sub> as H<sub>2</sub>O<sub>2</sub> Mediated by High Surface Area CuO. Evidence for a Reductive-Oxidative Interfacial Mechanism." *Langmuir* **21**(18): 8554-8559.

- Barakat, M. A., et al (2005). "Photocatalytic degradation of 2-chlorophenol by Co-doped TiO<sub>2</sub> nanoparticles." *Applied Catalysis B: Environmental* **57**(1): 23-30.
- barbuslinski, K. (2009). "Fenton reaction controversy concerning the chemistry." *ecological chemistry and engineering* **16**(3).
- Batistella, L., L. A. Lerin, P. Brugnerotto, A. J. Danielli, C. M. Trentin, A. Popiolski, H. Treichel, J. V. Oliveira and D. de Oliveira (2012). "Ultrasound-assisted lipase-catalyzed transesterification of soybean oil in organic solvent system." *Ultrasonics Sonochemistry* **19**(3): 452-458.
- Behnajady, M. A., N. Modirshahla and R. Hamzavi (2006). "Kinetic study on photocatalytic degradation of C.I. Acid Yellow 23 by ZnO photocatalyst." *Journal of Hazardous Materials* **133**(1–3): 226-232.
- Benhebal, H., M. Chaib, T. Salmon, J. Geens, A. Leonard, S. D. Lambert, M. Crine and B. Heinrichs (2013). "Photocatalytic degradation of phenol and benzoic acid using zinc oxide powders prepared by the sol–gel process." *Alexandria Engineering Journal* **52**(3): 517-523.
- Bettinelli, M. V. D., D. Falcomer (2007). "Photocatalytic activity of TiO<sub>2</sub> doped with boron and vanadium." *Journal of Hazardous Materials* **146**(3): 529-534.
- Binas, V. D., et al., 2012. 113-114(0): p. 79-86. (2012). "Synthesis and photocatalytic activity of Mn-doped TiO<sub>2</sub> nanostructured powders under UV and visible light." *Applied Catalysis B: Environmental*, **113-114**: 79-86.
- Bubacz, K., J. Choina, D. Dolat and A. W. Morawski (2010). "Methylene Blue and Phenol Photocatalytic Degradation on Nanoparticles of Anatase TiO<sub>2</sub>." *Polish Journal of Environmental Studies* **19**(4).
- Buyukbingol, E., A. Sisman, M. Akyildiz, F. N. Alparslan and A. Adejare (2007). "Adaptive neuro-fuzzy inference system (ANFIS): A new approach to predictive modeling in QSAR applications: A study of neuro-fuzzy modeling of PCP-based NMDA receptor antagonists." *Bioorganic & Medicinal Chemistry* **15**(12): 4265-4282.
- Carp, O., C. L. Huisman and A. Reller (2004). "Photoinduced reactivity of titanium dioxide." *Progress in Solid State Chemistry* **32**(1): 33-177.
- Carraway, E. R., A. J. Hoffman and M. R. Hoffmann (1994). "Photocatalytic Oxidation of Organic Acids on Quantum-Sized Semiconductor Colloids." *Environmental Science & Technology* **28**(5): 786-793.
- Carvalho, H. P. (2013). "TiO<sub>2</sub>–Cu photocatalysts: a study on the long- and short-range chemical environment of the dopant." *Journal of Materials Science* **48**(11): 3904.
- Chan, K. Y., S. H. Ling, T. S. Dillon and H. T. Nguyen (2011). "Diagnosis of hypoglycemic episodes using a neural network based rule discovery system." *Expert Systems with Applications* **38**(8): 9799-9808.

- Chen, S., W. Zhao, W. Liu and S. Zhang (2008). "Preparation, characterization and activity evaluation of p-n junction photocatalyst p-ZnO/n-TiO<sub>2</sub>." *Applied Surface Science* **255**(5, Part 1): 2478-2484.
- Chen, Y., C. Zhang, W. Huang, C. Yang, T. Huang, Y. Situ and H. Huang (2014). "Synthesis of porous ZnO/TiO<sub>2</sub> thin films with superhydrophilicity and photocatalytic activity via a template-free sol-gel method." *Surface and Coatings Technology* **258**(0): 531-538.
- Chen, Z., N. Zhang and Y.-J. Xu (2013). "Synthesis of graphene-ZnO nanorod nanocomposites with improved photoactivity and anti-photocorrosion." *CrystEngComm* **15**(15): 3022-3030.
- Chen, J. J. Xu, Y. H. A., M. D. and D. G. Fu (2009). "Lowtemperature preparation of Boron-doped titania by hydrothermal method and its photocatalytic activity." *Journal of Alloys and Compounds* **484**(1-2): 73-79.
- Cheng, J. G. Yu, W. G. W., B. and B. L. Su (2009). "Enhancement of photocatalytic activity of Mesoporous TiO<sub>2</sub> powders by hydrothermal surface fluorination treatment " *Journal of Physical Chemistry C* **113**(16): 6743-6750.
- Chin-Chuan Liu, Y.-H. H., Pao-Fan Lai, Chia-Hsin Li, Chao-Lang Kao ( 2006). "Dyes and Pigments." **68**: 191e195.
- Chin-Chuan Liu, Y.H.H. P.-F. L., Chia-Hsin Li, Chao-Lang Kao (2006). *Dyes and Pigments* **68**: 191-195.
- Chiou, C.-H. a. R.-S. J. (2007). "Photocatalytic degradation of phenol in aqueous solutions by Pr-doped TiO<sub>2</sub> nanoparticles." *Journal of Hazardous Materials* **149**(1): 1-7.
- Colon, G. (2006). " Cu-doped TiO<sub>2</sub> systems with improved photocatalytic activity." *Applied Catalysis B: Environmental* **67**: 41-51.
- Colón, G., M. Maicu, M. C. Hidalgo and J. A. Navío (2006). "Cu-doped TiO<sub>2</sub> systems with improved photocatalytic activity." *Applied Catalysis B: Environmental* **67**(1-2): 41-51.
- Cronmeyer, D. C. (1959). "Infrared Absorption of Reduced Rutile TiO<sub>2</sub> Single Crystals." *Physical Review* **113**(5): 1222-1226.
- Dalai Ajay, K., Ed. (2012). Nanocatalysis for Fuels and Chemicals. ACS Symposium Series, *American Chemical Society* **1092**.
- Daneshvar, N., S. Aber, M. Seyed Dorraji, A. Khataee and M. Rasoulifard (2007). "Photocatalytic degradation of the insecticide diazinon in the presence of prepared nanocrystalline ZnO powders under irradiation of UV-C light." *Separation and purification Technology* **58**(1): 91-98.

- Daneshvar, N., D. Salari and A. R. Khataee (2004). "Photocatalytic degradation of azo dye acid red 14 in water on ZnO as an alternative catalyst to TiO<sub>2</sub>." *Journal of Photochemistry and Photobiology A: Chemistry* **162**(2-3): 317-322.
- Daneshvar, N. S. A., M. Seyed Dorraji, A. Khataee, M. Rasoulifard (2007). "Photocatalytic degradation of the insecticide diazinon in the presence of prepared nanocrystalline ZnO powders under irradiation of UV-C light." *Separation and purification Technology* **58**: 91-98.
- Devi, L. G., B.N. Murthy, and S.G. Kumar (2009). "Photocatalytic activity of V<sup>5+</sup>, Mo<sup>6+</sup> and Th<sup>4+</sup> doped polycrystalline TiO<sub>2</sub> for the degradation of chlorpyrifos under UV/solar light." *Journal of Molecular Catalysis A: Chemical* **308**(1-2): 174-181.
- Deng, Q. R., Xia, X. H., Guo, M. L., Gao, Y., & Shao, G. (2011). Mn-doped TiO<sub>2</sub> nanopowders with remarkable visible light photocatalytic activity. *Materials Letters*, **65**(13), 2051-2054.
- Devi, L. G., B.N. Murthy, and S.G. Kumar (2010). "Photocatalytic activity of TiO<sub>2</sub> doped with Zn<sup>2+</sup> and V<sup>5+</sup> transition metal ions: Influence of crystallite size and dopant electronic configuration on photocatalytic activity." *Materials Science and Engineering: B* **166**(1): 1-6.
- Diebold, U. (2003). Structure and properties of TiO<sub>2</sub> surfaces: a brief review. *Applied Physics A: Materials Science & Processing*, **76**(5), 681-687.
- Du, Y. and J. Rabani (2003). "The Measure of TiO<sub>2</sub> Photocatalytic Efficiency and the Comparison of Different Photocatalytic Titania." *The Journal of Physical Chemistry B* **107**(43): 11970-11978.
- El-Shobaky, H. G., A. S. Ahmed and N. R. E. Radwan (2006). "Effect of  $\gamma$ -irradiation and ZnO-doping of CuO/TiO<sub>2</sub> system on its catalytic activity in ethanol and isopropanol conversion." *Colloids and Surfaces A: Physicochemical and Engineering Aspects* **274**(1-3): 138-144.
- Elghniji, K., M. Ksibi, and E. Elaloui (2012). "Sol-gel reverse micelle preparation and characterization of N-doped TiO<sub>2</sub>: Efficient photocatalytic degradation of methylene blue in water under visible light." *Journal of Industrial and Engineering Chemistry* **18**(1): 178-182.
- Estruga, M. C. D., X. Dom`enech, and J. A. Ayll ´ on (2010). "Zirconium-doped and silicon-doped TiO<sub>2</sub> photocatalysts synthesis from ionic-liquid-like precursors." *Journal of Colloid and Interface Science* **344**(2): 327-333.
- Fagan, R., McCormack, D. E., Hinder, S. J., & Pillai, S. C. (2016). Photocatalytic Properties of g-C<sub>3</sub>N<sub>4</sub>-TiO<sub>2</sub> Heterojunctions under UV and Visible Light Conditions. *Materials*, **9**(4), 286.
- Ferrari-Lima, A. M., R. P. de Souza, S. S. Mendes, R. G. Marques, M. L. Gimenes and N. R. C. Fernandes-Machado (2015). "Photodegradation of benzene, toluene

and xylenes under visible light applying N-doped mixed TiO<sub>2</sub> and ZnO catalysts." *Catalysis Today* **241, Part A(0)**: 40-46.

- Fragala, M. E., I. Cacciotti, Y. Aleeva, R. Lo Nigro, A. Bianco, G. Malandrino, C. Spinella, G. Pezzotti and G. Gusmano (2010). "Core-shell Zn-doped TiO<sub>2</sub>-ZnO nanofibers fabricated via a combination of electrospinning and metal-organic chemical vapour deposition." *CrystEngComm* **12(11)**: 3858-3865.
- Fujishima, A., T. N. Rao and D. A. Tryk (2000). "Titanium dioxide photocatalysis." *Journal of Photochemistry and Photobiology C: Photochemistry Reviews* **1(1)**: 1-21.
- Fotiou, T., Triantis, T. M., Kaloudis, T., O'Shea, K. E., Dionysiou, D. D., & Hiskia, A. (2016). Assessment of the roles of reactive oxygen species in the UV and visible light photocatalytic degradation of cyanotoxins and water taste and odor compounds using C-TiO<sub>2</sub>. *Water research*, **90**, 52-61.
- Ganesh, I., P. P. Kumar, I. Annapoorna, J. M. Sumliner, M. Ramakrishna, N. Y. Hebalkar, G. Padmanabham and G. Sundararajan (2014). Preparation and characterization of Cu-doped TiO<sub>2</sub> materials for electrochemical, photoelectrochemical, and photocatalytic application. *Applied Surface Science*.
- Ganesh, I., P. P. Kumar, I. Annapoorna, J. M. Sumliner, M. Ramakrishna, N. Y. Hebalkar, G. Padmanabham and G. Sundararajan (2014). "Preparation and characterization of Cu-doped TiO<sub>2</sub> materials for electrochemical, photoelectrochemical, and photocatalytic applications." *Applied Surface Science* **293(0)**: 229-247.
- Gao, J., R. Jiang, J. Wang, P. Kang, B. Wang, Y. Li, K. Li and X. Zhang (2011). "The investigation of sonocatalytic activity of Er<sup>3+</sup>:YAlO<sub>3</sub>/TiO<sub>2</sub>-ZnO composite in azo dyes degradation." *Ultrasonics Sonochemistry* **18(2)**: 541-548.
- Gao, J., X. Luan, J. Wang, B. Wang, K. Li, Y. Li, P. Kang and G. Han (2011). "Preparation of Er<sup>3+</sup>:YAlO<sub>3</sub>/Fe-doped TiO<sub>2</sub>/ZnO and its application in photocatalytic degradation of dyes under solar light irradiation." *Desalination* **268**: 68-75.
- Gaya, U. I. and A. H. Abdullah (2008). "Heterogeneous photocatalytic degradation of organic contaminants over titanium dioxide: a review of fundamentals, progress and problems." *Journal of Photochemistry and Photobiology C: Photochemistry Reviews* **9(1)**: 1-12.
- Geethanjali, M. and S. M. Raja Slochanal (2008). "A combined adaptive network and fuzzy inference system (ANFIS) approach for overcurrent relay system." *Neurocomputing* **71(4-6)**: 895-903.
- Gennari, F. C. and D. M. Pasquevich (1998). "Kinetics of the anatase-rutile transformation in TiO<sub>2</sub> in the presence of Fe<sub>2</sub>O<sub>3</sub>." *Journal of Materials Science* **33(6)**: 1571-1578.

- Gleick, P. H. ( 2004). "The World's Water 2004-2005: The Biennial Report On Freshwater Resources." *Island Press*.
- Gonçalves, G., et al., 2006. 352(32–35): p. 3697-3704. (2006). "Preparation and characterization of nickel based catalysts on silica, alumina and titania obtained by sol–gel method." *Journal of Non-Crystalline Solids* **352**(32-35): 3697-3704.
- Grabowska, E. A. Z., J. W. Sobczak, M. Gazda, and J. Hupka (2009). "Boron-doped TiO<sub>2</sub>: characteristics and photoactivity under visible light." *Procedia Chemistry* **1**(2): 1553–1559
- Habibi, M. H., N. Talebian and J.-H. Choi (2007). "The effect of annealing on photocatalytic properties of nanostructured titanium dioxide thin films." *Dyes and Pigments* **73**(1): 103-110.
- Hadj Benhebal , M. C., Thierry Salmon , Je´re´my Geens , and S. p. D. L. Ange´lique Leonard , Michel Crine , Benoiˆt Heinrichs (2013). "Photocatalytic degradation of phenol and benzoic acid using zinc oxide powders prepared by the sol–gel process." *Alexandria Engineering Journal* **52**: 517-523.
- Hamadani, M., A. Reisi-Vanani and A. Majedi (2009). "Preparation and characterization of S-doped TiO<sub>2</sub> nanoparticles, effect of calcination temperature and evaluation of photocatalytic activity." *Materials Chemistry and Physics* **116**(2–3): 376-382.
- Hamadani, M., A. Reisi-Vanani and A. Majedi (2010). "Synthesis, characterization and effect of calcination temperature on phase transformation and photocatalytic activity of Cu,S-codoped TiO<sub>2</sub> nanoparticles." *Applied Surface Science* **256**(6): 1837-1844.
- Han, C., M.-Q. Yang, B. Weng and Y.-J. Xu (2014). "Improving the photocatalytic activity and anti-photocorrosion of semiconductor ZnO by coupling with versatile carbon." *Physical Chemistry Chemical Physics* **16**(32): 16891-16903.
- Hadj Benhebal , M.C. T. S., Je´re´my Geens ,, S.p.D.L. Ange´lique Leonard , Michel Crine , Benoiˆt Heinrichs (2013). "Photocatalytic degradation of phenol and benzoic acid using zinc oxide powders prepared by the sol–gel process." *Alexandria Engineering Journal* **52**: 517-523.
- HeF, (2013). "Solvothermal synthesis of N-doped TiO<sub>2</sub> nanoparticles using different nitrogen sources, and their photocatalytic activity for degradation of benzene." *Chinese Journal of Catalysis* **34**(12): 2263-2270.
- He, C. B. T., and J. Zhang (2010). "Thermally stable SiO<sub>2</sub>- doped mesoporous anatase TiO<sub>2</sub> with large surface area and excellent photocatalytic activity." *Journal of Colloid and Interface Science* **344**(2): 382-389.
- He, Z. Y. Li, Q. Zhang and H. Wang (2010). "Capillary microchannel-based microreactors with highly durable ZnO/TiO<sub>2</sub> nanorod arrays for rapid, high



- efficiency and continuous-flow photocatalysis." *Applied Catalysis B: Environmental* **93**(3–4): 376-382.
- Hirano, M., C. Nakahara, K. Ota and M. Inagaki (2002). "Direct Formation of Zirconia-Doped Titania with Stable Anatase-Type Structure by Thermal Hydrolysis." *Journal of the American Ceramic Society* **85**(5): 1333-1335.
- Ho, W. K. J. C. Y., and S. C. Lee (2006). "Low-temperature hydrothermal synthesis of S-doped TiO<sub>2</sub> with visible light photocatalytic activity." *Journal of Solid State Chemistry* **179**(4): 1171-1176.
- Hung, W.C. S. H. F., J. J. Tseng, H. Chu, and T. H. Ko (2007). "Study on photocatalytic degradation of gaseous dichloromethane using pure and iron ion-doped TiO<sub>2</sub> prepared by the sol-gel method." *Chemosphere* **66**(11): 2142-2151.
- Huang, M. C. X., Z. Wu, Y. Huang, J. Lin, and J. Wu (2008). "Photocatalytic discolorization of methyl orange solution by Pt modified TiO<sub>2</sub> loaded on natural zeolite." *Dyes and Pigments* **77**(2): 327-334.
- Inturi, S. N. R., T. Boningari, M. Suidan and P. G. Smirniotis (2014). "Visible-light-induced photodegradation of gas phase acetonitrile using aerosol-made transition metal (V, Cr, Fe, Co, Mn, Mo, Ni, Cu, Y, Ce, and Zr) doped TiO<sub>2</sub>." *Applied Catalysis B: Environmental* **144**(0): 333-342.
- Ishibai, Y. J. S., T. Nishikawa, and S. Miyagishi (2008). "Synthesis of visible-light active TiO<sub>2</sub> photocatalyst with Pt modification: role of TiO<sub>2</sub> substrate for high photocatalytic activity." *Applied Catalysis B* **79**(2): 117-121.
- Jaiswal, R., Patel, N., Kothari, D. C., & Miotello, A. (2012). Improved visible light photocatalytic activity of TiO<sub>2</sub> co-doped with Vanadium and Nitrogen. *Applied Catalysis B: Environmental*, **126**, 47-54.
- Jin, C. R. Y. Z., Y. Guo, J. L. Xie, Y. X. Zhu, and Y. C. Xie (2009). "Hydrothermal synthesis and characterization of phosphorous-doped TiO<sub>2</sub> with high photocatalytic activity for methylene blue degradation." *Journal of Molecular Catalysis A* **313**(1-2): 44-48.
- Jin, R. Z. W., Y. Liu, B. Jiang, and H. Wang, —vol (2009). "Photocatalytic reduction of NO with NH<sub>3</sub> using Si-doped TiO<sub>2</sub> prepared by hydrothermal method." *Journal of Hazardous Materials* **161**(1): 42-48.
- Jing, D., Zhang, Y., & Guo, L. (2005). Study on the synthesis of Ni doped mesoporous TiO<sub>2</sub> and its photocatalytic activity for hydrogen evolution in aqueous methanol solution. *Chemical Physics Letters*, **415**(1), 74-78.
- Jiassi, M., H. Chorfi, M. Saadoun and B. Bessaïs (2013). "ZnO ratio-induced photocatalytic behavior of TiO<sub>2</sub>-ZnO nanocomposite." *Superlattices and Microstructures* **62**(0): 192-199.

- Johra, F. T. and W.-G. Jung (2015). "RGO–TiO<sub>2</sub>–ZnO composites: Synthesis, characterization, and application to photocatalysis." *Applied Catalysis A: General* **491**(0): 52-57.
- Jongnavakit, P., P. Amornpitoksuk, S. Suwanboon and N. Ndiege (2012). "Preparation and photocatalytic activity of Cu-doped ZnO thin films prepared by the sol-gel method." *Applied Surface Science* **258**(20): 8192-8198.
- Jongsomjit, B., C. Sakdamnusun, J. Goodwin, Jr. and P. Praserttham (2004). "Co-Support Compound Formation in Titania-Supported Cobalt Catalyst." *Catalysis Letters* **94**(3-4): 209-215.
- Jonidi-Jafari, A., M. Shirzad-Siboni, J.-K. Yang, M. Naimi-Joubani and M. Farrokhi "Photocatalytic degradation of diazinon with illuminated ZnO–TiO<sub>2</sub> composite." *Journal of the Taiwan Institute of Chemical Engineers*(0).
- Kanade, K.G. B. B. K., J.-O. Baeg, S.M. Lee, C.W. Lee, S.-J. Moon, H. Chang (2007). "Self-assembled aligned Cu doped ZnO nanoparticles for photocatalytic hydrogen production under visible light irradiation." *Materials Chemistry and Physics* **102**: 98-104.
- Kaur, A., & Kansal, S. K. (2016). Bi<sub>2</sub> WO<sub>6</sub> nanocuboids: An efficient visible light active photocatalyst for the degradation of levofloxacin drug in aqueous phase. *Chemical Engineering Journal*, **302**, 194-203.
- Kansal, S. K., M. Singh and D. Sud (2008). "Studies on TiO<sub>2</sub>/ZnO photocatalysed degradation of lignin." *Journal of Hazardous materials* **153**(1-2): 412-417.
- Karunakaran, C., G. Abiramasundari, P. Gomathisankar, G. Manikandan and V. Anandi (2011). "Preparation and characterization of ZnO–TiO<sub>2</sub> nanocomposite for photocatalytic disinfection of bacteria and detoxification of cyanide under visible light." *Materials Research Bulletin* **46**(10): 1586-1592.
- Karunakaran, C., P. Vinayagamoorthy and J. Jayabharathi (2013). "Electrical, optical and photocatalytic properties of polyethylene glycol-assisted sol-gel synthesized Mn-doped TiO<sub>2</sub>/ZnO core-shell nanoparticles." *Superlattices and Microstructures* **64**(0): 569-580.
- Khan, M. M., J. Lee and M. H. Cho (2014). "Au/TiO<sub>2</sub> nanocomposites for the catalytic degradation of methyl orange and methylene blue: An electron relay effect." *Journal of Industrial and Engineering Chemistry* **20**(4): 1584-1590.
- Khaki, M. R. D., Sajjadi, B., Raman, A. A. A., Daud, W. M. A. W., & Shmshirband, S. (2016). Sensitivity analysis of the photoactivity of Cu–TiO<sub>2</sub>/ZnO during advanced oxidation reaction by Adaptive Neuro-Fuzzy Selection Technique. *Measurement*, **77**, 155-174.
- Kim, C.-S., J.-W. Shin, Y.-H. Cho, H.-D. Jang, H.-S. Byun and T.-O. Kim (2013). "Synthesis and characterization of Cu/N-doped mesoporous TiO<sub>2</sub> visible light photocatalysts." *Applied Catalysis A: General* **455**(0): 211-218.

- Konyar, M., H. C. Yatmaz and K. Öztürk (2012). "Sintering temperature effect on photocatalytic efficiencies of ZnO/TiO<sub>2</sub> composite plates." *Applied Surface Science* **258**(19): 7440-7447.
- Krumme, M. L. and S. A. Boyd (1988). "Reductive dechlorination of chlorinated phenols in anaerobic upflow bioreactors." *Water Research* **22**(2): 171-177.
- Ku, Y., Y.-H. Huang and Y.-C. Chou (2011). "Preparation and characterization of ZnO/TiO<sub>2</sub> for the photocatalytic reduction of Cr(VI) in aqueous solution." *Journal of Molecular Catalysis A: Chemical* **342–343**(0): 18-22.
- Kwong, C. K., T. C. Wong and K. Y. Chan (2009). "A methodology of generating customer satisfaction models for new product development using a neuro-fuzzy approach." *Expert Systems with Applications* **36**(8): 11262-11270.
- Lakshminarayana, G., J. Qiu, M. G. Brik, G. A. Kumar and I. V. Kityk (2008). "Spectral analysis of Er<sup>3+</sup> -, Er<sup>3+</sup> /Yb<sup>3+</sup> - and Er<sup>3+</sup> / Tm<sup>3+</sup> / Yb<sup>3+</sup> -doped TeO<sub>2</sub> -ZnO-WO<sub>3</sub> -TiO<sub>2</sub> -Na<sub>2</sub>O glasses." *Journal of Physics: Condensed Matter* **20**(37): 375101.
- Lee, D. Y., M.-H. Lee, and N.-I. Cho (2012). "Preparation and photocatalytic degradation of erbium doped titanium dioxide nanorods." *Current Applied Physics* **12**(4): 1229-1233.
- Li, F. B. and X. Z. Li (2002). "The enhancement of photodegradation efficiency using Pt-TiO<sub>2</sub> catalyst." *Chemosphere* **48**(10): 1103-1111.
- Li, D. H. H., N. K. Labhsetwar, S. Hishita, and N. Ohashi (2005). "Visible-light-driven photocatalysis on fluorine-doped TiO<sub>2</sub> powders by the creation of surface oxygen vacancies." *Chemical Physics Letters* **401**(4-6): 579–584.
- Li, L., X. Zhang, W. Zhang, L. Wang, X. Chen and Y. Gao (2014). "Microwave-assisted synthesis of nanocomposite Ag/ZnO-TiO<sub>2</sub> and photocatalytic degradation Rhodamine B with different modes." *Colloids and Surfaces A: Physicochemical and Engineering Aspects* **457**(0): 134-141.
- Li, X., R. Xiong, and G. Wei (2009). "Preparation and photocatalytic activity of nanoglued Sn-doped TiO<sub>2</sub>." *Journal of Hazardous Materials* **164**(2-3): 587-591.
- Li, Y., et al (2010). "Activated carbon supported TiO<sub>2</sub>-photocatalysis doped with Fe ions for continuous treatment of dye wastewater in a dynamic reactor." *Journal of Environmental Sciences* **22**(8): 1290-1296.
- Liao, S., H. Donggen, D. Yu, Y. Su and G. Yuan (2004). "Preparation and characterization of ZnO/TiO<sub>2</sub>, SO<sub>4</sub><sup>2-</sup>/ZnO/TiO<sub>2</sub> photocatalyst and their photocatalysis." *Journal of Photochemistry and Photobiology A: Chemistry* **168**(1–2): 7-13.

- Lin, X., et al (2012). "Enhanced photocatalytic activity of fluorine doped TiO<sub>2</sub> by loaded with Ag for degradation of organic pollutants." *Powder Technology* **219**: 173-178.
- Liu, R., H. Ye, X. Xiong and H. Liu (2010). "Fabrication of TiO<sub>2</sub>/ZnO composite nanofibers by electrospinning and their photocatalytic property." *Materials Chemistry and Physics* **121**(3): 432-439.
- Liu, X., L. Pan, T. Lv, Z. Sun and C. Sun (2012). "Enhanced photocatalytic reduction of Cr(VI) by ZnO–TiO<sub>2</sub>–CNTs composites synthesized via microwave-assisted reaction." *Journal of Molecular Catalysis A: Chemical* **363–364**(0): 417-422.
- Liu, Y., et al (2005). "Photocatalytic degradation of azo dyes by nitrogen-doped TiO<sub>2</sub> nanocatalysts." *Chemosphere* **61**(1): 11-18.
- Marcì, G., V. Augugliaro, M. J. López-Muñoz, C. Martín, L. Palmisano, V. Rives, M. Schiavello, R. J. D. Tilley and A. M. Venezia (2001). "Preparation Characterization and Photocatalytic Activity of Polycrystalline ZnO/TiO<sub>2</sub> Systems. 1. Surface and Bulk Characterization." *The Journal of Physical Chemistry B* **105**(5): 1026-1032.
- McManamon, C., J.D. Holmes, and M.A. Morris, 2011. 193(0): p. 120-127. (2011). "Improved photocatalytic degradation rates of phenol achieved using novel porous ZrO<sub>2</sub>-doped TiO<sub>2</sub> nanoparticulate powders." *Journal of Hazardous Materials* **193**: 120-127.
- Mori, K. M., S. Kawasaki, S. Yuan, and H. Yamashita (2008). "Hydrothermal synthesis of TiO<sub>2</sub> photocatalysts in the presence of NH<sub>4</sub> F and their application for degradation of organic compounds." *Chemical Engineering Science* **63**(20): 5066–5070.
- Mugundan, S., Rajamannan, B., Viruthagiri, G., Shanmugam, N., Gobi, R., & Praveen, P. (2015). Synthesis and characterization of undoped and cobalt-doped TiO<sub>2</sub> nanoparticles via sol–gel technique. *Applied Nanoscience*, **5**(4), 449-456.
- Mohan, R., K. Krishnamoorthy and S.-J. Kim (2012). "Enhanced photocatalytic activity of Cu-doped ZnO nanorods." *Solid State Communications* **152**(5): 375-380.
- Mohd Omar, F., H. Abdul Aziz and S. Stoll (2014). "Aggregation and disaggregation of ZnO nanoparticles: influence of pH and adsorption of Suwannee River humic acid." *Sci Total Environ* **469**: 195-201.
- Moradi, S., P. Aberoomand-Azar, S. Raeis-Farshid, S. Abedini-Khorrami and M. H. Givianrad "The effect of different molar ratios of ZnO on characterization and photocatalytic activity of TiO<sub>2</sub>/ZnO nanocomposite." *Journal of Saudi Chemical Society*(0).
- Morikawa, T., Y. Irokawa and T. Ohwaki (2006). "Enhanced photocatalytic activity of TiO<sub>2</sub>-xNx loaded with copper ions under visible light irradiation." *Applied Catalysis A: General* **314**(1): 123-127.

- Murugan, R., V. J. Babu, M. M. Khin, A. S. Nair and S. Ramakrishna (2013). "Synthesis and photocatalytic applications of flower shaped electrospun ZnO–TiO<sub>2</sub> mesostructures." *Materials Letters* **97**(0): 47-51.
- Nadia, A. Laoufi, Sara Hout, T. Djilali, Amel Ounnar, A. Djouadi, N. C. and F. Bentahar (2013). "Removal of a Persistent Pharmaceutical Micropollutant by UV/TiO<sub>2</sub> Process Using an Immobilized Titanium Dioxide Catalyst: Parametric Study " *chemical engineering transactions* **32**.
- Naeem, K. a. F. O. (2010). " Preparation of Fe<sup>3+</sup>-doped TiO<sub>2</sub> nanoparticles and its photocatalytic activity under UV light." *Physica B: Condensed Matter* **405**(1): 221-226.
- Naimi-Joubani, M., M. Shirzad-Siboni, J.-K. Yang, M. Gholami and M. Farzadkia "Photocatalytic reduction of hexavalent chromium with illuminated ZnO/TiO<sub>2</sub> composite." *Journal of Industrial and Engineering Chemistry*(0).
- Nozik, A. J. (1978). "Photoelectrochemistry: Applications to Solar Energy Conversion." *Annual Review of Physical Chemistry* **29**: 189-222.
- Pang, Y. L. and A. Z. Abdullah (2013). " Fe<sup>3+</sup> doped TiO<sub>2</sub> nanotubes for combined adsorption-sonocatalytic degradation of real textile wastewater." *Applied Catalysis B: Environmental* **129**: 473-481.
- Pant, B., H. R. Pant, N. A. M. Barakat, M. Park, K. Jeon, Y. Choi and H.-Y. Kim (2013). "Carbon nanofibers decorated with binary semiconductor (TiO<sub>2</sub>/ZnO) nanocomposites for the effective removal of organic pollutants and the enhancement of antibacterial activities." *Ceramics International* **39**(6): 7029-7035.
- Pant, H. R., B. Pant, R. K. Sharma, A. Amarjargal, H. J. Kim, C. H. Park, L. D. Tijng and C. S. Kim (2013). "Antibacterial and photocatalytic properties of Ag/TiO<sub>2</sub>/ZnO nano-flowers prepared by facile one-pot hydrothermal process." *Ceramics International* **39**(2): 1503-1510.
- Pang, Y. L., & Abdullah, A. Z. (2013). Fe<sup>3+</sup> doped TiO<sub>2</sub> nanotubes for combined adsorption–sonocatalytic degradation of real textile wastewater. *Applied Catalysis B: Environmental*, **129**, 473-481.
- Pant, H. R., C. H. Park, B. Pant, L. D. Tijng, H. Y. Kim and C. S. Kim (2012). "Synthesis, characterization, and photocatalytic properties of ZnO nano-flower containing TiO<sub>2</sub> NPs." *Ceramics International* **38**(4): 2943-2950.
- Paola, A. D., M. Bellardita and L. Palmisano (2013). "Brookite, the Least Known TiO<sub>2</sub> Photocatalyst." *Catalysts*.
- Park, J.-Y., K.-I. Choi, J.-H. Lee, C.-H. Hwang, D.-Y. Choi and J.-W. Lee (2013). "Fabrication and characterization of metal-doped TiO<sub>2</sub> nanofibers for photocatalytic reactions." *Materials Letters* **97**(0): 64-66.

- Pawar, R. C., D.-H. Choi, J.-S. Lee and C. S. Lee (2015). "Formation of polar surfaces in microstructured ZnO by doping with Cu and applications in photocatalysis using visible light." *Materials Chemistry and Physics* **151**(0): 167-180.
- Pei, C. C. and W. W.-F. Leung (2013). "Enhanced photocatalytic activity of electrospun TiO<sub>2</sub>/ZnO nanofibers with optimal anatase/rutile ratio." *Catalysis Communications* **37**(0): 100-104.
- Peng, L. F. C., L. Huang, H. Yu, and H. J. Wang (2008). "Preparation of nitrogen-doped titanium dioxide with visible-light photocatalytic activity using a facile hydrothermal method." *Journal of Physics and Chemistry of Solids* **69**(7): 1657-1664.
- Pei, C. C. and W. W.-F. Leung (2013). "Photocatalytic degradation of Rhodamine B by TiO<sub>2</sub>/ZnO nanofibers under visible-light irradiation." *Separation and purification technology* **114**(0): 108-116.
- Pham, T.-D. and B.-K. Lee (2014). "Cu doped TiO<sub>2</sub>/GF for photocatalytic disinfection of Escherichia coli in bioaerosols under visible light irradiation: Application and mechanism." *Applied Surface Science* **296**(0): 15-23.
- Philip, J. S. a. L. (2010). "Photocatalytic degradation of lindane under UV and visible light using N-doped TiO<sub>2</sub>." *Chemical Engineering Journal* **161**(1-2): 83-92.
- Pozan, G. S. and A. Kambur (2014). "Significant enhancement of photocatalytic activity over bifunctional ZnO-TiO<sub>2</sub> catalysts for 4-chlorophenol degradation." *Chemosphere* **105**: 152-159.
- Pozan, G. S. and A. Kambur (2014). "Significant enhancement of photocatalytic activity over bifunctional ZnO-TiO<sub>2</sub> catalysts for 4-chlorophenol degradation." *Chemosphere* **105**(0): 152-159.
- Pongwan, P., Wetchakun, K., Phanichphant, S., & Wetchakun, N. (2016). Enhancement of visible-light photocatalytic activity of Cu-doped TiO<sub>2</sub> nanoparticles. *Research on Chemical Intermediates*, **42**(4), 2815-2830.
- Rahman, A., M. Ahmed, M. Absi-Halabi, J. Beshara, H. Qabazard and A. Stanislau, Eds. (1995). *Catalysts in Petroleum Refining and Petrochemical Industries*, Elsevier, Amsterdam.
- Raj, K. J. A.A. V. R., and B. Viswanathan (2009). "Surface area, pore size, and particle size engineering of titania with seeding technique and phosphate modification." *Journal of Physical Chemistry C* **113**(31): 13750-13757.
- Ramimoghadam, D., S. Bagheri and S. B. Abd Hamid (2014). "Biotemplated Synthesis of Anatase Titanium Dioxide Nanoparticles via Lignocellulosic Waste Material." *BioMed Research International* **2014**: 7.
- Reyes-Coronado, D., Rodríguez-Gattorno, G., Espinosa-Pesqueira, M. E., Cab, C., de Coss, R. D., & Oskam, G. (2008). Phase-pure TiO<sub>2</sub> nanoparticles: anatase, brookite and rutile. *Nanotechnology*, **19**(14), 145605.

- Rengaraj, S., et al (2006). "Photocatalytic degradation of methylparathion-An endocrine disruptor by Bi<sup>3+</sup>-doped TiO<sub>2</sub>." *Journal of Molecular Catalysis A: Chemical* **247**(1-2): 36-43.
- Robinson, T., G. McMullan, R. Marchant and P. Nigam (2001). "Remediation of dyes in textile effluent: a critical review on current treatment technologies with a proposed alternative." *Bioresource Technology* **77**(3): 247-255.
- Ryu, J. and W. Choi (2007). "Substrate-Specific Photocatalytic Activities of TiO<sub>2</sub> and Multiactivity Test for Water Treatment Application." *Environmental Science & Technology* **42**(1): 294-300.
- Ryu, T. B. N. M.-J. H. a. K.-S., 2011. 33(1): p. 243. (2011). " Synthesis and High Photocatalytic Activity of Zn-doped TiO<sub>2</sub> Nanoparticles by Sol-gel and Ammonia-Evaporation Method." *Bull. Korean Chem. Soc* **33**(1): 243.
- Sakthivel, S. M. V. S., M. Palanichamy, B. Arabindoo, D. W. Bahnemann, and V. Murugesan (2004). "Enhancement of photocatalytic activity by metal deposition: characterisation and photonic efficiency of Pt, Au and Pd deposited on TiO<sub>2</sub> catalyst." *Water Research* **38**(13): 3001-3008.
- Sabri, M. G. M., B. Z. Azmi, Z. Rizwan, M. K. Halimah, M. Hashim and M. H. M. Zaid (2011). "Effect of temperature treatment on the optical characterization of ZnO-Bi<sub>2</sub>O<sub>3</sub>-TiO<sub>2</sub> varistor ceramics." *International Journal of Physical Sciences* **6**(6): 1388-1394.
- Sagar, R. (1996). Together With Chemistry Xii, *Rachna Sagar Private Limited*. 1st. Rachana Sagar Pvt. Ltd. New Delhi.
- Sahu, D. R., L. Y. Hong, S.-C. Wang and J.-L. Huang (2009). "Synthesis, analysis and characterization of ordered mesoporous TiO<sub>2</sub>/SBA-15 matrix: Effect of calcination temperature." *Microporous and Mesoporous Materials* **117**(3): 640-649.
- Sahu, M. and P. Biswas (2011). "Single-step processing of copper-doped titania nanomaterials in a flame aerosol reactor." *Nanoscale Research Letters* **6**(1): 441-441.
- Sangpour, P., F. Hashemi and A. Z. Moshfegh (2010). "Photoenhanced Degradation of Methylene Blue on Cosputtered M:TiO<sub>2</sub> (M = Au, Ag, Cu) Nanocomposite Systems: A Comparative Study." *The Journal of Physical Chemistry C* **114**(33): 13955-13961.
- Schneider, J., M. Matsuoka, M. Takeuchi, J. Zhang, Y. Horiuchi, M. Anpo and D. W. Bahnemann (2014). "Understanding TiO<sub>2</sub> Photocatalysis: Mechanisms and Materials." *chemical reviews* **114**(19): 9919-9986.
- Serpone, N., G. Sauvé, R. Koch, H. Tahiri, P. Pichat, P. Piccinini, E. Pelizzetti and H. Hidaka (1996). "Standardization protocol of process efficiencies and

activation parameters in heterogeneous photocatalysis: relative photonic efficiencies. " *Journal of Photochemistry and Photobiology A: Chemistry* **94**(2–3): 191-203.

- Shaheen, B. S., Salem, H. G., El-Sayed, M. A., & Allam, N. K. (2013). Thermal/electrochemical growth and characterization of one-dimensional ZnO/TiO<sub>2</sub> hybrid nanoelectrodes for solar fuel production. *The Journal of Physical Chemistry C*, **117**(36), 18502-18509.
- Shi, J.-w., S.-h. Chen, S.-m. Wang, Z.-l. Ye, P. Wu and B. Xu (2010). "Favorable recycling photocatalyst TiO<sub>2</sub>/CFA: Effects of calcination temperature on the structural property and photocatalytic activity." *Journal of Molecular Catalysis A: Chemical* **330**(1–2): 41-48.
- Simphele P. Buthelezi, A. O. O., Balakrishna Pillay (2012). "Textile Dye Removal from Wastewater Effluents Using Biofloculants Produced by Indigenous Bacterial Isolates." *Molecules* **17**: 14260-14274.
- Singh, R., A. Kainthola and T. N. Singh (2012). "Estimation of elastic constant of rocks using an ANFIS approach." *Applied Soft Computing* **12**(1): 40-45.
- Siuleiman, S., N. Kaneva, A. Bojinova, K. Papazova, A. Apostolov and D. Dimitrov (2014). "Photodegradation of Orange II by ZnO and TiO<sub>2</sub> powders and nanowire ZnO and ZnO/TiO<sub>2</sub> thin films." *Colloids and Surfaces A: Physicochemical and Engineering Aspects* **460**(0): 408-413.
- Song, K., J. Zhou, J. Bao and Y. Feng (2008). "Photocatalytic Activity of (Copper, Nitrogen)-Codoped Titanium Dioxide Nanoparticles." *Journal of the American Ceramic Society* **91**(4): 1369-1371.
- Son, J. E., Chattopadhyay, J., & Pak, D. (2010). Electrochemical performance of Badoped TiO<sub>2</sub> hollow spheres in water electrolysis. *international journal of hydrogen energy*, **35**(2), 420-427.
- Sreethawong, T. and S. Yoshikawa (2005). "Comparative investigation on photocatalytic hydrogen evolution over Cu-, Pd-, and Au-loaded mesoporous TiO<sub>2</sub> photocatalysts." *Catalysis Communications* **6**(10): 661-668.
- Sun, H. S. W., H. M. Ang, M. O. Tad'e, and Q. Li (2010). "Halogen element modified titanium dioxide for visible light photocatalysis." *Chemical Engineering Journal* **162**(2): 437-447.
- Sun, W. S. Z., Z. Liu, C. Wang, and Z. Mao (2008). "Studies on the enhanced photocatalytic hydrogen evolution over Pt/PEG-modified TiO<sub>2</sub> photocatalysts." *International Journal of Hydrogen Energy* **33**(4): 1112-1117.
- Takeda, N. K. T., 40 (1988) 678-682. (1988). "Generation of superoxide anion radical from atmospheric organic matter." *Bulletin of environmental contamination and toxicology* **40**: 678-682.



- Todorova, N. T. G., T. Vaimakis, and C. Trapalis (2008). "Structure tailoring of fluorine-doped TiO<sub>2</sub> nanostructured powders." *Materials Science and Engineering B* **152**(1-3): 50-54.
- Tong, T. J. Z., B. Tian, F. Chen, and D. He (2008). "Preparation of Fe<sup>3+</sup>-doped TiO<sub>2</sub> catalysts by controlled hydrolysis of titanium alkoxide and study on their photocatalytic activity for methyl orange degradation." *Journal of Hazardous Materials* **155**(3): 572-579.
- Takeda, N. and K. Teranishi (1988). "Generation of superoxide anion radical from atmospheric organic matter." *Bulletin of environmental contamination and toxicology* **40**(5): 678-682.
- Tao, R.-H., J.-M. Wu, J.-Z. Xiao, Y.-P. Zhao, W.-W. Dong and X.-D. Fang (2013). "Conformal growth of ZnO on TiO<sub>2</sub> nanowire array for enhanced photocatalytic activity." *Applied Surface Science* **279**(0): 324-328.
- Tian, J., J. Wang, J. Dai, X. Wang and Y. Yin (2009). "N-doped TiO<sub>2</sub>/ZnO composite powder and its photocatalytic performance for degradation of methyl orange." *Surface and Coatings Technology* **204**(5): 723-730.
- Tian, H J. M., K. Li, and J. Li (2009). "Hydrothermal synthesis of Sdoped TiO<sub>2</sub> nanoparticles and their photocatalytic ability for degradation of methyl orange." *Ceramics International* **35**(3): 1289-1292.
- Trejo-Tzab, R., J. J. Alvarado-Gil, P. Quintana and P. Bartolo-Pérez (2012). "N-doped TiO<sub>2</sub> P25/Cu powder obtained using nitrogen (N<sub>2</sub>) gas plasma." *Catalysis Today* **193**(1): 179-185.
- Tryba, B., M. Toyoda, A. W. Morawski, R. Nonaka and M. Inagaki (2007). "Photocatalytic activity and OH radical formation on TiO<sub>2</sub> in the relation to crystallinity." *Applied Catalysis B: Environmental* **71**(3-4): 163-168.
- Vargas, X., et al (2012). "Fe-doped titanium dioxide synthesized: Photocatalytic activity and mineralization study for azo dye." *Journal of Photochemistry and Photobiology A: Chemistry* **243**: 17-22.
- Vemury, S. and S. E. Pratsinis (1995). "Dopants in Flame Synthesis of Titania." *Journal of the American Ceramic Society* **78**(11): 2984-2992.
- Vorontsov, E. A. K. a. A. V. (2007). "Influence of mesoporous and platinum-modified titanium dioxide preparation methods on photocatalytic activity in liquid and gas phase." *Applied Catalysis B* **77**(1-2): 35-45.
- Wang, W.-A.Q. S., Y.-P.Wang, J.-L. Cao, G.-Q. Liu, and P.Y. Peng (2011). "Preparation and characterization of iodine-doped mesoporous TiO<sub>2</sub> by hydrothermal method." *Applied Surface Science* **257**(8): 3688-3696.
- Wang, M. Z., Xie, W. J., Hu, H., Yu, Y. Q., Wu, C. Y., Wang, L., & Luo, L. B. (2013). p-type ZnS: N nanowires: Low-temperature solvothermal doping and optoelectronic properties. *Applied Physics Letters*, **103**(21), 213111.

- Wang, H. Y., Y. Yang, X. Li, L. J. Li and C. Wang (2010). "Preparation and characterization of porous TiO<sub>2</sub>/ZnO composite nanofibers via electrospinning." *Chinese Chemical Letters* **21**(9): 1119-1123.
- Wang, C. Y. H. A., P. F. Wang, J. Hou, J. Qian, and S. H. Zhang (2010). "Preparation, characterization, photocatalytic properties of titania hollow sphere doped with cerium." *Journal of Hazardous Materials* **178**(1-3): 517-521.
- Wang, J., J. Li, Y. Xie, C. Li, G. Han, L. Zhang, R. Xu and X. Zhang (2010). "Investigation on solar photocatalytic degradation of various dyes in the presence of Er<sup>3+</sup>:YAlO<sub>3</sub>/ZnO–TiO<sub>2</sub> composite." *Journal of Environmental Management* **91**(3): 677-684.
- Wang, J., W. Mi, J. Tian, J. Dai, X. Wang and X. Liu (2013). "Effect of calcinations of TiO<sub>2</sub>/ZnO composite powder at high temperature on photodegradation of methyl orange." *Composites Part B: Engineering* **45**(1): 758-767.
- Wang, J., Z. Wang, B. Huang, Y. Ma, Y. Liu, X. Qin, X. Zhang and Y. Dai (2012). "Oxygen Vacancy Induced Band-Gap Narrowing and Enhanced Visible Light Photocatalytic Activity of ZnO." *ACS Applied Materials & Interfaces* **4**(8): 4024-4030.
- Wang, Y., W. Duan, B. Liu, X. Chen, F. Yang and J. Guo (2014). "The Effects of Doping Copper and Mesoporous Structure on Photocatalytic Properties of TiO<sub>2</sub>." *Journal of Nanomaterials* **2014**: 7.
- Wang, Y., K. Lu, and C. Feng (2011). "Photocatalytic degradation of methyl orange by polyoxometalates supported on yttrium-doped TiO<sub>2</sub>." *Journal of Rare Earths* **29**(9): 866-871.
- Wang, Y., S. Zhu, X. Chen, Y. Tang, Y. Jiang, Z. Peng and H. Wang (2014). "One-step template-free fabrication of mesoporous ZnO/TiO<sub>2</sub> hollow microspheres with enhanced photocatalytic activity." *Applied Surface Science* **307**(0): 263-271.
- Wang, Q., Zhu, S., Liang, Y., Cui, Z., Yang, X., Liang, C., & Inoue, A. (2017). Onestep synthesis of size-controlled Br-doped TiO<sub>2</sub> nanoparticles with enhanced visiblelight photocatalytic activity. *Materials Research Bulletin*, **86**, 248-256.
- Wu, C., L. Shen, H. Yu, Y.-C. Zhang and Q. Huang (2012). "Solvothermal synthesis of Cu-doped ZnO nanowires with visible light-driven photocatalytic activity." *Materials Letters* **74**(0): 236-238.
- Wu, L., J. C. Yu and X. Fu (2006). "Characterization and photocatalytic mechanism of nanosized CdS coupled TiO<sub>2</sub> nanocrystals under visible light irradiation." *Journal of molecular catalysis A: Chemical* **244**(1): 25-32.
- Xiao, Q., et al (2008). "Photoinduced hydroxyl radical and photocatalytic activity of samarium-doped TiO<sub>2</sub> nanocrystalline." *Journal of Hazardous Materials* **150**(1): 62-67.

- Xiao, S., L. Zhao, X. Leng, X. Lang and J. Lian (2014). "Synthesis of amorphous TiO<sub>2</sub> modified ZnO nanorod film with enhanced photocatalytic properties." *Applied Surface Science* **299**(0): 97-104.
- Xiao, T. Y. P., R. Li, Z. H. Peng, and C. H. Yan (2006). "Preparation, phase transformation and photocatalytic activities of cerium-doped mesoporous titania nanoparticles." *Journal of Solid State Chemistry* **179**(4): 1161-1170.
- Xin, B., Wang, P., Ding, D., Liu, J., Ren, Z., & Fu, H. (2008). Effect of surface species on Cu-TiO<sub>2</sub> photocatalytic activity. *Applied surface science*, **254**(9), 2569-2574.
- Xu, X., J. Wang, J. Tian, X. Wang, J. Dai and X. Liu (2011). "Hydrothermal and post-heat treatments of TiO<sub>2</sub>/ZnO composite powder and its photodegradation behavior on methyl orange." *Ceramics International* **37**(7): 2201-2206.
- Xu, J. Y. A., D. Fu, and C. Yuan (2008). "Synthesis of fluorine-doped titania-coated activated carbon under low temperature with high photocatalytic activity under visible light." *Journal of Physics and Chemistry of Solids* **69**(10): 2366–2370
- YMa, J.-W. F., X. Tao, X. Li, and J.-F. Chen (2011). "Low temperature synthesis of iodine-doped TiO<sub>2</sub> nanocrystallites with enhanced visible-induced photocatalytic activity." *Applied Surface Science* **257**(11): 5046–5051.
- Yang, C., H. Fan, Y. Xi, J. Chen and Z. Li (2008). "Effects of depositing temperatures on structure and optical properties of TiO<sub>2</sub> film deposited by ion beam assisted electron beam evaporation." *Applied Surface Science* **254**(9): 2685-2689.
- Yang, G., Z. Yan and T. Xiao (2012). "Preparation and characterization of SnO<sub>2</sub>/ZnO/TiO<sub>2</sub> composite semiconductor with enhanced photocatalytic activity." *Applied Surface Science* **258**(22): 8704-8712.
- Yang, M.-Q., N. Zhang, M. Pagliaro and Y.-J. Xu (2014). "Artificial photosynthesis over graphene-semiconductor composites. Are we getting better?" *Chemical Society Reviews* **43**(24): 8240-8254.
- Yi, S., J. Cui, S. Li, L. Zhang, D. Wang and Y. Lin (2014). "Enhanced visible-light photocatalytic activity of Fe/ZnO for rhodamine B degradation and its photogenerated charge transfer properties." *Applied Surface Science* **319**(0): 230-236.
- Yogi, C., K. Kojima, T. Takai and N. Wada (2009). "Photocatalytic degradation of methylene blue by Au-deposited TiO<sub>2</sub> film under UV irradiation." *Journal of Materials Science* **44**(3): 821-827.
- Yu, J., J. Low, W. Xiao, P. Zhou and M. Jaroniec (2014). "Enhanced Photocatalytic CO<sub>2</sub>-Reduction Activity of Anatase TiO<sub>2</sub> by Coexposed {001} and {101} Facets." *Journal of the American Chemical Society* **136**(25): 8839-8842.

- Yu, C., Yang, K., Xie, Y., Fan, Q., Jimmy, C. Y., Shu, Q., & Wang, C. (2013). Novel hollow Pt-ZnO nanocomposite microspheres with hierarchical structure and enhanced photocatalytic activity and stability. *Nanoscale*, **5**(5), 2142-2151.
- Yu, C., Jimmy, C. Y., & Chan, M. (2009). Sonochemical fabrication of fluorinated mesoporous titanium dioxide microspheres. *Journal of Solid State Chemistry*, **182**(5), 1061-1069.
- Yu, C., Cai, D., Yang, K., Jimmy, C. Y., Zhou, Y., & Fan, C. (2010). Sol-gel derived S, I-codoped mesoporous TiO<sub>2</sub> photocatalyst with high visible-light photocatalytic activity. *Journal of Physics and Chemistry of Solids*, **71**(9), 1337-1343.
- Zaleska, A.J. W. S., E. Grabowska, and J. Hupka (2008). "Preparation and photocatalytic activity of boron-modified TiO<sub>2</sub> under UV and visible light." *Applied Catalysis B* **78**(1-2): 92-100.
- Zhang, Q.Y. L., E. A. Ackerman, M. Gajdardziska-Josifovska, and H. Li (2011). "Visible light responsive iodine-doped TiO<sub>2</sub> for photocatalytic reduction of CO<sub>2</sub> to fuels " *Applied Catalysis A* **400**(1-2): 195-202.
- Zhang, M., T. An, X. Liu, X. Hu, G. Sheng and J. Fu (2010). "Preparation of a high-activity ZnO/TiO<sub>2</sub> photocatalyst via homogeneous hydrolysis method with low temperature crystallization." *Materials Letters* **64**(17): 1883-1886.
- Zhang, P., C. Shao, X. Li, M. Zhang, X. Zhang, Y. Sun and Y. Liu (2012). "In situ assembly of well-dispersed Au nanoparticles on TiO<sub>2</sub>/ZnO nanofibers: A three-way synergistic heterostructure with enhanced photocatalytic activity." *Journal of Hazardous Materials* **237-238**(0): 331-338.
- Zhang, Y., Z.-R. Tang, X. Fu and Y.-J. Xu (2010). "TiO<sub>2</sub>-Graphene Nanocomposites for Gas-Phase Photocatalytic Degradation of Volatile Aromatic Pollutant: Is TiO<sub>2</sub>-Graphene Truly Different from Other TiO<sub>2</sub>-Carbon Composite Materials?" *ACS Nano* **4**(12): 7303-7314.
- Zhao, L., M. Xia, Y. Liu, B. Zheng, Q. Jiang and J. Lian (2012). "Micro-twins TiO<sub>2</sub> nanorods grown on seeded ZnO film." *Journal of Crystal Growth* **344**(1): 1-5.
- Zhao, Y., Li, C., Liu, X., Gu, F., Du, H. L., & Shi, L. (2008). Zn-doped TiO<sub>2</sub> nanoparticles with high photocatalytic activity synthesized by hydrogen-oxygen diffusion flame. *Applied Catalysis B: Environmental*, **79**(3), 208-215.
- Zheng, X., D. Li, X. Li, J. Chen, C. Cao, J. Fang, J. Wang, Y. He and Y. Zheng (2015). "Construction of ZnO/TiO<sub>2</sub> photonic crystal heterostructures for enhanced photocatalytic properties." *Applied Catalysis B: Environmental* **168**, 408-415.
- Zhong, J. b., et al., 2012. 12(3): p. 998-1001. (2012). "Improved photocatalytic performance of Pd-doped ZnO." *Current Applied Physics* **12**(3): 998-1001.
- Zhou, P., J. Yu and M. Jaroniec (2014). "All-Solid-State Z-Scheme Photocatalytic Systems." *Advanced Materials* **26**(29): 4920-4935.

- Zhou, X.-T., H.-B. Ji and X.-J. Huang (2012). "Photocatalytic Degradation of Methyl Orange over Metalloporphyrins Supported on TiO<sub>2</sub> Degussa P25." *Molecules*.
- Zhu, B. L., C. S. Xie, W. Y. Wang, K. J. Huang and J. H. Hu (2004). "Improvement in gas sensitivity of ZnO thick film to volatile organic compounds (VOCs) by adding TiO<sub>2</sub>." *Materials Letters* **58**(5): 624-629.
- Zhu, J., F. Chen, J. Zhang, H. Chen and M. Anpo (2006). "Fe<sup>3+</sup>-TiO<sub>2</sub> photocatalysts prepared by combining sol-gel method with hydrothermal treatment and their characterization." *Journal of Photochemistry and Photobiology A: Chemistry* **180**(1-2): 196-204.
- Zhu, J., Z. Deng, F. Chen, J. Zhang, H. Chen, M. Anpo, J. Huang and L. Zhang (2006). "Hydrothermal doping method for preparation of Cr<sup>3+</sup>-TiO<sub>2</sub> photocatalysts with concentration gradient distribution of Cr<sup>3+</sup>." *Applied Catalysis B: Environmental* **62**(3-4): 329-335.
- Zhu, J., W. Zheng, B. He, J. Zhang and M. Anpo (2004). "Characterization of Fe-TiO<sub>2</sub> photocatalysts synthesized by hydrothermal method and their photocatalytic reactivity for photodegradation of XRG dye diluted in water." *Journal of Molecular Catalysis A: Chemical* **216**(1): 35-43.
- Zhu, M., H. Wang, A. A. Keller, T. Wang and F. Li (2014). "The effect of humic acid on the aggregation of titanium dioxide nanoparticles under different pH and ionic strengths." *Sci Total Environ* **487**: 375-380.
- Zhu, Z., M. Hartmann, E. M. Maes, R. S. Czernuszewicz and L. Kevan (2000). "Physicochemical Characterization of Chromium Oxides Immobilized in Mesoporous MeMCM-41 (Me = Al, Ti, and Zr) Molecular Sieves." *The Journal of Physical Chemistry B* **104**(19): 4690-4698.
- Zou, X., X. Dong, L. Wang, H. Ma, X. Zhang and X. Zhang (2014). "Preparation of Ni Doped ZnO-TiO<sub>2</sub> Composites and Their Enhanced Photocatalytic Activity." *International Journal of Photoenergy* **2014**: 8.
- Zuo, F., L. Wang, T. Wu, Z. Zhang, D. Borchardt and P. Feng (2010). "Self-doped Ti<sup>3+</sup> enhanced photocatalyst for hydrogen production under visible light." *J Am Chem Soc* **132**(34): 11856-11857.

## LIST OF PUBLICATIONS

### Academic journal

1. **Mohammad Reza Delsouz Khaki**, Abdul Aziz Abdul Raman, Wan Mohd Ashri Wan Daud, Baharak Sajjadi (2016) –Sensitivity Analysis of the Photoactivity of Cu-TiO<sub>2</sub>/ZnO during Advanced Oxidation Reaction by Adaptive Neuro-Fuzzy Selection Technique”, *Journal of Measurement*, Impact Factor: 1.484, **77** (2016), Pages 155-174.
2. **Mohammad Reza Delsouz Khaki**, Mohammad Saleh Shafeeyan , Abdul Aziz Abdul Raman, Wan Mohd Ashri Wan Daud (2017) –Application of doped photocatalysts for organic pollutant degradation - A review ”, *Journal of Environmental Management*, Impact Factor: 3.131, **198** (2017), Pages 78-94.
3. **Mohammad Reza Delsouz Khaki**, Abdul Aziz Abdul Raman, Wan Mohd Ashri Wan Daud, Baharak Sajjadi (2015) –Enhanced Photocatalytic Activity Using a New Hybrid of Cu Doped ZnO/TiO<sub>2</sub> under Visible Light Irradiation: Synthesis, Characterization and Efficiency Evaluation”, *Journal of water process Engineering*, Impact Factor: 3.14, (24/09/2016), Under Review.
4. **Mohammad Reza Delsouz Khaki**, Abdul Aziz Abdul Raman, Wan Mohd Ashri Wan Daud, Baharak Sajjadi (2015) –Evaluation the Efficiency of New Hybrid Cu Doped TiO<sub>2</sub>/ZnO Nano-Sized Photocatalyst for Degradation of MO and MB under Visible Light Irradiation; *Journal of water Reuse and Desalination*; Impact Factor: 0.409, (19/10/20162015), Under review.

## Conference Proceeding

1. **Mohammad Reza Delsouz Khaki**, Abdul Aziz Abdul Raman, Wan Mohd Ashri Wan Daud, Baharak Sajjadi (2015). –Effect of New Hybrid of doped photocatalyst Cu - ZnO/TiO<sub>2</sub> on an energy level for reducing of Band gap: Synthesis, Characterization and Effectiveness on Band gap”, *5rd International Conference on Environment (ICENV)*, Page 8, Penang, Malaysia.

University of Malaya